HIGH SPIN STATES IN

^{176,177}Ta

By

· LILY BUJA-BIJUNAS, B.Sc.

A Thesis

Submitted to the School of Graduate Studies

in Partial Fulfilment of the Requirements

for the Degree

Doctor of Philosophy

McMaster University

October 1978

HIGH SPIN STATES IN ^{176,177}Ta

DOCTOR OF PHILOSOPHY (1978)   McMASTER UNIVERSITY
(Physics)   Hamilton, Ontario

TITLE: High Spin States in ^{176,177}Ta

AUTHOR: Lily Buja-Bijunas

SUPERVISOR: Dr. J.C. Waddington

NUMBER OF PAGES: xiii,175

ii

ABSTRACT

The level structures of the odd and odd-odd deformed nuclei ^{177}Ta and ^{176}Ta have been studied by means of (Heavy Ion, xn) reactions. Gamma singles, γ-angular distribution, delayed gamma singles, γ-γ prompt coincidence, γ-γ delayed coincidence and delayed conversion electron measurements were used. Isomeric states with half-lives of 78 ns and 3.8 μs were established at (1309.0) keV and 2826.8 keV in ^{176}Ta and ^{177}Ta, respectively.

The interpretation of the high spin states has been carried out within the framework of the quasiparticle model, these states being assigned many-quasiparticle configurations. Experimentally deduced energy levels in ^{177}Ta were found to agree well with calculated values using the experimentally determined energies of lower-order many-quasiparticle states in ^{176}Hf and ^{177}Ta and a zero-range interaction between unpaired nucleons.

ACKNOWLEDGEMENTS

I wish to thank my supervisor and research director, Dr. J.C. Waddington, for his interest and guidance during the course of my studies. Also, to the members of my supervisory committee, Dr. A.B. Volkov and Dr. J.H. Crocket, I wish to express my gratitude.

Special thanks go to Dr. T.L. Khoo who generously assisted in both the theoretical and experimental aspects of this work. Dr. F.M. Bernthal is also thanked for help extended during experiments at Michigan State University.

It is difficult if not impossible to successfully complete a study without the help and co-operation of many people. I wish, therefore, to thank the faculty, students and staff of the Tandem Accelerator Laboratory and especially the members of my research group who have contributed many long hours to my work. A special thank you to my fellow student Arlene Larabee who had the dubious privilege of being my roommate during the final year of my studies.

I would like to express my thanks to a very talented Patti Petty who drew the many diagrams and to Susan Hanna who expertly typed the pages of this thesis.

And to my husband Ross, for his patience, understanding and encouragement, I extend a thousand thank yous. Very few could have been as lucky as I.

And last, but not least, my roommate's cat 'Stupid' despite whose help I still managed to complete this thesis.

iv

TABLE OF CONTENTS

θ

x

LIST OF TABLES

To My Grandfather

Stanley Verbyla

CHAPTER 1

INTRODUCTION

The goal of the study of nuclear physics is the development
of a suitable theory to explain observed nuclear phenomena. Con-
siderable experimental work is carried out to provide the required
evidence to substantiate or refute interpretations of these nuclear
properties.

The properties of deformed nuclei in the rare-earth region
(150 < A < 190) have been found to be well-explained in terms of a
unified model, which is an attempt to describe collective and
particle-like phenomena simultaneously. This model is applied to
the two nculei of this study, ^{177}Ta and ^{176}Ta, which are well-
deformed with deformations $\delta \sim 0.25$ and which exhibit characteristic
'rotational' behaviour.

The nuclei near the region Z = 72, N = 104 are known to have
high Ω single particle states near the Fermi level. This leads
to formation of high-K many particle rotational bands which are
often yrast and thus may be populated in heavy particle reactions.
In particular, the even-even nucleus ^{176}Hf has been extensively
studied (Khoo et al, 1972; Khoo et al, 1976) and many-quasiparticle
bands have been found in this nucleus. These high-K states are
often isomeric, their subsequent decay to lower-lying levels

1

being K-forbidden. Many 3 – and 5-quasiparticle states are found in the odd nucleus ^{177}Ta and a 7-quasiparticle configuration of spin $43/2^+$ is proposed for a level of ~ 4 MeV excitation. Similarly, 2- and 4-quasiparticle configurations are proposed for levels found in the odd-odd ^{176}Ta.

The excitation energies of the 3 –, 5 – and 7-quasiparticle states in ^{177}Ta are calculated assuming the higher-order states to be combinations of lower-order quasiparticle states found in ^{176}Hf and ^{177}Ta. The residual nucleon-nucleon interactions are calculated using a zero-range interaction found by Khoo et al (1975) to give values in good agreement with experimental results in ^{176}Hf. Similarly, the values calculated for ^{177}Ta give satisfactory agreement.

CHAPTER 2

THEORY

2.1 Introduction

The study of the structure of nuclei is a formidable problem because of the complexity of the system involved. Obviously, such a dynamical system, with all the degrees of freedom open to it, is not a trivial one, and therefore the use of a model which can give a systematic description of the nucleus is sought.

One of the most successful attempts at developing a model was the shell model (Mayer and Jensen, 1955). Within the framework of this model, each nucleon is considered to move independently within a stationary orbit, the effective force of all the other nucleons within the system being represented by an average common potential. This model has found its greatest applicability to spherical nuclei.

The nonspherical equilibrium shape of nuclei in the deformed mass regions $18 \leq A \leq 28$, $150 \leq A \leq 190$, $A > 224$ cannot be handled properly with the simple shell model approach as correlated motion of several nucleons must be taken into account to properly explain such properties as large quadrupole moments. For such properties, the liquid drop model of the nucleus (Bohr, 1936), where the nucleus is treated as a deformable liquid drop, is more applicable.

3

Clearly, then, the most desirable approach would be a blending of both approaches to describe collective and particle-like phenomena simultaneously. The unified model developed by Bohr (1952) and Bohr and Mottelson (1953) treats the nucleus in this way.

A great deal of detail has been eliminated in the discussion of theory in this thesis. The reason for this is an effort to avoid duplication as the facts regarding the basic theoretical approach to deformed nuclei have already been laid down in a number of theses. Only the pertinent ideas are mentioned. For a full discourse, excellent treatments can be found by Preston and Bhaduri (1975), Rowe (1970) and Khoo (Ph.D. thesis, McMaster 1972). A detailed discussion is given in the case of new ideas developed expressly for this study.

2.2 The Unified Model for Rotations

2.2.1 Deformed Nuclei

The phenomenon of a deformed nucleus is simple to under-stand if one considers the way in which particles couple in a nucleus. There are two basically different coupling schemes which lead to a spherical or else a deformed equilibrium shape. The first is to couple pairs of particles to $J = 0$ configurations. This leads to a spherical shape. The second is reflected by the tendency of a nucleon to align its orbit with the average field produced by the other nucleons in the system. This is "aligned"

coupling and leads to a deformed equilibrium shape.

To understand the latter, consider the addition of one extra particle to the next empty $(j, m = j)$ orbit of a closed shell nucleus. The presence of this particle leads to a non-spherical density distribution concentrated along the equatorial plane. Thus, any other additional particles added to the system will align their orbits with the non-spherical field and produce an oblate (pancake shaped) nucleus. Similarly, the addition of the odd nucleon into the $(j, m = 1/2)$ orbit will lead to a non-spherical density distribution concentrated along the polar axis and, hence, a prolate (cigar shaped) nucleus.

The angular momentum of the aligned system is not a good quantum number and so the nucleus thus described is not in a stationary state. The nucleus, therefore, rotates. Within the framework of the unified model for rotations, the rotational angular momentum of the core couples with the intrinsic angular momentum of the extra-core nucleons travelling within the deformed average potential to yield constant total angular momentum. This system is described in Figure 2.1.(a).

The total angular momentum of the system, $\vec{I}$, is composed of the angular momentum of the rotational core and the extra-core particles, $\vec{R}$ and $\vec{J}$, respectively. The projection of $\vec{I}$ upon a space fixed axis, z, is given by m_I, while the projection upon a symmetry axis, z', is given by K. The projection of the intrinsic

Figure 2.1

Coupling of angular momenta in an axially

symmetric a) odd A and b) doubly odd or even nucleus.

a)

b)
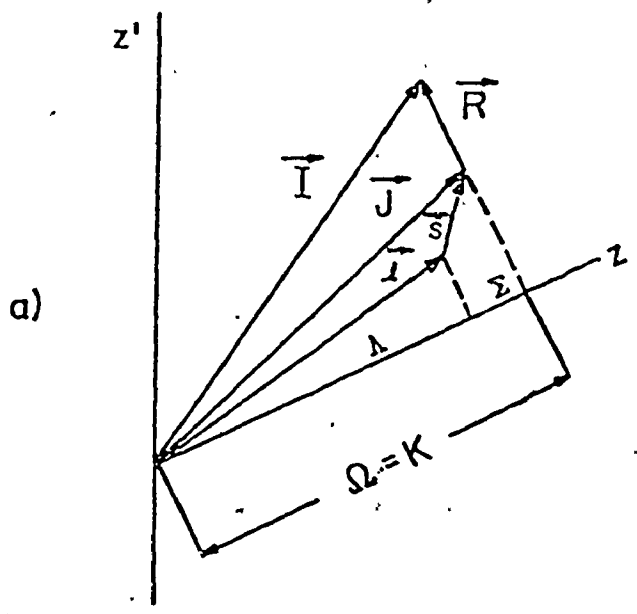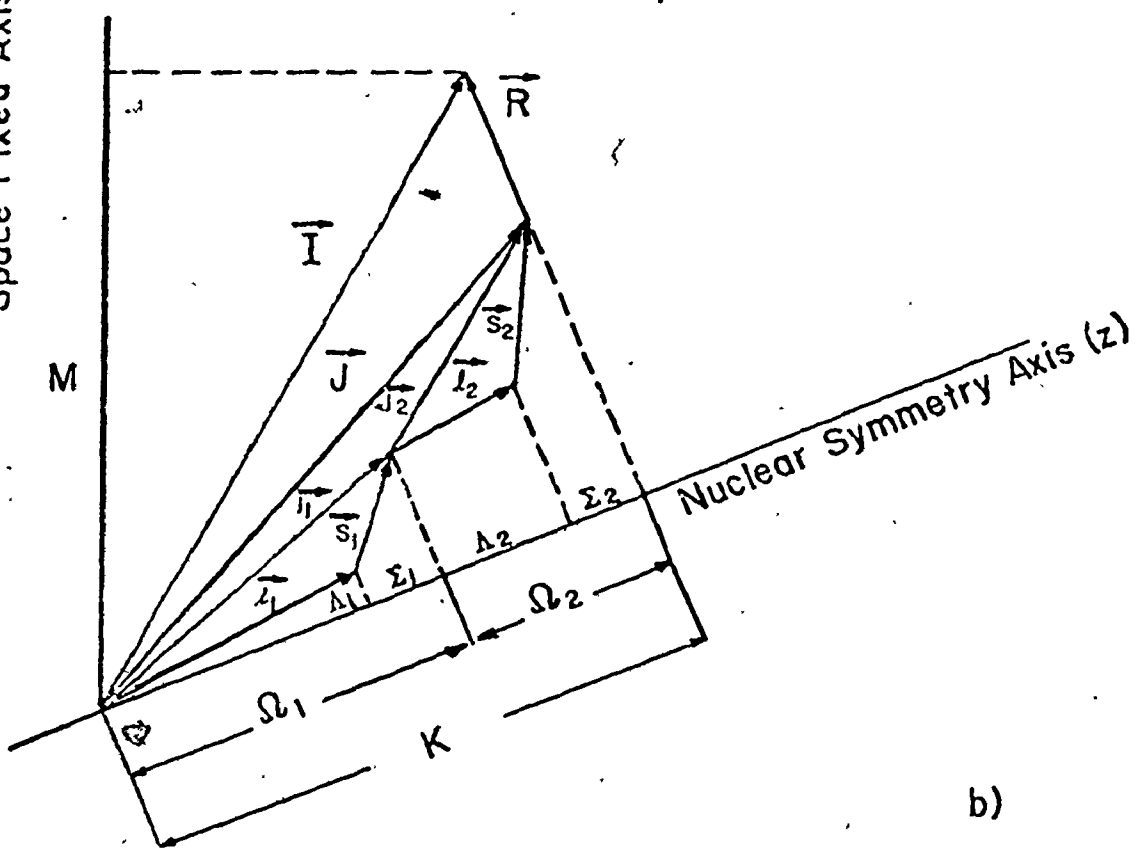
angular momentum $\vec{J}$ upon the symmetry axis, Ω, is a constant of the motion as are m_I and K. The intrinsic angular momentum is composed of orbital and intrinsic spin components, $\vec{\ell}$ and $\vec{s}$, with their respective components on the symmetry axis, Λ and Σ. This gives $\Omega = \Lambda + \Sigma$, with $\Sigma = \pm 1/2$. Rotational motion of an axially symmetric nucleus must be perpendicular to the axis of symmetry, and so, in such a case, $K = \Omega$.

For the case of two extra core particles as in an odd-odd or even-even nucleus (see Figure 2.1. (b)) the respective intrinsic angular momenta $\vec{j_1}$ and $\vec{j_2}$ couple to yield the total intrinsic angular momentun, $\vec{J}$. The respective projections of $\vec{j_1}$ and $\vec{j_2}$ upon the symmetry axis, Ω_1 and Ω_2, can couple either parallel or anti-parallel leading to two possible values of K, i.e.

$$K_1 = |\;|\Omega_1|\; - \;|\Omega_2|\;| \quad \text{anti-parallel} \quad (2.2.1)$$

$$K_2 = |\Omega_1|\; + \;|\Omega_2| \quad \text{parallel} \quad (2.2.2)$$

The difference in energy between these two coupling modes will be discussed in Section 2.5.

2.2.2 Coupling of Rotational and Particle Motions

The complete Schrödinger equation describing a nucleus with p extra-core nucleons is given by

$$(T_{rot} + \sum_p H_p)\chi = \mathcal{E}\chi \quad (2.2.3)$$

The rotational kinetic energy is given by

$$T_{rot} = \sum_{k=1}^{3} \frac{\hbar^2}{2\mathcal{J}_k} R_k^2 = \sum_k \frac{\hbar^2}{2\mathcal{J}_k} (I_k - j_k)^2 \qquad (2.2.4)$$

where the summation is extended over the three body-fixed axes, and $\mathcal{J}_k$ is the moment of inertia about the axis k. Expanding for the axially symmetric case, one obtains

$$\begin{aligned} T_{rot} &= \frac{\hbar^2}{2\mathcal{J}} [(\vec{I}-\vec{j})^2 - (I_3-j_3)^2] + \frac{\hbar^2}{2\mathcal{J}_3} (I_3-j_3)^2 \\ &= \frac{\hbar^2}{2\mathcal{J}} [I(I+1) + j^2 - 2\vec{I} \cdot \vec{j} - (K-\Omega)^2] + \frac{\hbar^2}{2\mathcal{J}_3}(K-\Omega)^2 \\ &= \frac{\hbar^2}{2\mathcal{J}} [I(I+1) - K^2 - \Omega^2] + \frac{\hbar^2}{2\mathcal{J}_3}(K-\Omega)^2 \\ &\quad - \frac{\hbar^2}{2\mathcal{J}}(I_+j_- + I_-j_+) + \frac{\hbar^2}{2\mathcal{J}} j^2 \end{aligned} \qquad (2.2.5)$$

In the above expression, $\mathcal{J} = \mathcal{J}_1 = \mathcal{J}_2$. The first two terms contain only constants, while the last contains only particle motion and is usually included with the particle Hamiltonian. The term of interest contains the operators I_+j_- and I_-j_+ which couple the rotational and particle angular momenta. This is the so-called RPC or Coriolis interaction. The operators $I_\pm$ have non-zero matrix elements only for states that differ by one unit in K and so the RPC term "mixes" states of K with $K \pm 1$.

$$\langle IK|I_\pm|IK\underline{\pm}1\rangle = \sqrt{(I\mp K)(I\pm K+1)} \qquad (2.2.6)$$

The only diagonal contribution of the RPC term is in the $K = 1/2$ states as both $\pm K$ are included in the collective wavefunction.

The off-diagonal contribution is particularly important when states of the same angular momentum I and parity but differing in K by one unit come very close together. The effect of the mixing is similar to that of states of the same spin repelling each other. For the case of two rotational bands, the lower band becomes compressed while the upper is expanded. In extreme cases, the band structure may not be recognizable. A calculation of the band mixing effect is given in Section 2.7.

In the adiabatic limit where the rotational motion of the core is slow in comparison to the particle motion and, in essence, the particles are unaware of the rotational motion of the core, RPC is neglected.

2.3 Single Particle States in a Deformed Nucleus -- the Nilsson Model

The calculation of the single particle orbitals in a deformed shell-model potential was carried out by Nilsson (1955). A spheriodal harmonic oscillator potential with axial symmetry is chosen as the common potential with the single particle Hamiltonian taken to be

$$H = H_0 + C\vec{\ell} \cdot \vec{s} + D\vec{\ell} \cdot \vec{\ell}$$ (2.3.1)

where

$$H_0 = -\frac{\hbar^2}{2m} \nabla^2 + \frac{1}{2} m(\omega_\perp^2 (x^2 + y^2) + \omega_z^2 z^2) \quad .$$ (2.3.2)

The harmonic oscillator potential is split into two parts, one of which is spherically symmetric and the other part is a function of the

deformation δ. The terms $C\vec{\ell} \cdot \vec{s}$ and $D\vec{\ell} \cdot \vec{\ell}$ are added so that, for the limiting case of spherical symmetry, energy levels agree with those calculated by the shell model. The $\vec{\ell} \cdot \vec{s}$ term is the familiar spin-orbit coupling, while the $\vec{\ell} \cdot \vec{\ell}$ depresses the states of high angular momentum.

For the axially symmetric case, the oscillator frequencies are defined as

$$\omega_{\perp} = \omega_0 (1 + \tfrac{2}{3} \delta)^{1/2} = \omega_x = \omega_y$$

$$\omega_z = \omega_0 (1 - \tfrac{4}{3} \delta)^{1/2} \qquad\qquad\qquad (2.3.3)$$

To ensure the volume contained by the equipotential surface is independent of deformation, the restriction is applied that

$$\omega_x \omega_y \omega_z = \text{constant.} \qquad\qquad (2.3.4)$$

This restriction implies that ω_0 should be deformation dependent:

$$\omega_0(\delta) = \omega_0^0 \, (1 - \tfrac{4}{3} \delta^2 - \tfrac{16}{27} \delta^3)^{-1/6} \qquad\qquad (2.3.5)$$

where ω_0^0 is the value of ω_0 at $\delta = 0$.

To solve (2.3.1) Nilsson (1955) used $|N\ell\Lambda\Sigma\rangle$ as a set of basis vectors, the eigenfunctions of the Hamiltonian, χ_Ω, being a linear combination of these basis vectors. The results of his calculations are tabulated in the form of coefficients $a_{\ell\Lambda\Sigma}^{\Omega}$, the eigenfunctions of the Hamiltonian being expressed as:

$$\chi_\Omega = \sum_{\ell\Lambda\Sigma} a_{\ell\Lambda\Sigma}^{\Omega} \, |N\ell\Lambda\Sigma\rangle \qquad\qquad (2.3.6)$$

In the same manner, Chi(1966,67) has undertaken to use the basis vectors of the isotropic harmonic oscillator $|N\ell j\Omega\rangle$ in his solution of the Hamiltonian. The coefficients as calculated by Chi, $C_{j\ell}^{\Omega}$, are related to Nilsson's $a_{\ell\Lambda\Sigma}^{\Omega}$ through the Clebsch-Gordon transformation

$$C_{j\ell}^{\Omega} = \sum_{\Lambda\Sigma} \langle \ell 1/2\Omega\Sigma | j\Omega\rangle a_{\ell\Lambda\Sigma}^{\Omega} \qquad (2.3.7)$$

Figures 2.2 and 2.3 give the Nilsson results for proton and neutron single particle states in the region of interest in this study. The line representing each single particle orbital as a function of deformation δ is labelled by $\Omega\pi$ and the triad $[Nn_3\Lambda]$. The asymptotic quantum numbers N and n_3 give the total number of oscillator quanta and the component along the symmetry axis, respectively. They are constants of the motion only in the limit of large deformation.

Within the spherical shell model, each j orbital is (2j+1) - fold degenerate. For the deformed shell model potential this degeneracy is lifted so that each shell model state separates into j + 1/2 levels, each level 2-fold degenerate with values $\pm \Omega$.

The energy of a nuclear state, equation 2.2.3, for the axially symmetric nucleus is given as

$$E_{I,K} = \varepsilon_K + \frac{\hbar^2}{2\mathcal{J}} [I(I+1) - 2K^2 + \delta_{K1/2} a(-)^{I+1/2}(I+1/2)] \qquad (2.3.8)$$

where ε_K is the intrinsic state energy characterized by the K value. Upon each intrinsic state is built a rotational band, each member having the same value of K and spins I = K, K+1 etc. The decoupling

Figure 2.2

Nilsson diagram for proton orbitals for 50 < Z < 94

$\frac{1}{2}+[400]$

$\frac{3}{2}+[402]$

$\frac{11}{2}-[505]$

$\frac{5}{2}+[642]$

$\frac{1}{2}-[530]$

$\frac{3}{2}-[532]$

$\frac{3}{2}+[651]$

$\frac{5}{2}+[402]$

$\frac{9}{2}-[514]$

$\frac{7}{2}+[404]$

$\frac{1}{2}+[660]$

$\frac{1}{2}-[541]$

$\frac{1}{2}+[411]$

$\frac{7}{2}-[523]$

$\frac{3}{2}+[411]$

$\frac{5}{2}+[413]$

$\frac{5}{2}-[532]$

$\frac{5}{2}-[541]$

$\frac{1}{2}+[420]$

$\frac{3}{2}+[422]$

$\frac{1}{2}-[550]$

$h_{\frac{9}{2}}$

(82)

$s_{\frac{1}{2}}$

$d_{\frac{3}{2}}$

$h_{\frac{11}{2}}$

$d_{\frac{5}{2}}$

$g_{\frac{7}{2}}$

(50)

$\frac{E}{\hbar\omega_o}$

6.4

6.2

6.0

5.8

5.6

5.4

0   0.1   0.2   0.3

δ
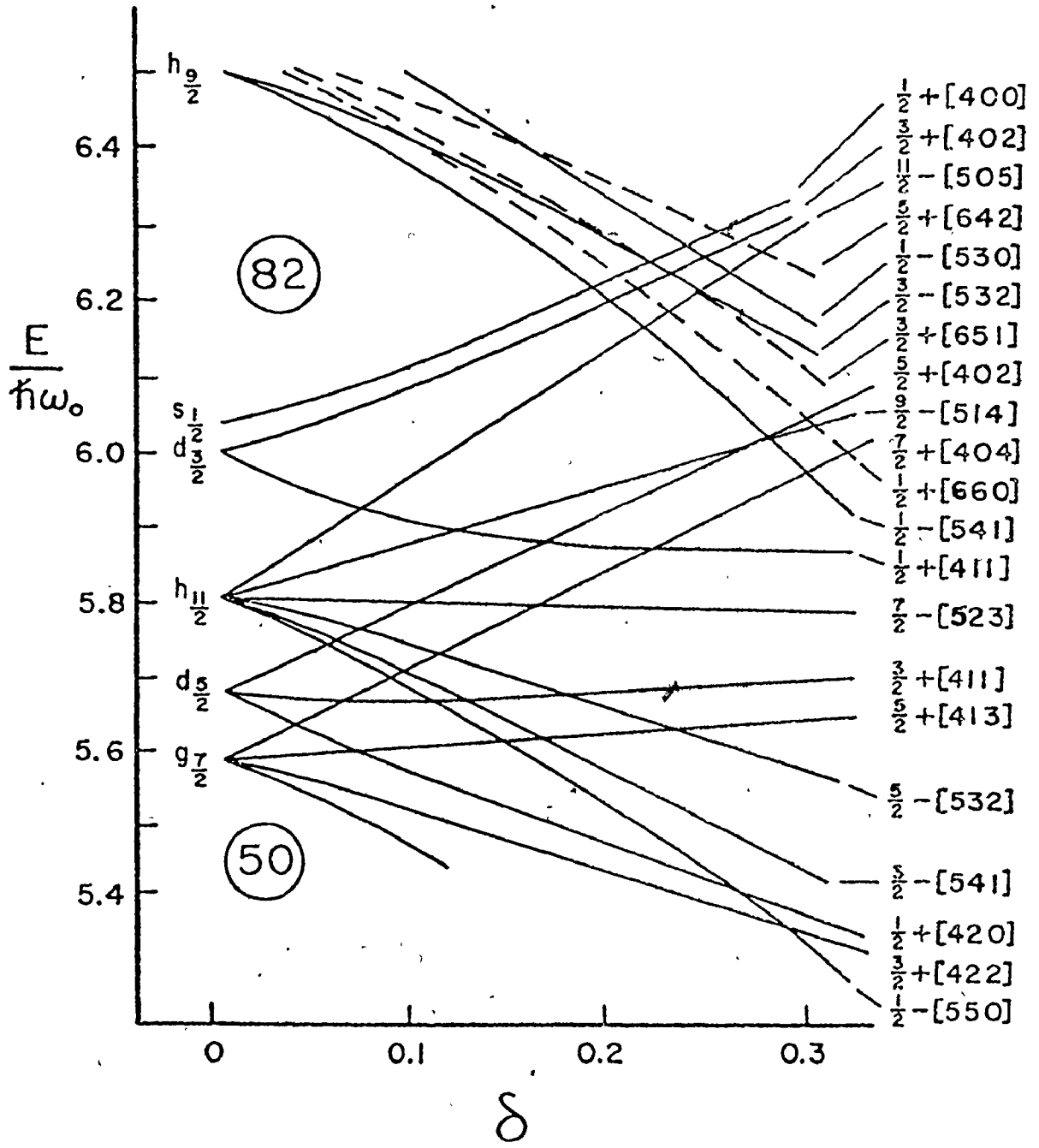
Figure 2.3

Nilsson diagram for neutron orbitals for 82 < N < 126.

A Nilsson diagram showing single-particle energy levels $E/\hbar\omega_o$ as a function of the deformation parameter δ.

Left-side axis labels: $\frac{E}{\hbar\omega_o}$ with values 6.50, 6.25, 6.00, 5.75.

Spherical shell labels (left): p 1/2, f 5/2, p 3/2, i 13/2, h 9/2, f 7/2, h 11/2.

Circled numbers: 126, 82, 90.

Top labels: 1/2− [501], 5/2− [503], 3/2− [501], 13/2+ [606].

Right-side labels (top to bottom):
9/2− [505]
11/2+ [615]
7/2− [503]
3/2− [512]
1/2− [510]
9/2+ [624]
7/2− [514]
5/2− [512]
7/2+ [633]
1/2− [521]
11/2− [505]
5/2− [523]
3/2− [521]
5/2+ [642]

Bottom labels: [541] 1/2−, [530] 1/2−, [532] 3/2−, [660] 1/2+, [651] 3/2+.

Bottom axis δ with values: 0, 0.1, 0.2, 0.3.

parameter 'a' is non zero only for K = 1/2 bands and is a result of the Coriolis contribution as discussed in Section 2.2.

2.4 The Pairing Interaction

To explain the tendency of Fermi particles to pair to spin J = 0, a short-range interaction must be introduced. The pairing phenomenon forms the basis of the BCS theory of superconductivity developed by Bardeen, Cooper and Schrieffer (1957). This theory was adapted to the theory of nuclei through the work of Bohr, Mottelson and Pines. (1958), a review article subsequently being presented by Nathan and Nilsson (1965).

The inclusion of the pairing force destroys the simple picture of independent particles and produces a diffuseness of the Fermi surface. Whereas in the independent particle model a state 'ν' is either empty or full if it is above or below the Fermi surface, the state now is characterized by a probability V_ν^2 of being filled by a pair of particles and U_ν^2 of being empty. Conservation of probability requires that

$$U_\nu^2 + V_\nu^2 = 1 \ . \qquad\qquad (2.4.1)$$

An independent particle formalism can be regained through the mathematical device of independent quasiparticles. Particle excitations in nuclei can then be thought of as quasiparticle excitations where the quasiparticle is a fermion which is particle-like to the extent U_ν and hole-like to the extent V_ν.

The energy of a quasiparticle state is given by

$$E_\nu = \sqrt{(\epsilon_\nu - \lambda)^2 + \Delta^2} \qquad (2.4.2)$$

where ϵ_ν is the single particle energy (e.g. Nilsson model energy), λ is the non-diffuse Fermi level and 2Δ is the energy gap. This energy gap can be seen by a comparison of the first excited intrinsic state in an even-even as opposed to an odd or odd-odd nucleus where the former is seen to be an energy $2\Delta \simeq 1\,\mathrm{MeV}$ above the ground state whereas no such gap appears in the latter case. The value of 2Δ is determined by the strength of the pairing force and can be measured through odd-even mass differences. Since an odd proton nucleus has a nucleon which cannot be paired, it is less tightly bound than a proton in an even-even nucleus. Therefore, the difference in proton separation energies gives a measure of the pairing gap,

$$\Delta_p \simeq \frac{1}{4}[2S_p(Z,N) - S_p(Z+1,N) - S_p(Z-1,N)] \qquad (2.4.3)$$

The same mass difference holds in the case of neutrons. The energy gap ranges from about 900 keV to 1.5 MeV, the gap being larger for lighter nuclei.

The quantities U_ν^2 and V_ν^2 are calculated using the expressions

$$V_\nu^2 = \frac{1}{2}\left[1 - \frac{\epsilon_\nu - \lambda}{\sqrt{(\epsilon_\nu - \lambda)^2 + \Delta^2}}\right] \qquad (2.4.4)$$

$$U_\nu^2 = \frac{1}{2}\left[1 + \frac{\epsilon_\nu - \lambda}{\sqrt{(\epsilon_\nu - \lambda)^2 + \Delta^2}}\right] \qquad (2.4.5)$$

For a single particle state far above the Fermi level

λ, $(\varepsilon_\nu - \lambda)^2 \gg \Delta^2$ and $V_\nu^2 = 0$. Similarly, far below the Fermi

level $V_\nu^2 = 1$.

2.5 Splitting Energy in Deformed Nuclei

As mentioned in Section 2.2, the respective projections of

$\vec{j}_1$ and $\vec{j}_2$ upon the symmetry axis, Ω_1 and Ω_2, can couple either parallel

or anti-parallel leading to two possible values of K. After

rotational energies are subtracted, the difference in energy between

the two K-states is due to the interaction between the two unpaired

nucleons. The empirical rule of Gallagher and Moszkowski (1958) for

the case of odd-odd nuclei predicts that the band with the value

of K such that $\Sigma = |\Sigma_1 + \Sigma_2| = 1$ would lie lower in energy than the

band with $\Sigma = |\Sigma_1 - \Sigma_2| = 0$. The rule is opposite for the case of

even-even nuclei.

These splitting energies, then, can be used as a probe for

the residual neutron-proton interaction. First efforts at the

calculation of the parallel-antiparallel splitting energy were carried

out by dePinho and Picard (1965) and Newby (1962). A more systematic

approach which led to consistent results for a number of odd-odd

deformed nuclei was tried by Jones et al (1971) and Pyatov (1963).

In his calculations, Pyatov considered a zero-range spin-dependent

central potential for the odd nucleon interaction of the form

$$H_{int} = -4\pi g \cdot \delta(\vec{r}_p - \vec{r}_n)[1 - \alpha + \alpha\vec{\sigma}_n \cdot \vec{\sigma}_p]. \qquad (2.5.1)$$

In the above expression, α is the extent of contribution of the spin

forces while g is dimensionless and is usually expressed in terms

of the parameter W,

$$W = g\sqrt{\frac{2\upsilon^3}{\pi}}$$

(2.5.2)

where υ is a quantity which appears in the expressions for the

radial wavefunction. An extensive review article on the effective

neutron-proton interaction in rare earth nuclei has been written

by Boisson et al (1976).

The energy shift for the odd-odd case is given by

$$\Delta E = E(K_1) - E(K_2) = -2\alpha\{A[1+(-1)^{I+N_1+N_2} \delta_{K,0}] + B$$

(2.5.3)

where the expressions for A and B are given by Pyatov. The value

of ΔE is found to be proportional to the quantity αW.

The programme SPLIT (Cheung, 1975) was used for the

calculation of splitting energies for various two-quasiparticle con-

figurations in ^{176}Ta. The value $\alpha W = 0.85$ was used in the calculation.

2.6 Calculation of the Excitation Energies of Many-Quasiparticle States

The energy of a many-quasiparticle state is a combination of

the single-quasiparticle energies of its constituent nucleons and the

neutron-neutron, proton-proton and neutron-proton interactions between

them. It is then theoretically possible to calculate the energy

of such a state if the required quantities can be experimentally

measured or theoretically estimated. The energy of a state of N

quasiparticles would then be given by

$$E(Nq.p.) = \varepsilon_1 + \varepsilon_2 + \ldots + \varepsilon_N + \Delta^1_p + \Delta^2_p + \ldots + \Delta^X_p + \Delta^1_n + \Delta^2_n + \ldots +$$

$$\Delta^Y_n + V_{nn}(Nq.p.) - V_{nn}(gs) + V_{pp}(Nq.p.)$$

$$-V_{pp}(gs) + V_{np}(Nq.p.) - V_{np}(gs) \quad . \tag{2.6.1}$$

The Δ_p and Δ_n are the pairing energies lost in breaking a neutron or proton pair with X equaling A/2 for a system of A unpaired protons, A even, and (A-1)/2 for A odd. Similarly Y equals B/2 for a system of B unpaired neutrons, B even, and (B-1)/2 for B odd.

$\varepsilon_1, \ldots, \varepsilon_N$	are the single particle energies of the unpaired nucleons
$V_{nn}(Nq.p.)-V_{nn}(gs)$	is the difference in energy of the neutron-neutron interaction in the N-quasiparticle state and the ground state
$V_{pp}(Nq.p.)-V_{pp}(gs)$	is the difference in energy of the proton-proton interaction in the N-quasiparticle state and the ground state
$V_{np}(Nq.p.)-V_{np}(gs)$	is the difference in energy of the neutron-proton interaction in the N-quasiparticle state and the ground state.

Alternatively, one can get a better estimate of the energy by grouping the constituent quasiparticles into two or more multi-quasiparticle states whose energies are accurately known. Using this new grouping, the energy of a state of N quasiparticles which can

be grouped into a state of A-quasiparticles and a state of B-quasiparticles would then be given by

$$
\begin{aligned}
E(Nq.p.) = {} & \varepsilon_1 + \varepsilon_2 + \ldots + \varepsilon_A + \varepsilon_{A+1} + \ldots + \varepsilon_{N-A} \\
& + V_{nn}(Aq.p.) - V_{nn}(gs)_A + V_{nn}(Bq.p.) \\
& - V_{nn}(gs)_B + D' + V_{pp}(Aq.p.) - \\
& V_{pp}(gs)_A + V_{pp}(Bq.p.) - V_{pp}(gs)_B \\
& + D'' + V_{np}(Aq.p.) - V_{np}(gs)_A + \\
& V_{np}(Bq.p.) - V_{np}(gs)_B + D'''. \\
= {} & E(Aq.p.) + E(Bq.p.) + D' + D'' + D''' \quad\quad (2.6.2)
\end{aligned}
$$

where $E(Aq.p.)$ and $E(Bq.p.)$ are the measured A-quasiparticle and B-quasiparticle state energies and $V(gs)_{A,B}$ refer to the ground states in the respective nuclei where the A and B are found. The quantities D', D'' and D''' give the difference in nucleon-nucleon interaction in the N-quasiparticle state and the constituent A- and B- quasiparticle states.

The quantities to be calculated, then, are the nucleon-nucleon interactions. For the case of a state of p quasiprotons and n quasineutrons, the value of the neutron-proton interaction can be expressed as (Khoo et al (1975); Khoo (1978))

$$
\begin{aligned}
V_{np}(Nq.p.) - V_{np}(gs) = {} & \sum_{\substack{i=p \\ j=n}} \langle ij \rangle + \sum_{\substack{i=p \\ j \neq n}} \langle ij \rangle v_j^{*2} \\
& + \sum_{\substack{i \neq p \\ j=n}} \langle ij \rangle v_i^{*2} + \sum_{\substack{i \neq p \\ j \neq n}} \langle ij \rangle 2 v_i^{*2} v_j^{*2}
\end{aligned}
$$

$$- \sum_{\substack{i \\ j}} <ij> \, 2v_i^2 v_j^2 \; . \qquad\qquad (2.6.3)$$

The summations are carried over the interactions between the p quasiprotons and n quasineutrons, the p quasiprotons with the paired neutrons, the paired protons with the n quasineutrons, and the paired protons with the paired neutrons. The $<ij>$ and the time-reversed $<i\bar{j}>$ are the nucleon -nucleon interaction matrix elements which are calculated assuming some form of interaction potential while the v^{*2} and v^2 give occupation probabilities in the excited and ground states, respectively. The terms in the ground state can be regrouped with corresponding terms in the N-quasiparticle state to yield

$$V_{np}(Nq.p.) - V_{np}(gs) = \sum_{\substack{i=p \\ j=n}} [<ij> - 2v_i^2 v_j^2 (<ij> + <i\bar{j}>)$$

$$+ \; \overline{<ij>} \; \{ \sum_{\substack{i=p \\ j\neq n}} v_j^{*2} - 2v_i^2 v_j^2 + \sum_{\substack{i\neq p \\ j=n}} v_i^{*2} - 2v_i^2 v_j^2$$

$$+ \; \sum_{\substack{i\neq p \\ j\neq n}} (2v_i^{*2} v_j^{*2} - 2v_i^2 v_j^2) \; \} \qquad (2.6.4)$$

An average interaction $\overline{<ij>}$ has been substituted for the individual contributions as the large number of interactions would make this a good approximation. The expression can be further simplified by noting that if the case were taken where all the interactions are the same in the N-quasiparticle and ground states and, of course,

there are the same number of interactions in both cases, then the sum of the coefficients of all the matrix elements must be zero. Therefore, in any case,

$$\sum_{\substack{i=p \\ j\neq n}} + \sum_{\substack{i\neq p \\ j=n}} + \sum_{\substack{i\neq p \\ j\neq n}} + \sum_{\substack{i=p \\ j=n}} (1 - 4v_i^2 v_j^2) = 0 \quad . \tag{2.6.5}$$

Therefore,

$$V_{np}(Nq.p.) - V_{np}(gs) = \sum_{\substack{i=p \\ j=n}} [<ij> - 2v_i^2 v_j^2$$

$$(<ij> + <i\bar{j}>) -$$

$$<\bar{i}\bar{j}>(1 - 4v_i^2 v_j^2)]. \tag{2.6.6}$$

For the case of the neutron-neutron or proton-proton interaction between N neutrons or between N protons, this result can be expressed as,

$$V_{k\ell}(Nq.p.) - V_{k\ell}(gs) = \sum_{\substack{k=N \\ \ell=N}} [\frac{<k\ell>}{2}(1 - \delta_{k\ell}) -$$

$$2v_k^2 v_\ell^2(1 - \delta_{k\ell})(\frac{<k\ell> + <k\bar{\ell}>}{2}) -$$

$$\overline{<k\ell>}(1 - \delta_{k\ell})(\frac{1 - 4v_k^2 v_\ell^2}{2})]. \tag{2.6.7}$$

To calculate the values of the interaction matrix elements, the zero-range spin-dependent central potential proposed by Pyatov (1963) was used. (See equation 2.5.1). The values of the parameters $4\pi g(\nu/2\pi)^{3/2}$ and α were set at 5.82 MeV and 0.146, respectively. These parameters were adjusted to these values by Khoo et al (1975)

so as to reproduce the splittings of singlet-triplet pairs in odd-odd (Jones et al, 1971) and even-even (Khoo et al, unpublished data) nuclei.

Khoo et al (1975) also carried out the same calculation of the interaction matrix elements using what he termed a 'realistic' interaction, including spin-orbit and tensor terms, obtained from the Reid potential following Brueckner theory. The details are given by Bertsch (1972). Khoo et al (1975) found that whereas the δ-interaction could account quite well for the energy of the many-quasiparticle states in ^{176}Hf he was calculating, the 'realistic' interaction gave much poorer agreement. The matrix elements calculated using the δ-force were, therefore, used in the energy calculations in ^{177}Ta.

Tables 2.1 to 2.5 list the values of the nucleon-nucleon interaction matrix elements and the neutron and proton occupation probabilities v^2 in ^{176}Hf and ^{177}Ta which were used in the calculations. The experimental values of v^2 were obtained through the use of equations 2.4.2 and 2.4.4 and experimental quasiparticle energies.

Table 2.1

Neutron-Proton Interaction Matrix Elements Using δ-Force
Interaction.   Force strengths set at $4\pi g(\nu/2\pi)^{3/2} = 5.82$
MeV and $\alpha = 0.146.$ Upper member of each pair gives the
singlet value, the lower member gives the triplet value.
All matrix elements are negative.   Average matrix
element $\doteq 503$.

	$5/2^+[402]\downarrow_p$	$7/2^+[404]\downarrow_p$	$9/2^-[514]\downarrow_p$
$1/2^-[521]\downarrow_n$	345/439	234/292	283/341
$7/2^+[633]\downarrow_n$	241/302	381/481	(457/595)*
$5/2^-[512]\downarrow_n$	526/686	351/438	477/626
$7/2^-[514]\downarrow_n$	376/482	588/761	796/1074
$9/2^+[624]\downarrow_n$	286/374	432/567	544/708

*estimated

Table 2.2

Proton-Proton Interaction Matrix Elements Using

δ-Force Interaction. Force strengths set at

$4\pi g(\nu/2\pi)^{3/2}$ = 5.82 MeV and α = 0.146. Upper

member of each pair gives the singlet value, .

the lower member gives the triplet value. All

matrix elements are negative. Average matrix

element = 170.

	$5/2^+[402]\uparrow_p$	$7/2^+[404]\downarrow_p$	$9/2^-[514]\uparrow_p$
$5/2^+[402]\uparrow_p$		340/8.1	(330/15)*
$7/2^+[404]\downarrow_p$			327/23
$9/2^-[514]\uparrow_p$			

* estimated

Table 2.3

Neutron-Neutron Matrix Elements Using δ-Force Interaction.

Force strengths set at $4\pi g(\nu/2)^{3/2} = 5.82$ MeV and $\alpha = 0.146$.

Upper member of each pair gives the singlet value, the lower member gives the triplet value. All matrix elements are negative. Average matrix element = 116.

	$1/2^-[521]\downarrow_n$	$7/2^+[633]\uparrow_n$	$5/2^-[512]\uparrow_n$	$7/2^-[514]\downarrow_n$	$9/2^+[624]\uparrow_n$
$1/2^-[521]\downarrow_n$					
$7/2^+[633]\uparrow_n$	177/38				
$5/2^-[512]\uparrow_n$	180/42	(178/30)*			
$7/2^-[514]\downarrow_n$	139/23	202/39	241/27		
$9/2^+[624]\uparrow_n$	204/30	(216/34)*	165/40	280/32	

* estimated

25

Table 2.4

Experimental Values of Occupation Probabilities
v^2 for Proton States in ^{176}Hf and ^{177}Ta.

Orbital	v^2	
	^{176}Hf	^{177}Ta
$5/2^+[402]\uparrow_p$	.169	.322
$7/2^+[404]\downarrow_p$	.442	.500
$9/2^-[514]\uparrow_p$	.329	.678

Table 2.5

Experimental Values of Occupation Probabilities
v^2 for Neutron States in ^{176}Hf and ^{177}Ta.

Orbital	v^2
$7/2^+[633]\uparrow_n$	.883
$1/2^-[521]\downarrow_n$	.797
$5/2^-[512]\uparrow_n$	.743
$7/2^-[514]\downarrow_n$	.341
$9/2^+[624]\uparrow_n$	.194

2.7 Band Mixing

As mentioned in Section 2.2, the effect of the Coriolis term is to bring about a mixing of two states. The mixed state will, therefore, be a combination of the two unperturbed states, i.e.

$$\psi = C_1 \ \psi_a + C_2.\psi_b \tag{2.7.1}$$

where ψ_a and ψ_b are the unperturbed wavefunctions. The Schrödinger equation for the state is

$$H\psi = E(C_1\psi_a + C_2\psi_b), \tag{2.7.2}$$

E being the Coriolis perturbed energy. This leads to the set of equations

$$C_1(E_a-E) + C_2 H_{ab} = 0$$

$$C_1 H_{ba} + (E_b-E)C_2 = 0 \tag{2.7.3}$$

whose solution requires that

$$\begin{vmatrix} E_a-E & H_{ab} \\ H_{ba} & E_b-E \end{vmatrix} = 0 \tag{2.7.4}$$

The values of E_a and E_b are the unperturbed energies of the states ψ_a and ψ_b, respectively. The Coriolis matrix element $H_{ab} = \langle\psi_a|H'|\psi_b\rangle$ is given by

$$H_{ab} = -\frac{\hbar^2}{2\vartheta} \langle\Omega \pm 1|j_+|\Omega\rangle \ \sqrt{(I\mp K)(I\pm K+1)} \ f(U,V) \tag{2.7.5}$$

where the $f(U,V)$ is a reduction factor due to pairing (F.S. Stephens and R.S. Simon, 1972). The solutions of (2.7.4) are

$$E_{\pm} = \frac{1}{2} \left[(E_a + E_b) \pm (E_a - E_b) [1 + (\frac{2H_{ab}}{E_a - E_b})^2]^{1/2} \right] , \qquad (2.7.6)$$

Substitution into (2.7.3) yields the values of the mixing amplitudes C_1 and C_2.

$$C_{1\pm} = \left[1 + \frac{E_a - E_{\pm}}{H_{ab}} \right]^{-1/2}$$

$$C_{2\pm} = \left(\frac{E_{\pm} - E_a}{H_{ab}} \right) C_{1\pm} \qquad (2.7.7)$$

The importance of band mixing was first emphasized by Kerman (1956) who, with its inclusion produced a dramatic improvement in the rotational model of ^{183}W. A calculation of this effect as applied to ^{176}Ta is given in Section 5.7.

2.8 .Electromagnetic Transition Rates

The possible multipolarities, λ, of transitions between states of angular momentum and parity $|I_i \pi_i\rangle$ and $|I_f \pi_f\rangle$ are governed by the selection rule

$$|I_i - I_f| \leq \lambda \leq I_i + I_f \qquad (2.8.1)$$

and

$$\pi_i \pi_f = (-)^{\lambda} \qquad \text{for an electric } \lambda\text{-pole transition}$$
$$= (-)^{\lambda+1} \qquad \text{for a magnetic } \lambda\text{-pole transition.}$$

The transition probability for the emission of a photon of energy $\hbar\omega$ and angular momentum λ is

$$T(\lambda, I_i \rightarrow I_f) = \frac{8\pi(\lambda+1)}{[\lambda(2\lambda+1)!!]^2} \frac{1}{\hbar} \left(\frac{\omega}{c}\right)^{2\lambda+1} B(\lambda, I_i \rightarrow I_f) \text{ sec.}^{-1} \qquad (2.8.2)$$

where $B(\lambda, I_i \rightarrow I_f)$ is the reduced transition probability and is given by

$$B(\lambda, I_i \rightarrow I_f) = \sum_{\mu M_f} |<I_f M_f|O(\lambda,\mu)|I_i M_i>|^2 . \qquad (2.8.3)$$

The operator connecting the state $|I_i M_i>$ to $|I_f M_f>$ is the μ-component of the electric or magnetic λ-pole transition operator.

An estimate of the transition probability for a single particle model without inclusion of configuration mixing or collective effects was made by Weisskopf (1952). The values of T_{sp} for the lowest multipolarities are given in Table 2.6.

Considering equations (2.8.2) and (2.8.3), transitions between different K-bands connected by the operator $O_{\lambda\mu}$ require the evaluation of the matrix element $<\overline{K_f}|O(\lambda,\mu)|K_i>$. The value of this integral is nonzero provided

$$\Delta K = |K_f - K_i| \leq \lambda \qquad (2.8.4)$$

This gives rise to the so-called K-selection rule governing electromagnetic transitions. This rule is not strictly obeyed to the extent that K is not a good quantum number and so decay can proceed through the admixture of other K values in the wavefunction.

The quantity ν defined as

$$\nu = |K_i - K_f| - \lambda \qquad (2.8.5)$$

Table 2.6

Estimates of single particle transition probabilities E_γ is the energy
of the transition in MeV and A is the mass of the nuclide

Multipolarity	T_{sp}
E1	$1.5 \times 10^{14} A^{2/3} E_\gamma^3$
M1	$3.15 \times 10^{13} E_\gamma^3$
E2	$7.25 \times 10^7 A^{4/3} E_\gamma^5$
M2	$1.2 \times 10^8 A^{2/3} E_\gamma^5$
E3	$1.1 \times 10^2 A^2 E_\gamma^7$
M3	$1.8 \times 10^2 A^{4/3} E_\gamma^7$

is referred to as the degree of K-forbiddeness.   In addition, the
concept of the retardation factor, the ratio of the measured half-life
to the Weisskopf single particle estimate is often used.

$$F_W = T_{1/2}(\text{exp.}) / T_{1/2}(\text{S.P.}) \qquad (2.8.6)$$

And,

$$F_W = (f_W)^\nu \qquad (2.8.7)$$

where f_W is the degree of forbiddeness per unit of ν.   The values of
f_W have been systematically investigated by K.E.G. Löbner (1968).
It is found that the reduced transition probabilities decrease approx-
imately by a factor of 100 per degree of K-forbiddeness.

2.9   Internal Conversion

The de-excitation of a state through electromagnetic transitions
can proceed through one of two ways: emission of a γ-ray or internal
conversion of an orbital electron.   Both can occur in the de-excitation
of a level, the relative contribution being determined by the energy
and multipolarity of the transition.   The latter process occurs when
the atomic electrons orbiting the nucleus are affected by changes in
the nuclear electromagnetic field.   Sufficient energy may be trans-
ferred to the electron to leave the atom, the energy of the converted
electron being

$$E_e = E_\gamma - E_{B.E.} \qquad (2.9.1)$$

where E_γ is the transition energy between the states and $E_{B.E.}$ is the
binding energy of the electron.   Conversion can originate from the

K, L_I, L_{II} etc. atomic orbitals.

Because of the presence of both processes, the rate of de-excitation is the sum of the rate of γ-emission and the rate of electron conversion. The ratio of these two rates is given by the conversion coefficient $\alpha = T_e/T_\gamma$ which increases with the multipolarity and decreases with the energy of the transition.

CHAPTER 3

EXPERIMENTAL TECHNIQUES

3.1 Introduction

·The project which is the subject of this thesis relied heavily on the sophisticated use of apparatus which could isolate those data which were of interest. The task required the use of many different electronics set-ups as well as the use of two laboratory facilities -- McMaster University Tandem Van de Graaff and Michigan State University Cyclotron.

This chapter deals with the various techniques used in carrying out these studies. Where the same basic principle is used in an experiment carried out at McMaster and at Michigan State, only the details of one set-up are given, the analogy being straightforward.

3.2 Production of High Angular Momentum States; (Heavy Ion, xn) Reactions

The use of (Heavy Ion, xn) reactions in nuclear spectroscopy studies has become more and more widespread with the ready availability of numerous heavy ion beams. A review article on the subject of the use of such reactions was published by Newton (1969). The ideas presented in this section are a summary of those presented in the article.

34

To understand the various types of reactions which can occur with heavy ion projectiles, it is simplest to consider three sets of conditions. When the separation between the nuclear surface of the target and projectile is much larger than the extent of the nuclear force, then only the Coulomb force determines the interaction between the bodies. This leads to Rutherford (elastic) scattering or else to Coulomb excitation of the target. As the separation decreases and approaches the limits where nuclear forces come into play, then the possibility arises for inelastic scattering. In addition, particle transfer reactions are feasible in which one or more particles are transferred from projectile to target, or vise versa. In the case of greatest overlap of the nuclear wavefunctions in which the nuclei "collide", then the possibility arises for the formation of a compound nucleus system.

A (Heavy Ion, xn) reaction can be classified as the type of reaction where the incoming projectile forms a compound nucleus with the target and then proceeds to evaporate several neutrons or charged particles. It is because of the fact that the heavy ion projectile can, because of its mass bring high values of orbital angular momentum into the two-nucleus system that it is valuable in the study of high spin states in nuclei. For example, a 54 MeV ^{11}B projectile can, after allowing for Coulomb effects, bring in as much as ℓ_{max} = 24 to the compound system.

The strength of the Coulomb barrier has a great effect on the type of reaction that will occur. Since light nuclei have small Coulomb barriers, charged particles such as protons and alphas can be emitted in addition to neutrons. However, in the case of heavier nuclei where the Coulomb barrier is much stronger, charged particle emission is strongly inhibited, and neutron evaporation is the basic mode of decay. An illustration of the reaction mechanism for this mode of decay is given in Figure 3.1.

In the illustration shown, a compound nucleus (A,Z) is formed at an excitation energy of about 25 MeV. Since the average binding energy of a neutron is of the order of 8 MeV, a neutron is easily boiled off to form the nucleus (A-1,Z) with a lower excitation energy. The average energy of an evaporated neutron is only about 2 MeV and so the system is unstable to neutron emission to (A-2,Z). Once this nucleus is formed, however, most of the states may be stable to neutron emission and thus decay to the ground state via γ-emission instead. It is, therefore, expected that the reaction will mainly produce the nucleus (A-2,Z) with small admixtures of the nuclei (A-1,Z) and (A-3,Z).

This reaction mechanism makes the choice of appropriate projectile energy very important. In the case illustrated in Figure 3.1, if the compound nucleus had been formed at an energy of about 33 MeV instead, then it would have been possible to make mainly the nucleus (A-3,Z) instead. This is a highly useful tool since selection of a

Figure 3.1

An illustration of the reaction mechanism
of an (α, xn) reaction.
(Reproduced from Newton et al, 1967).
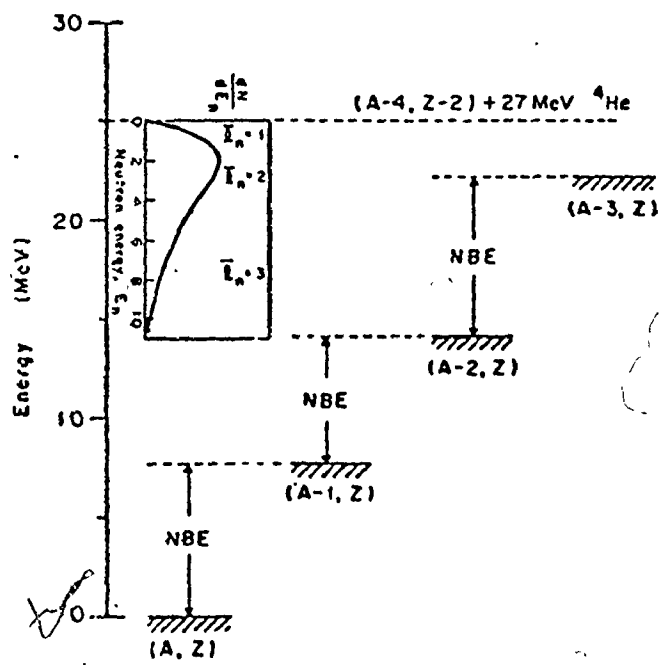
Ground state locations

final nucleus is possible. Computer calculated excitation functions for the reactions $^{170}Er(^{11}B,xn)$ and $^{174}Yb(^{7}Li,xn)$ are given in Figure 3.2(a) and (b) respectively. Unfortunately, because of the width of the neutron spectrum, more of the nuclei on either side of the desired final nucleus would be made as the number of evaporated neutrons increase. Hence, the close overlap of successive peaks.

Although decay through γ-ray emission is always a possibility, it is not normally competitive with particle emission until the nucleus is about one neutron binding energy above the yrast line. Figure 3.3 illustrates the two basic types of γ-decay. In the figure, excitation energy is plotted versus angular momentum. For a given angular momentum, I, the state of lowest energy in a nucleus is called the yrast state. Of course, the decay of an excited state is not limited to only one "path" of transitions because of the proximity of several states to the yrast line. Any of these closely situated states can at some time take part in the de-excitation. It is, therefore, more appropriate to consider the decay as a cascade near the yrast band.

Well above the yrast band the high level density gives rise to electric dipole transitions which carry off about half the excitation energy but very little angular momentum. This type of decay continues until a region is reached where the level density is no longer high. This region is located just above the yrast line. At this point the decay will enter a cascade from one yrast level to the next, a larger amount of angular momentum being carried off, and the spectrum will then be decidedly different from the evaporation spectrum above. On the

Figure 3.2

Computer calculated excitation functions for
the reactions
a) $^{170}Er("B,xn)$ and
b) $^{174}Yb(^{7}Li,xn)$.

^{7}Li on ^{174}Yb
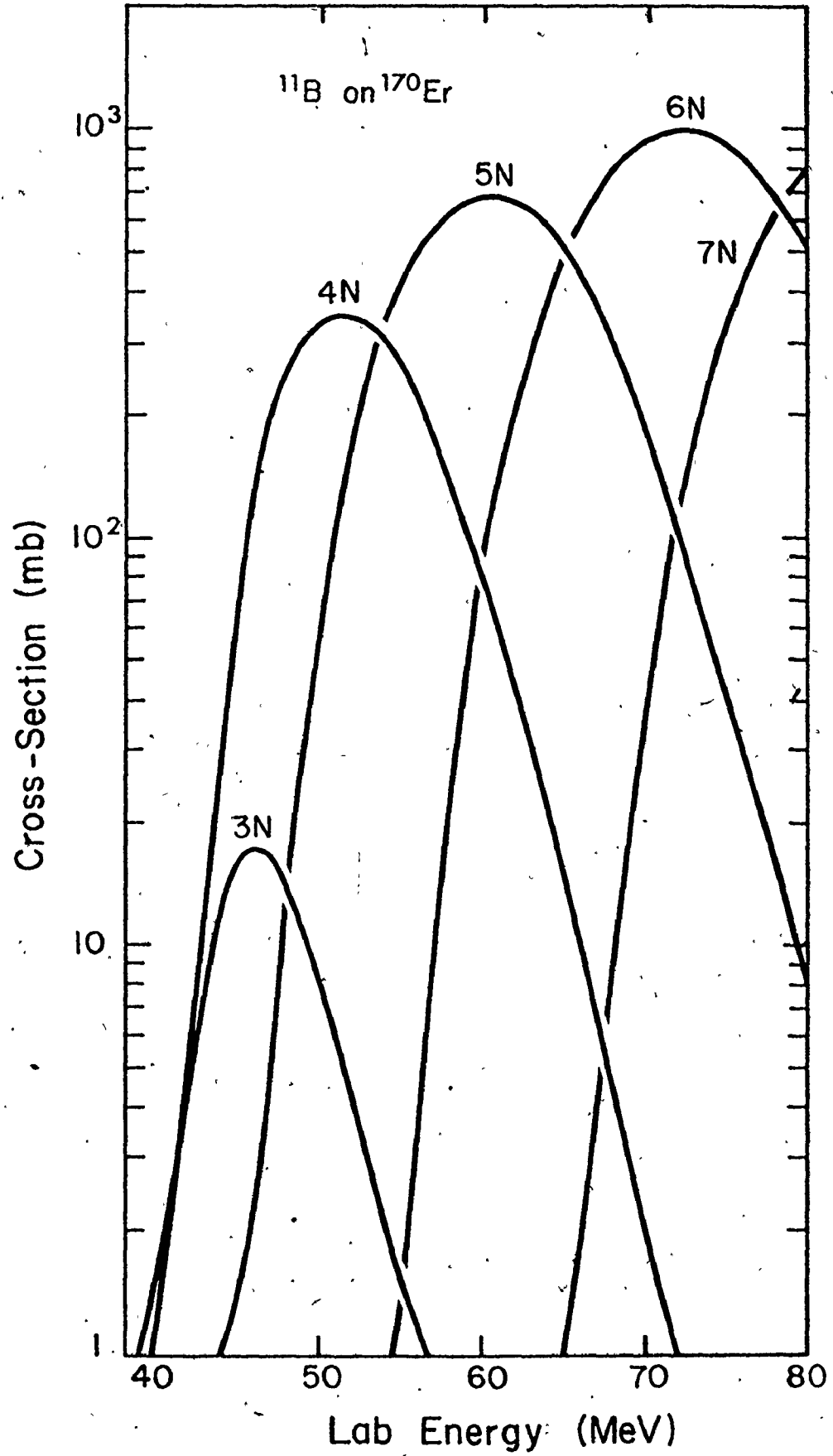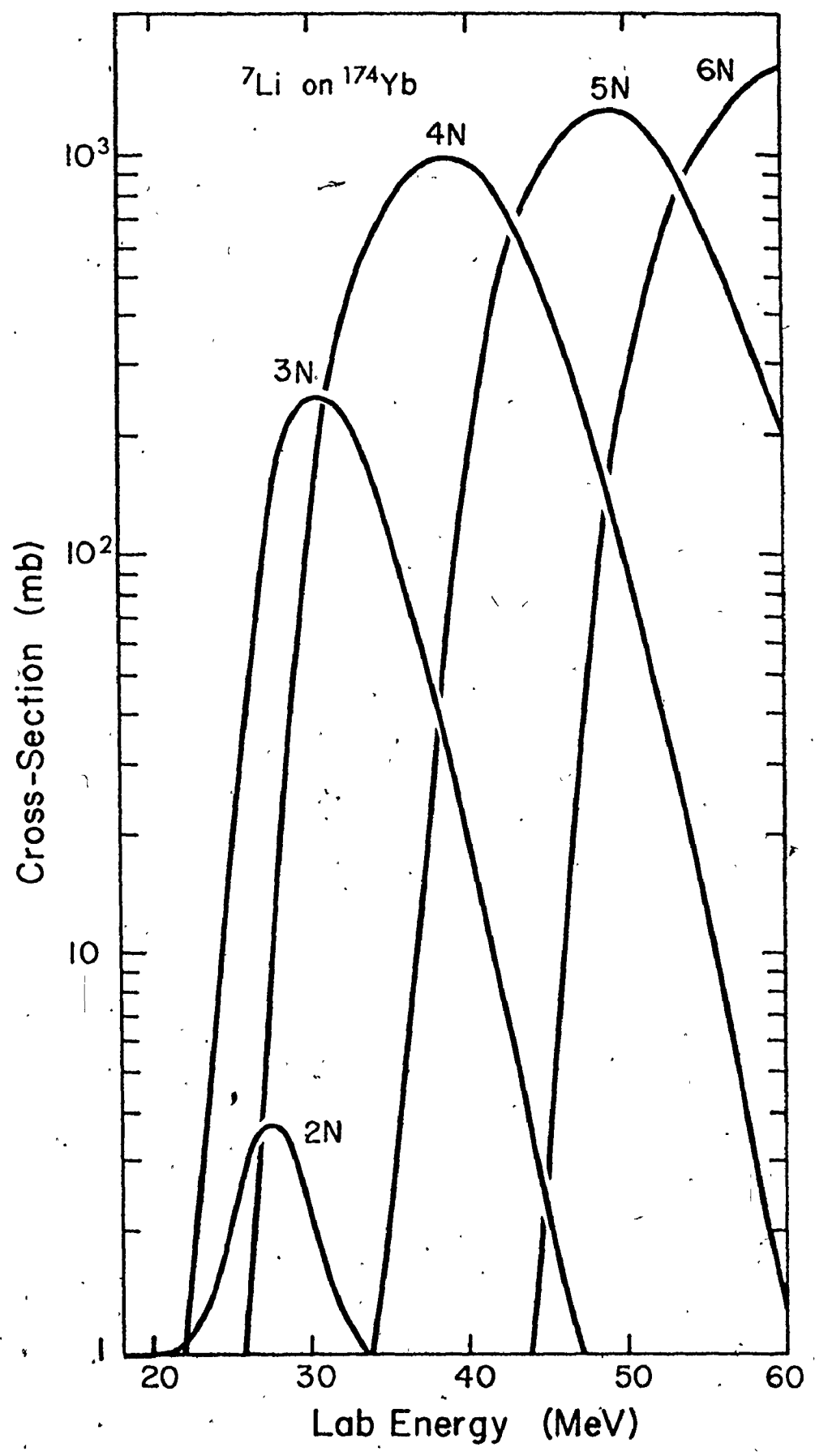
Figure 3.3

Figure illustrating the energy levels plotted

versus angular momenta in a nucleus of mass

$\sim$ 160 populated by an (^{40}Ar,4n) reaction.

(Reproduced from Stephens et al, 1972).

Figure: Plot of Excitation energy (MeV) versus I for $A \sim 160$, showing yrast levels, ground state band (gsb), quasi-particle states, statistical cascade, yrast cascade, and population following $^{40}Ar, 4n$. Region marked "No levels."
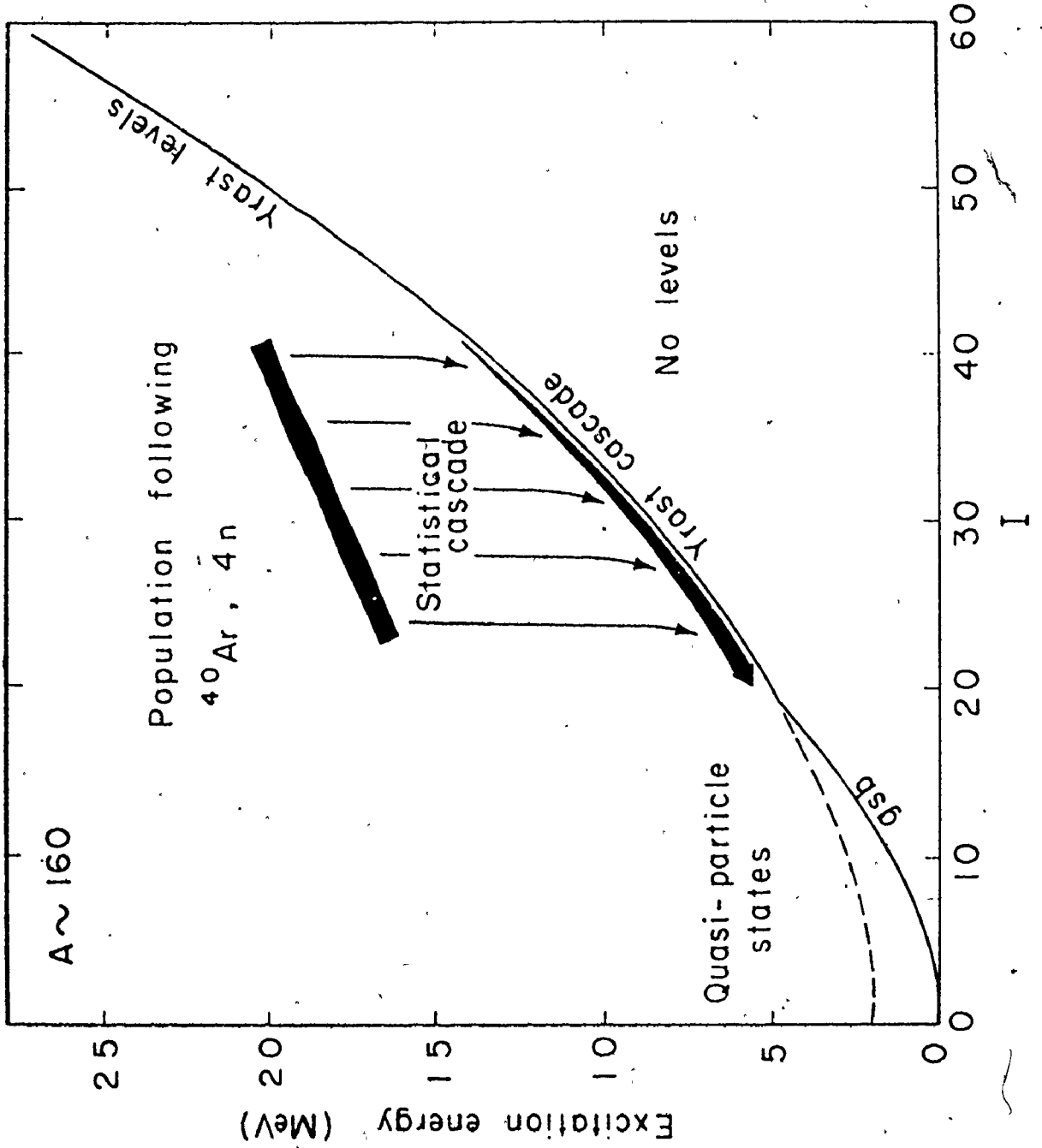
average, the energy of a transition will be lower. Also, an yrast level, unlike the high-density levels above, will collect a sizable proportion of the γ-rays cascading from states with angular momentum higher than its own. The larger amount of angular momentum being carried off with each step is seen by the presence of quadrupole transitions. The main problem in studying the decay of states thus populated by (Heavy Ion, xn) reactions is the masking brought about by the continuum γ-rays. One must be able to distinguish the transitions of interest from the transitions in the high density region.

3.3 Beam Transport Systems

3.3.1 McMaster University Tandem Van de Graaff Facilities

A general schematic of the beam transport system is given in Figure 3.4. Positive ions are produced in the duoplasmatron and are accelerated to an energy of ∿ 40 keV. They are subsequently passed through an adder gas in which ≃ 1% of the ions are converted to negative ions through the pick-up of two electrons. In the case of the triconex source the production of negative ions is more direct. Positive cesium ions produced in a cesium boiler knock atoms of the required projectile from a cone. These atoms become negatively charged while passing through a cesium coating on the cone. An inflection magnet then directs the desired negative ions into the accelerator where they are attracted to the positive terminal. This first phase of acceleration produces ions of energy eV; where V is the positive terminal voltage. Once the ions have arrived at the

Figure 3.4

A general schematic of the beam transport
system at the McMaster University Tandem
Van de Graaff facilities.
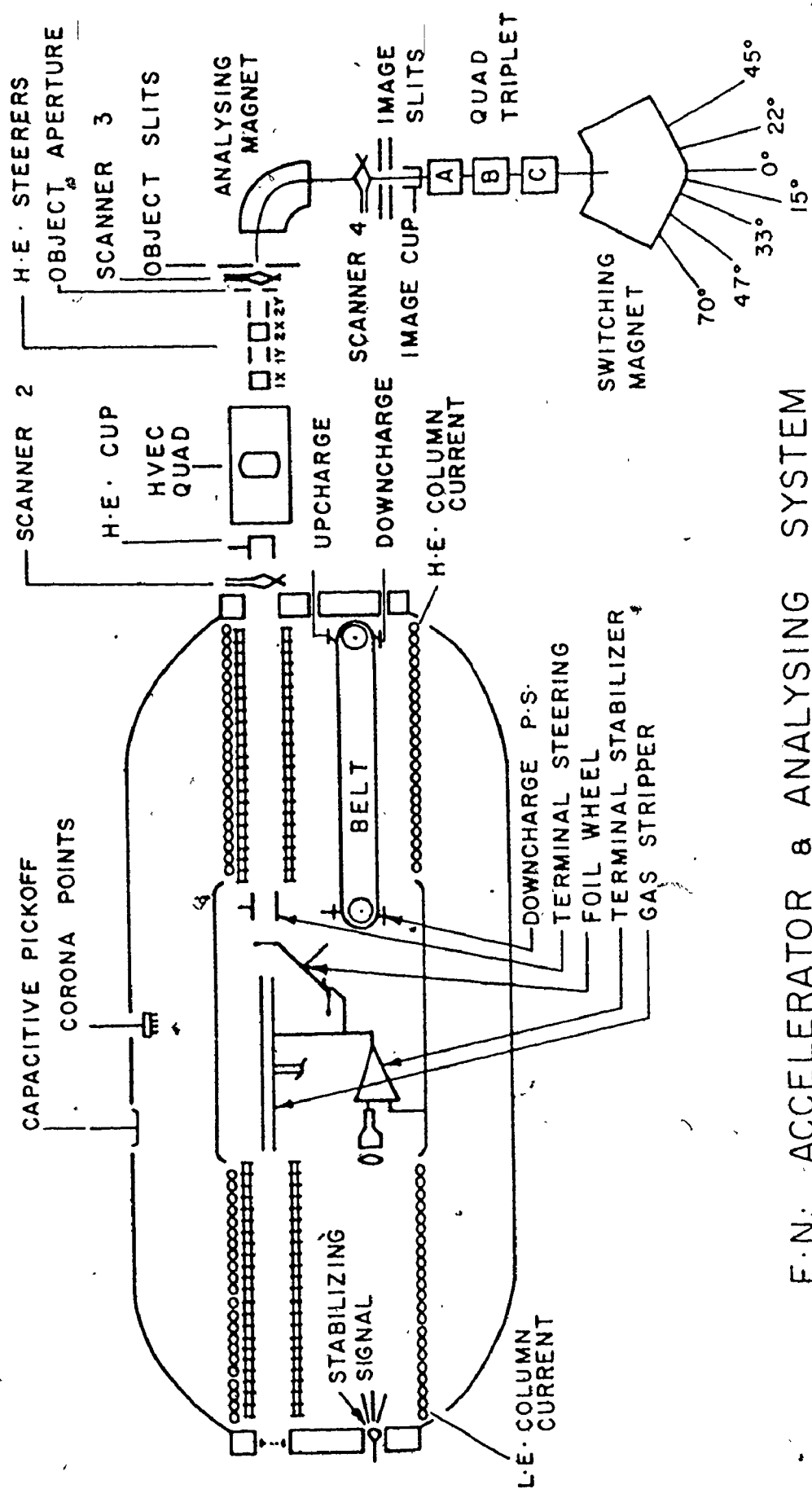
F·N· ACCELERATOR & ANALYSING SYSTEM

terminal they are passed through a gas or foil stripper which will remove   electrons from the ions. This newly acquired positive charge will now repel the ions from the positive terminal down to the ground end of the machine. The acceleration of the now positive ions through the second stage of the machine will now add an energy (ne)V, assuming +ne is the charge on the positive ions. Upon leaving the machine the beam is then focussed through the use of quadrupole magnets. An analyzing dipole magnet ensures that the beam will be of the chosen energy, all but the chosen beam being directed away from the path leading into the further stages of the system. Again, quadrupole magnets focus the beam. The various target stations are situated at different angles to the beam line at this stage. A switching magnet is then set to send the beam down to the required target area.

3.3.2 Michigan State University Cyclotron Facilities

Michigan State University houses a conventional cyclotron fed by an internal rf source of positive ions. The cyclotron basically consists of a vacuum chamber containing two semicircular electrodes coupled by an rf power source such that the dees form the high voltage end of a quarter-wave line. The chamber is placed between the pole faces of an electromagnet such that the dees are perpendicular to the uniform external magnetic field. Typical magnet strength is of the order of 15 kgauss. Ions produced at the ion source located at the

centre of the dees are acted upon by the rf field coupling the dees as well as the external magnetic field. The rf field accelerates the positive ions across the dee gap while the external perpendicular field guides the ions in circular orbits. The acceleration across the gap, and hence increase in velocity, causes the ions to move in orbits of ever increasing radii. To achieve proper phasing the external magnetic field is adjusted so that the angular velocity of the ions is equal to the angular velocity of the rf power coupling the dees. Upon reaching the edge of the magnetic field, the ions are deflected by a negatively charged deflection plate and pass through a window to the rest of the beam transport system as given in Figure 3.5. The usual system of quadrupole and dipole magnets follows for beam focusing and steering. The use of two analyzing magnets instead of the customary one, makes this facility particularly favourable for studies demanding high resolution.

3.4 Target Preparation and Choice of Beam Intensity

The target thicknesses which were chosen were a result of two basic considerations. An increase in the thickness of the target would, of course, lead to an increase in the intensity of desirable γ-rays from the target. However, a thick target produces a degradation of beam energy within the target and hence has undesirable features as well. To make up for the undesired thickness effects, one could use a thin target with a large beam current. Large beam currents

Figure 3.5

A general schematic of the beam transport
system at the Michigan State University
Cyclotron facilities.
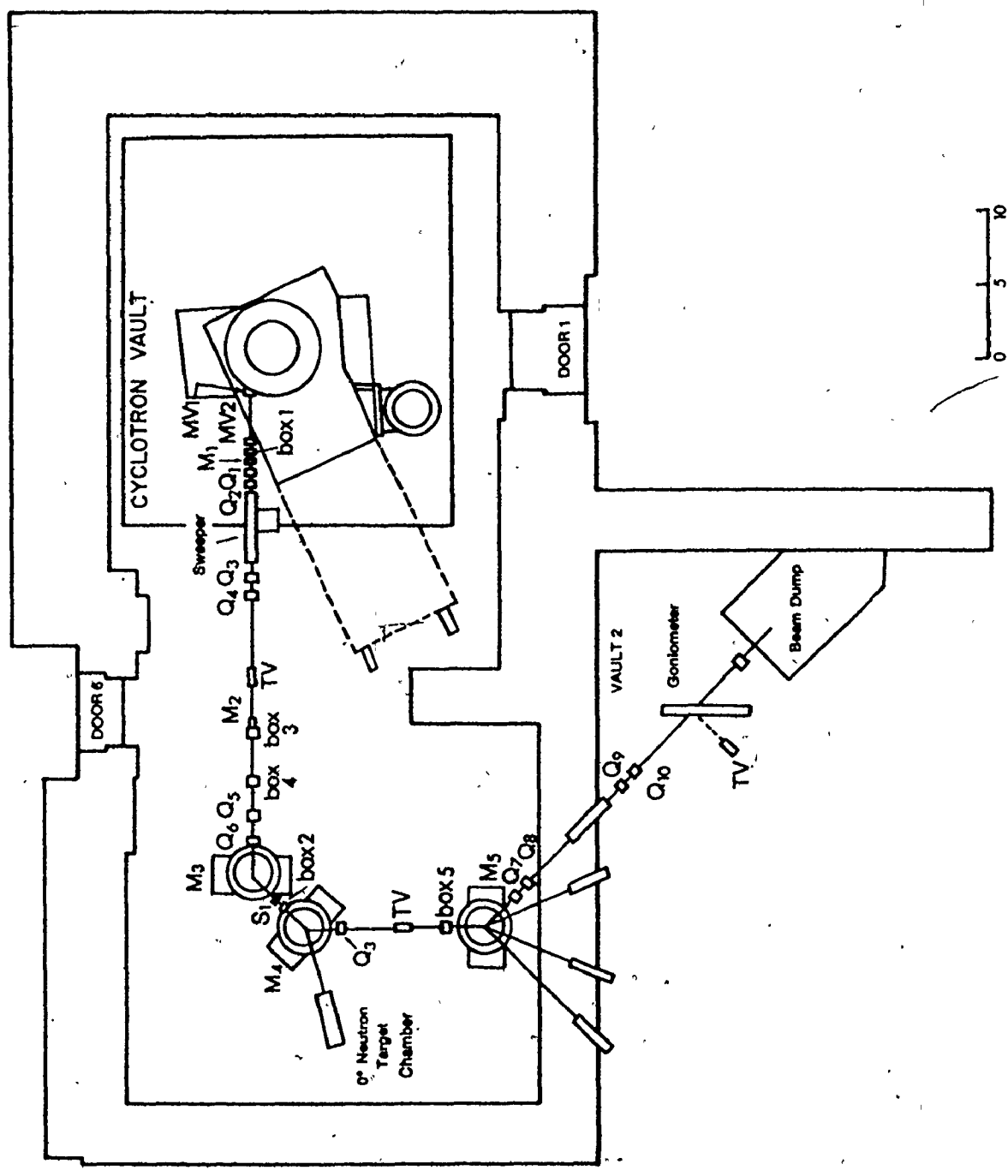
should be avoided, however, because of the production of beam induced background radiation which could mask the gamma rays of interest. The choice is a trade-off of the above considerations. The target thicknesses used in the case of ^{173}Yb, ^{170}Er and ^{176}Lu were 3.3 mg/cm^2, 8.5 mg/cm^2 and 3.0 mg/cm^2, respectively. The beam currents used were of the order of a fraction of a nanoamp (.1 → .3) for the coincidence experiments and about 10 to 20 nanoamps for direct singles measurements.

3.4.1 ^{170}Er, ^{173}Yb

Target material was obtained in powder oxide form from the Isotope Sales Division of the Oak Ridge National Laboratory. The relative isotope abundances are listed in Table 3.1. Because of the nature of lutetium metal, its preparation will be treated later.

Targets of ^{173}Yb and ^{170}Er were prepared in the normal procedure. A mixture of the oxide of interest was mixed with some lanthanum or thorium and placed in a tantalum crucible. An electron gun (maximum temperature 2000°C) was used to reduce and evaporate the desired metal onto tantalum metal strips. The accumulated metal was peeled off and rolled to the desired thickness.

3.4.2 ^{176}Lu

The difficulty in preparing the lutetium target arose from the high temperature (2200-2300°C) required to properly reduce the oxide/ thorium mixture. Figure 3.6A illustrates the normal procedure for the

Table 3.1

Relative Isotopic Abundance of Target Materials

Mass Number	Erbium	Ytterbium	Lutetium
162	0.02		
164	0.04		
166	0.87		
167	0.72		
168	1.46	<0.02	
170	96.89	0.05	
171		0.3	
172		1.41	
173		95.0	
174		2.89	
175			25.5
176		0.34	74.5

Figure 3.6

An illustration of target making techniques
showing (A) the normal procedure for the
evaporation of target metal onto metal strips,
(B) the difficulty of heating rare earth metals
within a conventional crucible, (C) crucible -
within -crucible method which was devised to
overcome the problem.

A.

Plug

Electron
Bombardment

Tantalum
Crucible

Oxide & Reductant
Mixture

B.

C.
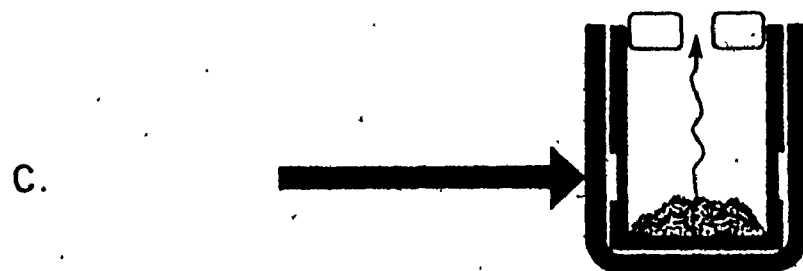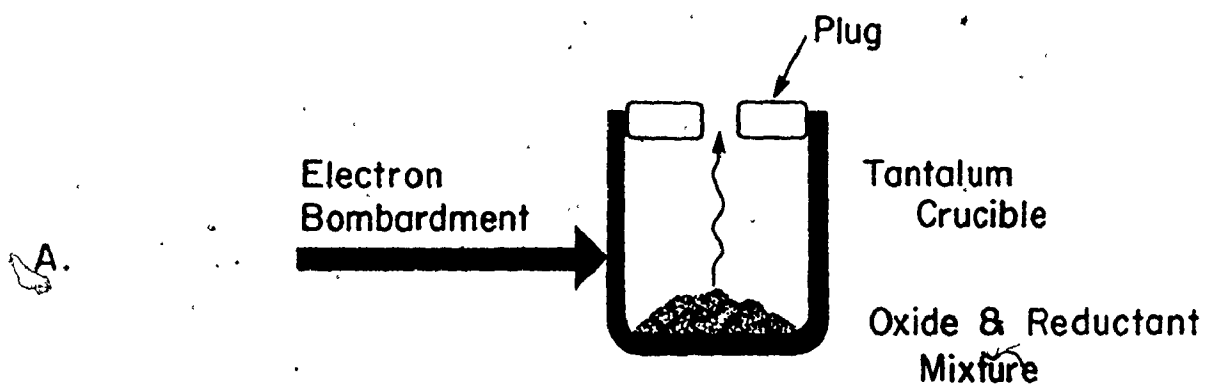
evaporation of the metal onto metal strips. Rare earth metals readily form alloys with tantalum at high temperatures, unfortunately, since high temperatures were required to reduce the oxide, a difficulty arose. Figure 3.6B shows the problem with using the standard electron gun. Since its beam is concentrated at basically one spot, the heating of the crucible is highly non-uniform and the spot being heated now at an extremely high temperature, will turn into an alloy leading to the collapse of the wall of the crucible. Once the wall is perforated, the metal can spurt out the sides instead of onto metal strips as required. The expensive nature of the lutetium oxide makes this highly undesirable.

A crucible-within-a-crucible method was finally devised by Dr. Y. Peng and is illustrated in Figure 3.6C. Two tantalum crucibles were fitted, one inside the other. The inner crucible's outside wall has a groove bored around its circumference towards the bottom. If the electron beam should penetrate the wall of the outside crucible, the inner crucible would still be intact. In addition, the indentation of the inner crucible wall makes more uniform heating possible and, therefore, provides a second benefit.

3.5 Experimental Facilities in Target Areas

3.5.1 Gamma Studies

3.5.1i McMaster University

One of the experimental arrangements used at McMaster for γ-ray measurements is illustrated in Figure 3.7. The Orange Beta Spectrometer line (33°) was used because of its advantageous low background

Figure 3.7

Target chamber arrangement for γ-ray measurements
using Orange Beta Spectrometer line (33°) at
McMaster University Tandem Accelerator
facilities.

51

SCALE: 3/4

TARGET

TARGET FRAME

AL TARGET HOLDER

Beam Direction

LUCITE

TANTALUM

$\phi = .280''$

STAINLESS STEEL
TARGET POSITION

$\frac{1}{32}''$

$\frac{3}{4}''$
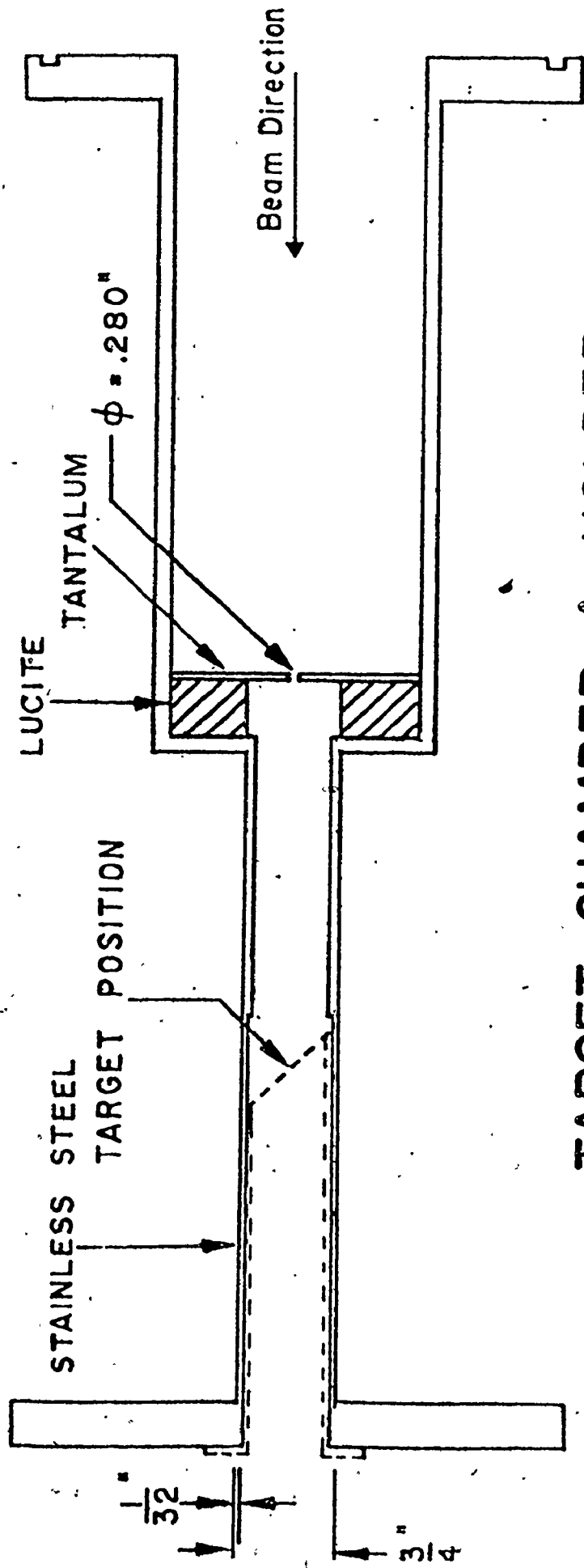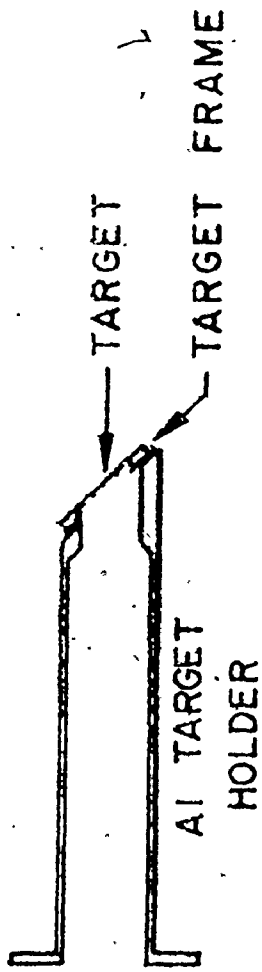
TARGET CHAMBER & HOLDER

properties (see T.L. Khoo Ph.D. thesis, McMaster, 1972). A section of the beam pipe in front of the faraday cup was replaced by a section designed for γ-ray studies. The thin foil targets were mounted on lead frames, attached to the target holder, and oriented at 45° to the beam direction. The detector was placed at 90° to the beam direction. To reduce the number of background γ-rays, a lead toroid was placed around the target chamber, just before the target position. Because of the high rate of X-ray production which would be processed by the Ge(Li) detector and lead to large dead time problems, absorbers were placed in front of the detector faces to attenuate undesirable counts from background. These absorbers took the form of a copper shield or else a cadmium/copper graded shield.

For the γ-γ coincidence experiments, two Ge(Li) detectors were placed facing each other, at 90° to the beam direction. A view of the set-up as seen from above is shown below.

BEAM

DET #1

DET #2

TARGET

TARGET CHAMBER
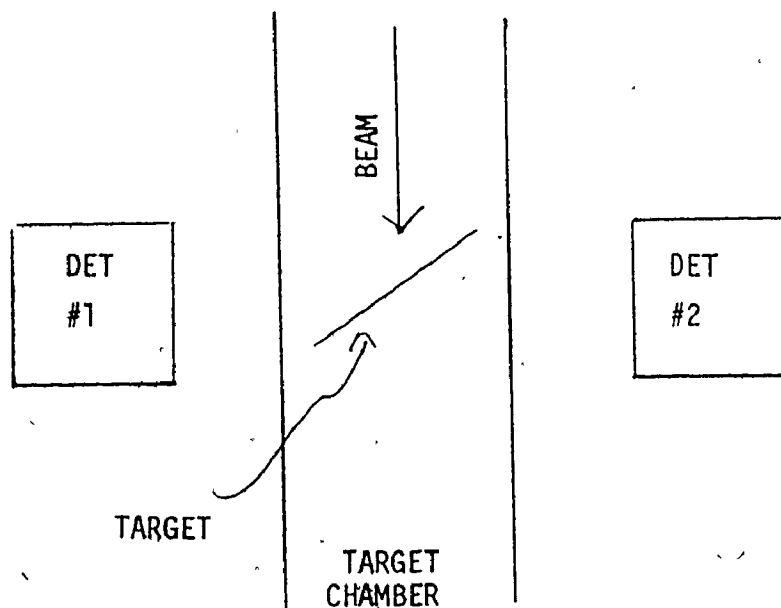
In order to maximize counting statistics, the detectors were placed with their faces as close together as physical dimensions would permit. The above arrangement, unfortunately, does have the disadvantage of enhancing electron-position annihilation events (511 keV) which are emitted at 180° to each other. A lead shield was therefore placed straddling on the top and the bottom of the chamber to partly reduce scattering from one detector to the other.

3.5.1ii Michigan State University

Gamma ray experiments were carried out on the goniometer beam line. Figure 3.8 illustrates a side view of the chamber used in γ-γ coincidence experiments. The width across the chamber is approximately 3.8 cm with a plane of symmetry through the middle. The self-supporting rolled target was placed on an aluminum target holder suspended by an aluminum rod. The positioning of the target with respect to the beam line and the use of absorbers was similar to the case already considered for experiments carried out at McMaster. Once positioned, the two detector faces were approximately two inches from the target.

Figure 3.9 gives a schematic of the γ-angular distribution chamber. A mylar window is inserted into the side of the aluminum chamber so as to make viewing possible between the angles 60° and 159° to the beam direction. A self-supporting rolled target was placed on an aluminum frame, positioned 45° to the beam direction. The Ge (Li) detector face was placed at a radial distance from the

Figure 3.8

Side view of the target chamber used in
γ-γ coincidence experiments at Michigan
State University Cyclotron facilities.

TO CYCLOTRON

TARGET

EXTENSION

TO BEAM DUMP

TV CAMERA PORT

GONIOMETER ARM

Figure 3.9

Top and side views of the target chamber used

in γ-angular distribution experiments at

Michigan State University Cyclotron facilities.

2.865"

target

Window

Ge(Li)

Beam

4.812"

2.50"

target

4.00"

2.00"

Beam

5.00"
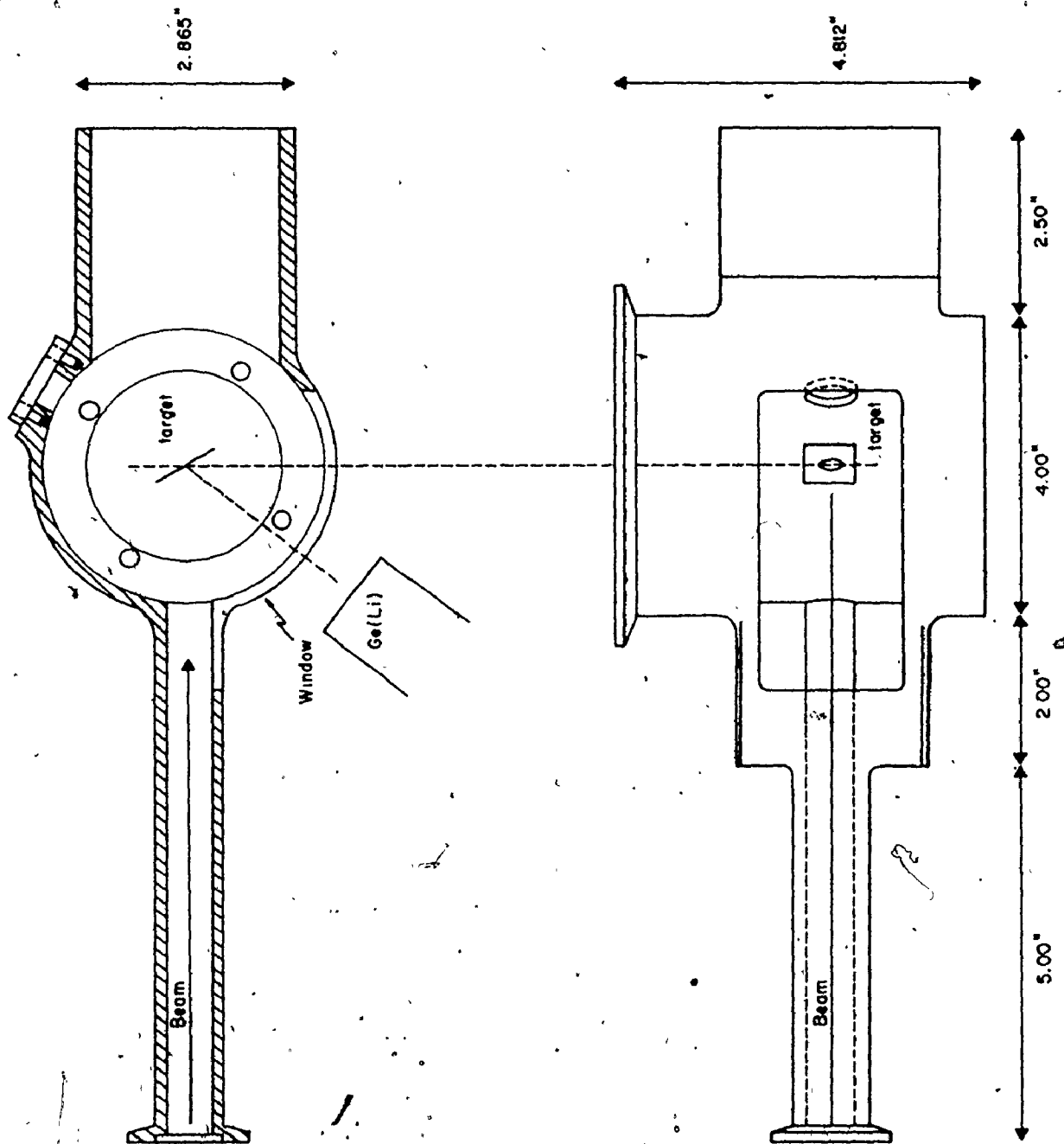
target sufficiently far   that a problem would not arise from
the contribution of too large an angular spread.

3.5.2 Conversion Electron Facilities at Michigan State University

The basic assembly of the MSU electron spectrometer is
depicted in Figure 3.10. Electrons travel from the target chamber,
around a Pb γ-ray shield and through a set of helical anti-positron
vanes. A double-focussing solenoid provides momentum selection. The
anti-positron vanes, which form a helix around the axis of the magnet
coil, were installed to prevent unwanted counts from positrons which,
because of their positive charge, spiral in a direction opposite
to that of the electrons.

A high resolution Si(Li) detector is used for electron energy
determination. The Si(Li) is 3 mm deep with an active area of 80 mm^2.
Resolution was warranted for 2.5 keV at 975 keV. The detector is
mounted on a 3/8" diameter cold finger and enclosed in a right-angle
cryostat. The cryostat vacuum is isolated by a 1/4 mil aluminized
mylar foil. A 2" gate valve and sliding seal arrangement was con-
structed to permit the experimenter to change targets without breaking
the thin mylar window or warming the detector. Targets are typically
1-3 mg/cm^2 thick. The arrangement also allows operation without the
mylar window, should better resolution for low-energy transitions be
required.

Figure 3.10

The basic assembly of the Michigan State
University electron spectrometer showing
the helical anti-positron vanes and
sliding seal arrangment.

Ge(Li)

57

Beam
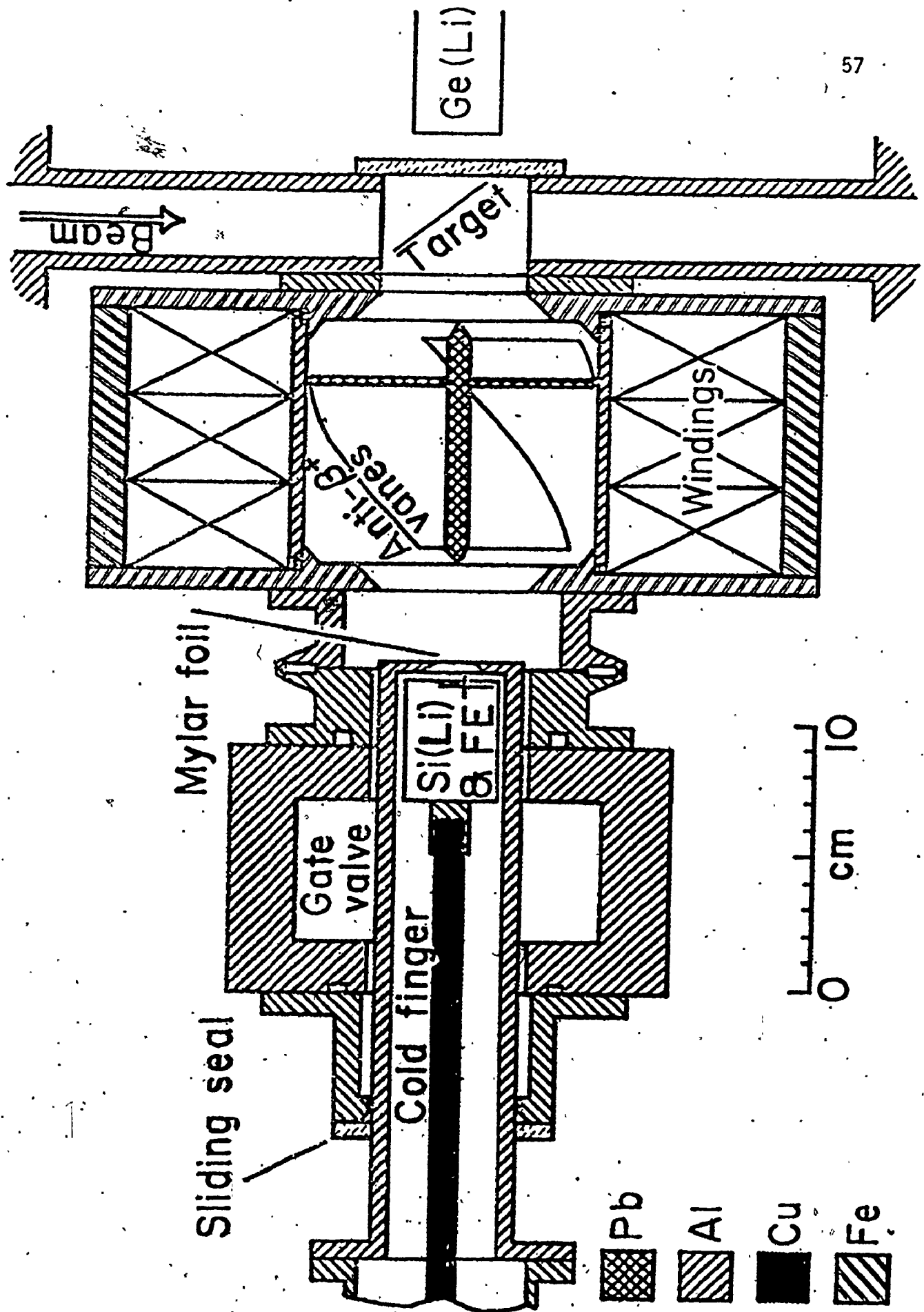
Target

Anti-β vanes

Windings

Mylar foil

Si(Li) & FE

Gate valve

Cold finger

Sliding seal

0   cm   10

Pb

Al

Cu

Fe

In order to allow a range of electron energies to enter the detector, the magnet current is swept with a triangular waveform of period about 100 seconds. This current supply is capable of providing a stable regulated current of up to 200 amperes.

A Ge(Li) detector is positioned facing the electron spectrometer at 45° to the target to accept the corresponding γ-radiation. The electron and γ-radiation are collected simultaneously.

A more detailed explanation of the operation of the spectrómeter can be found in a report by L.L. Kneisel (1975, Michigan State University, M.Sc. thesis).

3.6 Detectors

The following Ge(Li) detectors were used for γ-ray measurements:

Detector	Resolution
10 cc (planar)	1.2 keV at 122 keV
17%	2.9 keV at 1333 keV
ND 10%	2.1 keV at 937 keV
EDAX 8%	2.7 keV at 937 keV
65 cc	2.9 keV at 618 keV

The decision as to which detector should be used depends on the energy range of interest. The smaller volume detector, although of very low efficiency for higher energy gammas, nonetheless has much better resolution in the low energy range and should, therefore, be used when investigating low energy lines. Conversely, if the interest is in higher energy lines, a detector of larger volume should

be used. Typically, a 1 cc detector is appropriate for gammas
below ∿ 500 keV while a 17% is appropriate for investigation in
the 1 MeV range.

Energy calibration is accomplished by collecting γ
events from standard IAEA and TRC sources either in or out of beam.
If calibration is done separately, care should be taken to limit
source intensities to values that produce dead times within the
detector of approximately the same length as during the actual
experiment. A much larger counting rate could produce a gain·shift
that would upset the channel/energy correspondence as compared to
that obtained during the experiment. The channel/energy correspondence
is calculated by fitting the known γ-energies of the standard sources
and the corresponding peak positions to a polynomial.

$$\text{Energy} = a + bx + cx^2 + dx^3 \qquad (3.6.1)$$

where x gives the channel number. The ADC's used were found to be
quite linear so that only two terms were required for calibration
purposes. Having established the calibration function, it is then a
simple matter to calculate energies of unknown γ-ray peaks in the
spectrum collected.

Since the intensities of the peaks are of vital importance, one
must correct for the efficiency of the Ge(Li) detector used. Here
again standard sources as well as a ^{152}Eu source were used which emit
γ-rays whose relative intensities are accurately known. Care should
be taken when doing the calibration that the original set-up of the

experiment be exactly duplicated or else compensated for later since target chamber walls etc. absorb photon radiation and must be considered. A typical efficiency correction curve, in this case for the 65 cc, is given in Figure 3.11. It should be noted that efficiency curves should be recorded often because of the deterioration of detectors with age.

3.7 Beam Pulsing Systems

3.7.1 Michigan State University Cyclotron rf Beam Sweeper

The pulsed nature of a cyclotron beam makes it ideal for studying isomers whose half-lives are < 50 ns -- the time between beam bursts being typically 46-70 ns. However, in order to use such a beam to measure longer half-lives, it is necessary to lengthen the period between beam bursts. In order to do this, a beam pulser has been constructed to sweep the beam off for the required interval.

A method to accomplish this is to intercept the beam by deflecting it with an electric field across a pair of slits. The deflection plates constructed are 1 meter long and 25 mm apart and are illustrated in Figure 3.12.

The sweeper itself is an amplitude stabilized rf amplifier at a submultiple of the cyclotron frequency. A sinusoidal voltage of 13-26 kV is applied to the deflection plates located between quadrupoles 2 and 3. The phase of the applied voltage is adjusted

Figure 3.11

An efficiency correction curve for the 65 cc

Ge(Li) detector used at McMaster University

Tandem facilities.

65cc Ge(Li)

Relative Efficiency

Energy (keV)
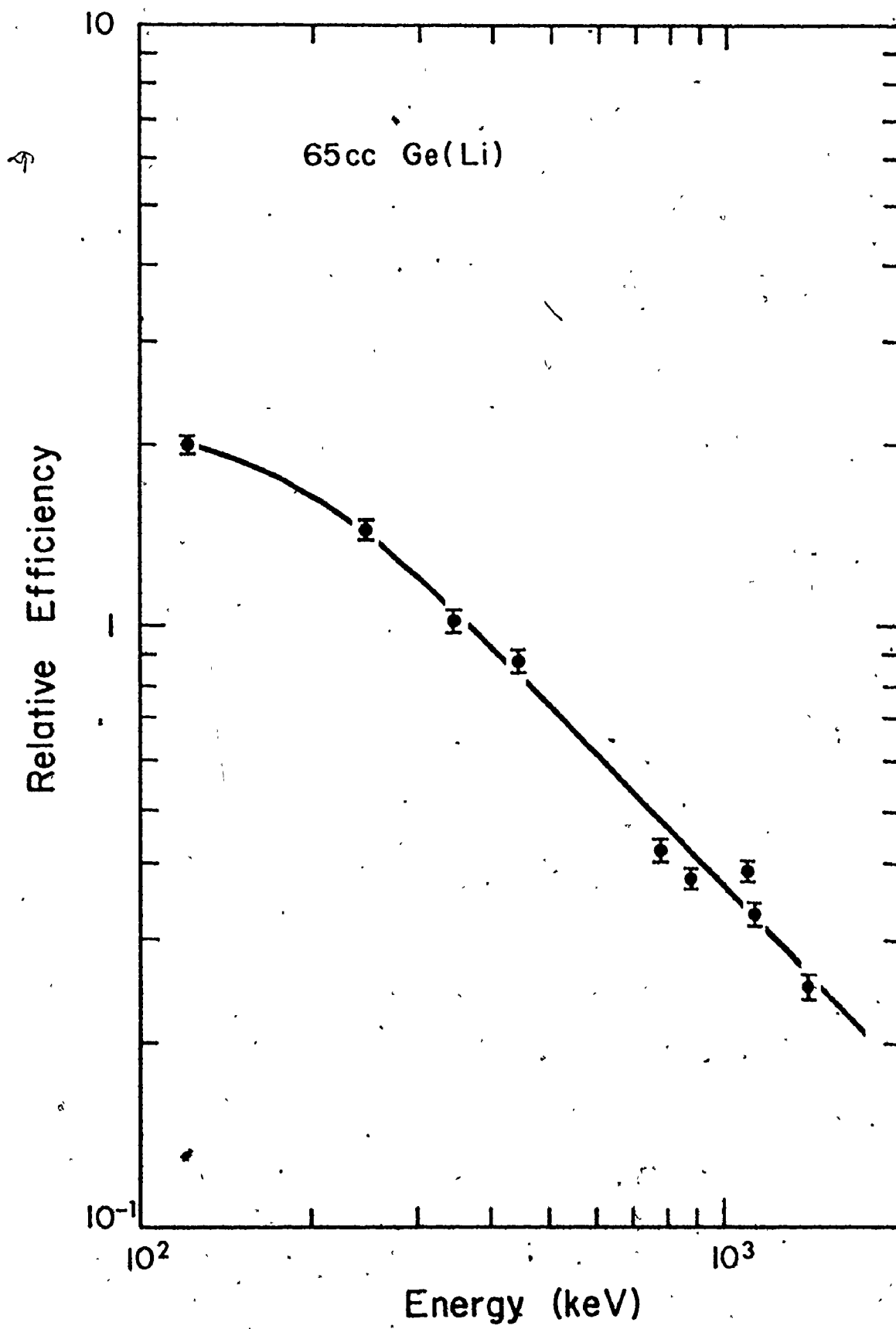
Figure 3.12

An illustration of the beam deflection plates

used in the Michigan State University beam

sweeping system.

Slits

25 mm

V

1 m
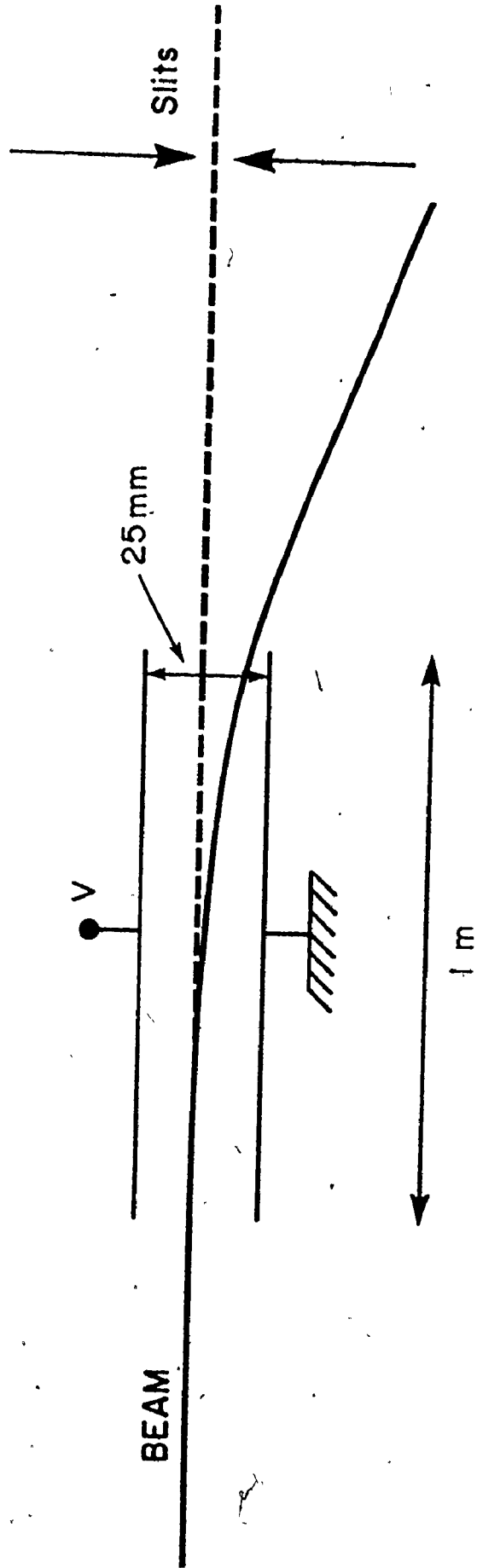
BEAM

so that unwanted pulses are swept onto a pair of slits located downstream. The beam sweeping system, then, permits one of "n" beam bursts to be accepted. At the maximum cyclotron frequency, the system has been used successfully with "n" values up to 9 with particles as energetic as 48 MeV α's.

3.7.2 McMaster University Van de Graaff Beam Pulser

The beam pulsing for the McMaster Van de Graaff is also accomplished through deflection with an electric field. The system is somewhat simpler since the Van de Graaff is a continuous beam machine. The deflecting plates in this case are actually a pair of the low energy steerers which are driven by a voltage supply set at 600 volts. The on-off periods are provided by a reference pulser which governs the voltage on the plates. The length and time between positive pulses from the reference pulser are adjusted to correspond to the beam pulsing rate required. The pulser pattern below would yield an on-off ratio of 40 µs/100 µs.

100 µs

40 µs
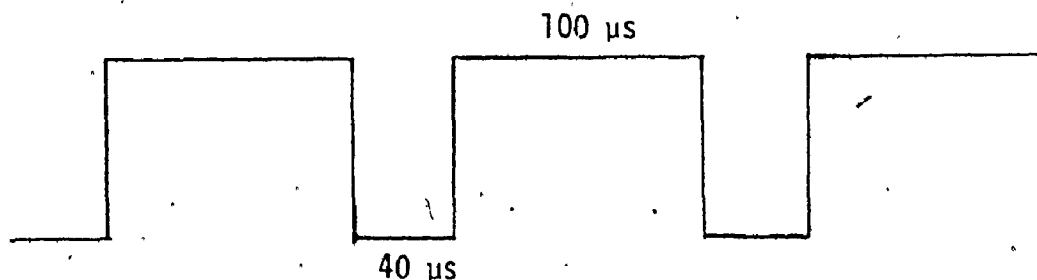
Because the beam pulsing apparatus is situated a certain distance before the target itself, there is a time lag between the signal from the reference pulser turning the beam off and the

actual stopping of the beam at the position of the target. The time
lag is of the order of 5 μs. It is necessary to take into account
this time lag when designing an experiment.

3.8 Prompt Gamma Studies

3.8.li Singles

Pulses from a Ge(Li) detector were amplified by commercial
FET preamplifiers and linear spectroscopy amplifiers (eg. Tennelec
TC203 or TC205). The gain on the amplifier was set so as to
contain the full range of energies of interest within the maximum
pulse height acceptable by the ADC's input. A 2 μs time constant
for the linear amplifier is used with most Ge(Li)'s.

The pulses were fed to a computer (PDP-9 at McMaster
or Xerox Sigma 7 at Michigan State) interfaced to the ADC's.
Programmes used for data acquisition were POLYPHEMUS (Michigan
State University Cyclotron Program Library) and ADCS (McMaster
University Tandem Accelerator Programme Library). The data collected
were transferred onto magnetic tape or dectape for further analysis.

Peak area extractions, energy calibrations and other
peak analysis were carried out either using the programme SOFT
on the PDP-15 computer or else the programme JAGSPLOT on the CDC-6400.
Comprehensive write-ups for these programmes can be found in the
Tandem Accelerator Laboratory Programme Documentation Library for
the former and a report by W.B. Cook (Cook, W.B., 1972. McMaster
University, Ph.D. thesis) for the latter. A very simple peak area

analysis was carried out in the case of SOFT. The first and last channels containing the desired peak were defined as well as a background determined by chosen points on either side of the peak. The areas were derived simply by calculating the total number of events within the range defined by the two channels and subtracting the appropriate amount of background. No fitting was carried out.

The peak analysis programme JAGSPLOT is more sophisticated in that it performs a least squares fit to the peak shape which is a convolution of a decaying exponential curve (tail) and a Gaussian curve. The mathematical representation is as follows:

$$I(x) = \alpha + \beta x + \sum_{j=1}^{N} \gamma_j \int_{-\infty}^{x_{pj}} e^{\varepsilon(y-x_{pj})} e^{-\delta(x_{pj}-y)^2} \, dy \qquad (3.8.1)$$

where

x = channel number

$I(x)$ = counts in channel x

N = number of peaks in window ($N \leq 6$)

$\alpha + \beta x$ = linear background

γ_j = intensity of the Gaussian located at x_{pj}

ε = constant determining the exponential fall-off of the Gaussian intensity

x_{pj} = peak position of Gaussian in peak j

$\delta = \dfrac{1}{2\sigma^2}$ of normal Gaussian distribution.

A number of regions are chosen from the spectrum to be analyzed. Initial values for the background parameters α and β and for the Gaussian intensity γ_j are calculated from the data. Starting values of δ and ϵ are supplied by the programme. A non-linear least-squares fit to the data, in which all the parameters may be varied, is then performed.

3.8.1 ii γ-angular Distribution Study

An angular distribution study for ^{177}Ta was carried out at Michigan State University. Data were collected at $\theta = 90°$, $107°$, $125°$, $136°$, $147°$ and $159°$, where θ is the angle between the direction of γ-emission and the beam.

In order to normalize the yields at the various angles, the peak intensities of the various transitions were compared to the intensity of a transition which was isotropic and, therefore, should have equal yield at all angles. A transition de-exciting an isomer was chosen since its delayed nature permits the extranuclear electron field to distunb the nuclear orientation before emission.

The PDP-15 programme LEGPOL, documented with the Tandem Accelerator Laboratory Programme Documentation Library, was used to normalize the intensities at respective angles and fit to the data to a function of the form

$$W(\theta) = A_0 + A_2 P_2(\cos\theta) + A_4 P_4(\cos\theta) \qquad (3.8.2)$$

where

$W(\theta)$ = yield at angle θ

$P_2(\cos\theta)$ = 2nd order Legendre polynomial

$P_4(\cos\theta)$ = 4th order Legnedre polynomial.

The $\dfrac{A_2}{A_0}$ and $\dfrac{A_4}{A_0}$ coefficients are characteristic of the multipolarity

of the transition. A more advanced analysis of the data was not

attempted because of the weak nature of the transitions of interest.

3.8.2 γ-γ Prompt Coincidence Studies

Standard prompt coincidence pulse analysis was used. A

block diagram of the circuitry used is illustrated in Figure 3.13.

The fast output signals from the detectors were fed into timing

filters and constant fraction discriminators. This method produced

timing pulses whose cross-over points are independent of both rise

time and amplitude effects. These pulses then produced the "start"

and "stop" signals for the timing analyzer (TAC). The time

distribution obtained from the TAC during the course of an experiment

gives a good indication of the timing resolution of the system

used. Typically, the width of the TAC peak for prompt timing is of

the order of 20-50 ns. Tailing in the distribution is mainly due

to low energy gamma rays.

Delays were adjusted such that an event consisting of a valid

"start" and valid "stop" should occur within the pulse length of a

logic coincidence gating signal. If the timing between two

pulses arriving at the two detectors was such that both occurred

Figure 3.13

A block diagram of the circuitry used in standard
prompt coincidence pulse analysis. Abbreviations
used are:

AMP   - linear spectroscopy amplifier

PRE AMP - FET preamplifier

T.F.A.   - timing filter amplifier

C.F.D.   - constant fraction discriminator

D   - delay

L.G.S.   - linear gate stretcher

TAC   - time to amplitude converter

L.S.&D. - logic shaper and delay

ADC   - analog to digital converter

P
D
P

9

A		A		A	
D		D		D	
C		C		C	
1		2		3	

Coincidence Gate

MAG

L.S.&D.

TAC

Valid
Stop

T
A
C

L.G.S.

L.G.S.

D

C.F.D.

C.F.D.

AMP

AMP

T.F.A.

T.F.A.

Ge
(Li)

PRE
AMP

Ge
(Li)

PRE
AMP

within the length of time the coincidence gate was open, the pulses were admitted to their respective ADC's and analyzed. The digital outputs of the two ADC's storing energy information and the third storing TAC information were stored as 18 bit words. The accumulation programme (AR3P, McMaster; IIEVENT, MSU) was used to read all three coincidence mode ADC's and store the information in a buffer. When a number of sets of data had been read from the ADC's and the buffer was full, the data buffer was then written onto magnetic tape. Each word contained not only a digital representation of the pulse height but also identification of the ADC from which the word originated.

For experiments at McMaster the data thus written onto magnetic tape were sorted using the Tandem Accelerator PDP-15 computer programme DS3H1. The basic procedure used is as follows. A set of channels corresponding to a given peak of interest (up to 32 different peaks) is chosen in one ADC as well as suitable background channels above and below the peak gate to make subtraction possible of events associated with underlying compton background. A 'true' and 'chance' TAC gate is also set on the TAC ADC so that the results may be 'chance' event corrected. An illustration of a typical coincidence TAC spectrum is given in Figure 3.14. The programme then scans all records for events in the second ADC which are matched with the gated channels of the other two ADC's. A spectrum can thus be isolated of all transitions coincident with the photopeak in the spectrum of the other detector.

Figure 3.14

An illustration of a typical TAC spectrum showing
'true' and 'chance' gates.
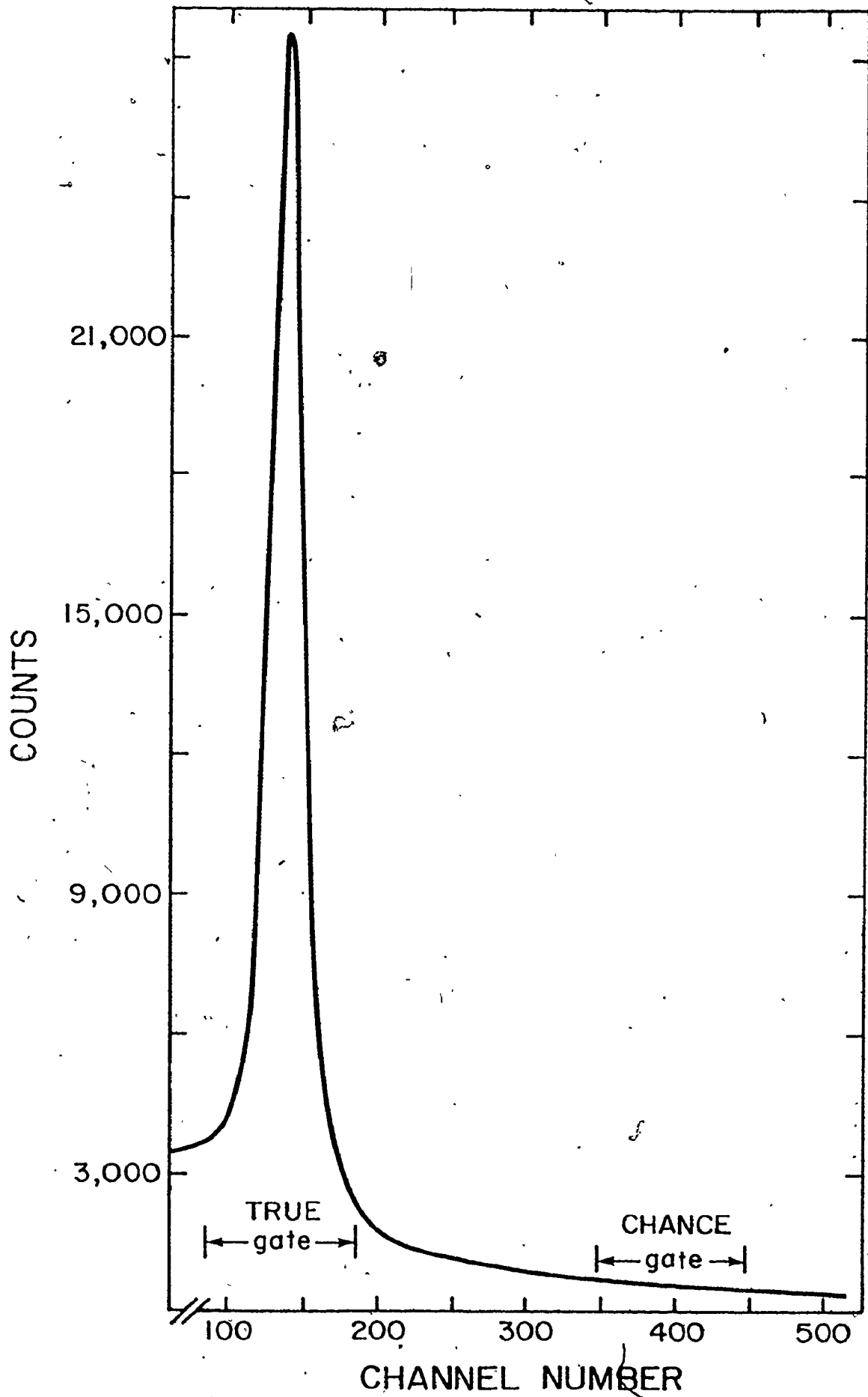
Sorting of γ-γ-t' coincidence events was carried out in a similar fashion at MSU using the programme KKRECOVERY (C.B. Morgan, MSU). The advantage of this programme is that up to 120 × 2K channel spectra may be generated -- the sorting only requiring approximately thirty minutes per 2400-foot tape. It is then possible to set gates on a large number of peaks.

3.9 Delayed Decay Studies

3.9.1 Delayed Singles and Half-Life Determinations

Since the isomers of interest were in the tens of nanoseconds to ∿ 10 μs range, it was possible to use pulsed beam techniques to study the transitions associated with the decay of these isomers. The basic method used in determining the half-life was to irradiate the target for a preset period of time, (at MSU this meant the natural 1 ns beam burst) and then to study the change in intensity with time of transitions occuring during the period when the beam is no longer on the target. If an event occurred during the beam-off period, both the energy of the γ and its time of occurrence were recorded. In the set-up at McMaster, the TAC was started by the turn-off of the beam and was stopped by a γ-ray, or else if no event occurred, the cycle was restarted. The reverse procedure was used at MSU in that an out-of-beam γ event started the TAC with the next beam pulse stopping it. This latter procedure was used to cut down on the number of unnecessary starts. A block diagram of a typical system for such a measurement is given in Figure 3.15.

Figure 3.15

Block diagram of the circuitry used in delayed singles
and half-life determinations. Abbreviations used are:

AMP   - linear spectroscopy amplifier

PREAMP   - FET Preamplifier

T.F.A.   - Timing filter amplifier

C.F.D.   - constant fraction discriminator

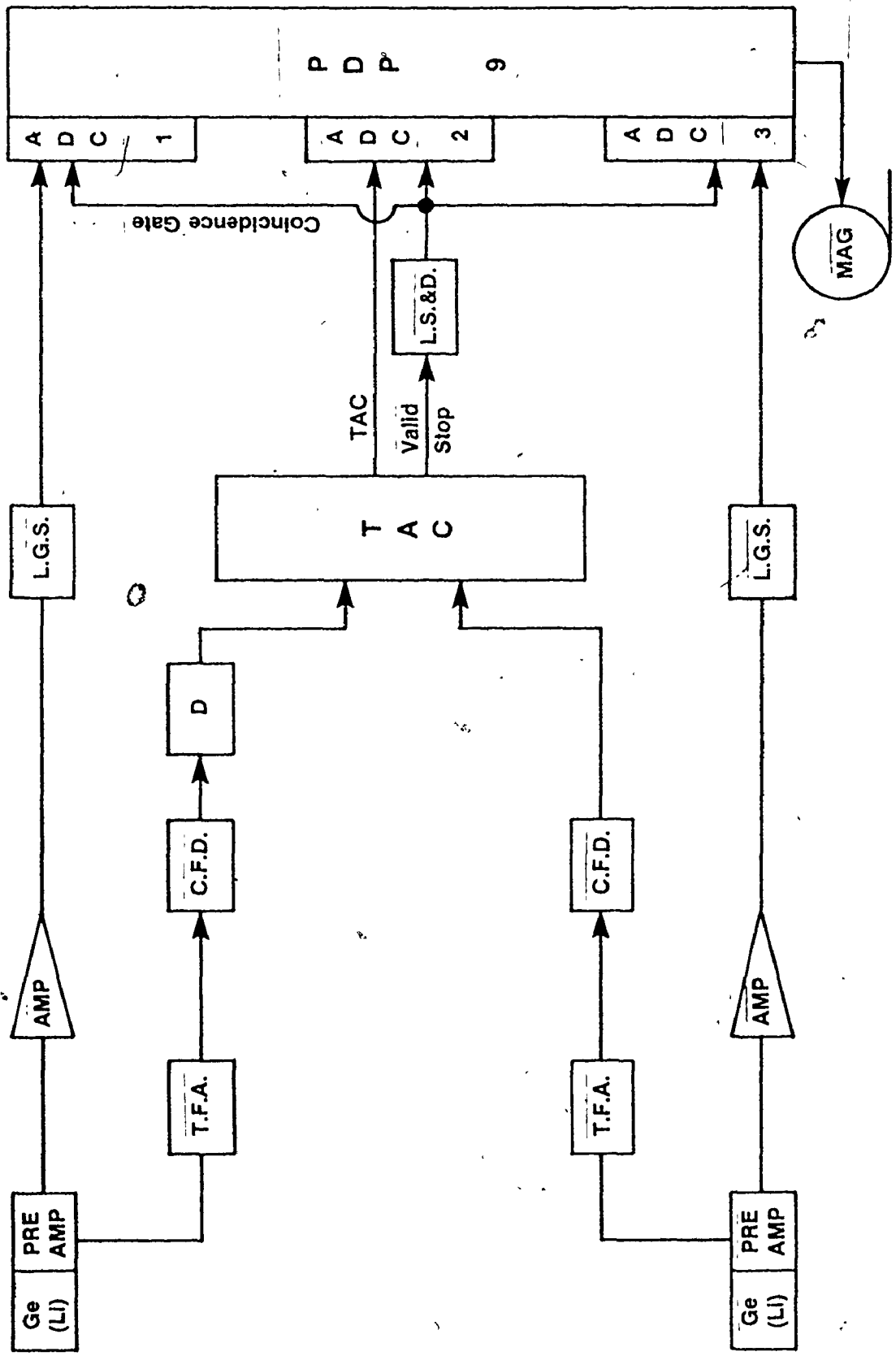G.&D.   - gate and delay generator

L.G.S.   - linear gate stretcher

TAC   - time to amplitude converter

L.S.&D.   - logic shaper and delay

ADC   - analog to digital converter

BEAM DEFLECTION PLATES

PULSER

L.S.D.

G.&D.

S T A R T

T A C

S T O P

TAC

True Stop

L.G.S.

L.S.&D.

Coincidence Gate

A D C 1

P D P 9

A D C 2

C.F.D.

T.F.A.

L.G.S.

AMP

PRE AMP

Ge (Li).
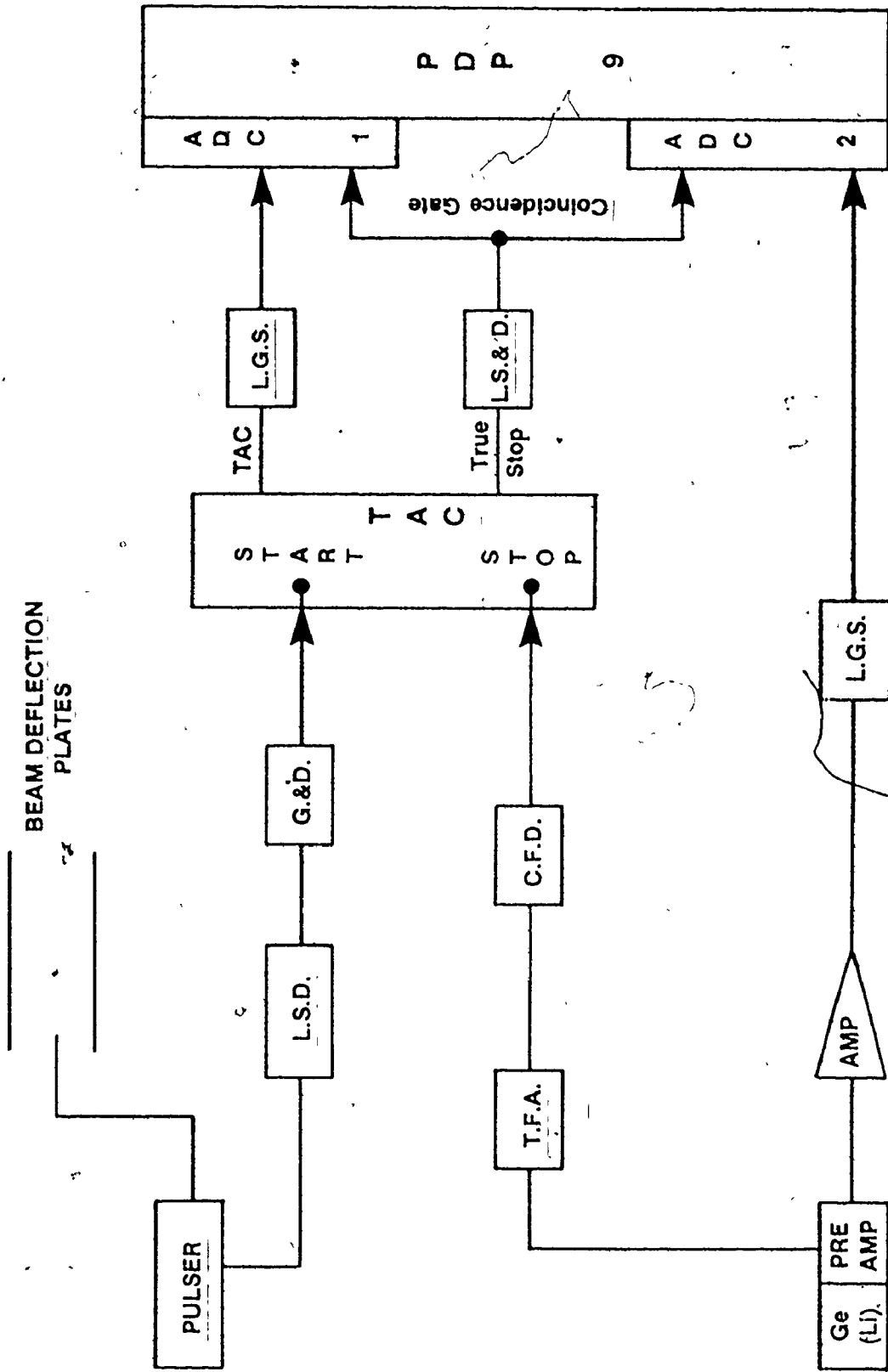
In order to carry out the measurements on ^{176}Ta at McMaster, the target was periodically irradiated for 40 µs by a ^{10}B beam and the subsequent γ spectra recorded. The (E,t) information was fed in a two parameter mode to the Nuclear Data 3300 analyzer whose memory stored incoming data within sixteen consecutive 1024 channel groups, each group representing 1.18 us intervals. It should be noted that although the beam remained turned off a total of 40 µs, the TAC range used for data accumulation was only 20 µs. This was done to allow for such extra time requirements as the TAC reset time. This allowance was not a mandatory condition for the correct operation of the equipment and was usually not considered in other experimental set-ups.

The cyclotron facilities at MSU were particularly suited to the measurement of a 78 ns isomer in ^{177}Ta since the beam is naturally pulsed with a beam-off period of ∿ 50 ns. The data were acquired in the two parameter (E,t) mode by the programme TOOTSIE (D. Bayer, MSU). The programme is capable of collecting data in up to ten evenly spaced intervals. The beam sweeper was adjusted so that eight spectral groups, each separated by 76.6 ns could be collected between 1 ns irradiations.

The resulting energy spectra were analyzed in the manner described in Section 3.8.1 for prompt γ-studies.

3.9.2 γ-γ Delayed Coincidence Studies

After having established the presence of an isomer, it is then of interest to somehow isolate those transitions which feed into it. A delayed coincidence experiment is used which searches for pairs of coincident events delayed in time relative to each other. The delay represents the presence of an intervening isomer.

In principle, then, the procedure was to irradiate the target until such time as a Ge(Li) detector, designated as the "start" detector, detects an event. This signals the pulsing system to turn the beam off for a prescribed period of time during which a second Ge(Li) detector, designated as the "stop" detector, awaits the arrival of a coincident γ-event. If a stop event is found for a start event, both events along with the time between were stored by the computer. The main difference between the MSU and McMaster experiments was that the MSU experiment allowed the coincident gamma event to be prompt or delayed and the different pairs were only later sorted by gating with appropriate areas of the TAC spectrum. The experiments at McMaster tried to eliminate all but delayed coincidences.

Figure 3.16 gives a schematic of the basic circuit used in the experiments at McMaster. The beam is left on until such time as an event is detected by the "start" detector. This pulse is not only used to start the timing unit but also to trigger a pulse of preset length at the pulser. This pulse, then, turns the beam off and allowing for beam transit time the system is now ready

Figure 3.16

Block diagram of circuitry used in γ-γ delayed

coincidence experiments. Abbreviations used are:

AMP   - linear spectroscopy amplifier

PRE AMP - FET preamplifier

T.F.A.   - timing filter amplifier

C.F.D.   - constant fraction discriminator

L.G.S.   - linear gate stretcher

G.B.A.   - gated biased amplifier

L.S.&D. - logic shaper and delay

TAC   - time to amplitude converter

INV   - inverter

ADC   - analog to digital converter

BEAM DEFLECTION PLATES

PDP 9

ADC 1

ADC 2

ADC 3

Coincidence Gate

G.B.A.

Ext Strobe

PULSER

SCA

G.&D.

True Stop

L.S.&D.

TAC

INV.

Busy

T A C

Start — inhibit — Stop

AMP

C.F.D.

C.F.D.

L.G.S.

T.F.A.

T.F.A.

AMP

PRE AMP

Ge (Li)

PRE AMP

Ge (Li)
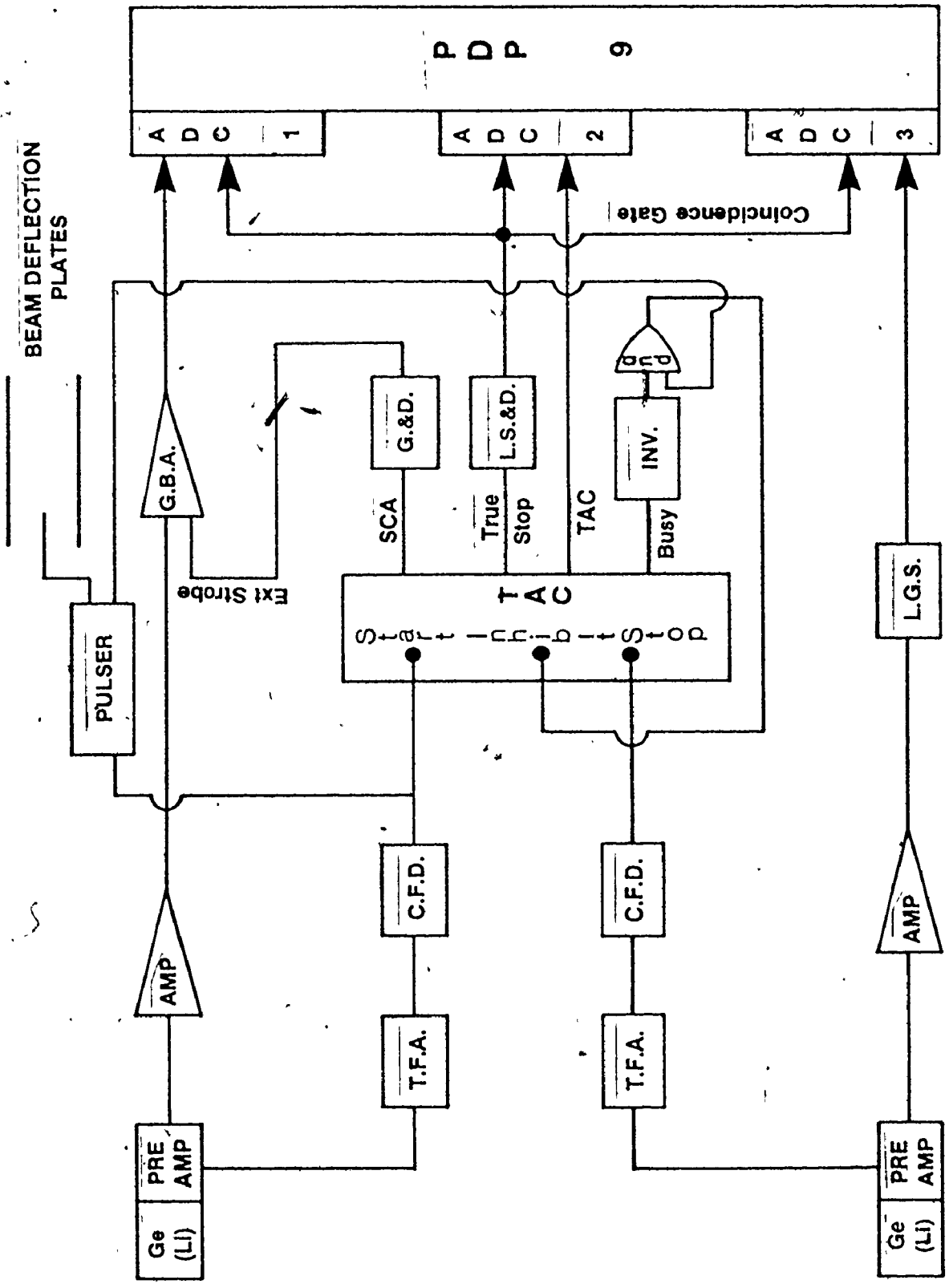
to await a possible delayed event occurring during the beam off period.

Since there may be a sizable time delay between the occurrence of a 'start' event and the "stop" event at the respective ADC's, a module (Gated Biased Amplifier Ortec 444) is used to store the first bit of information until such time as there is a TAC output to externally strobe the module and release the signal to its ADC. All three parameters (E_1, E_2, t) then are processed as a coincident triplet.

An additional problem which might easily arise occurs while the TAC is awaiting a 'stop' signal during the long (of the order of µs) beam off time. A new 'start' signal might appear and await processing by the TAC. Therefore, the start inhibit mode is used on the TAC such that another 'start' cannot be accepted either while the TAC is processing a 'start' signal or while the beam is turned off. In addition, the stop inhibit mode was used such that no 'stops' were accepted for $\simeq$ 100 ns after a 'start.'

3.9.3 γ-γ Prompt Coincidence, Out-of-Beam Studies

An experiment was carried out at MSU which carried the γ-γ delayed experiment one step further. An additional TAC, called the beam TAC, was used to monitor the occurrence of the 'start' signal relative to the beam burst since the 'start' could occur between beam bursts also. The highest probability, of course, is that the 'start' signal occur during the beam-on time. With the addition of this TAC, one can later sort for γ-γ coincidences

delayed or prompt with respect to each other, with the first event either delayed or prompt itself. The advantage of such a set-up is that γ-γ coincidences out-of-beam emphasize the isomer decay lines and can make otherwise weak lines visible.

3.9.4 Electron Studies

A conversion electron study was carried out at MSU primarily to obtain the multipolarities of the 555.4 and 789.4 keV transitions depopulating the 78 ns isomer in ^{177}Ta. Since the transitions of interest were isomer decay lines, a pulsed beam experiment was used. Just as in the delayed singles experiment, only out-of-beam γ's and associated electrons were collected. The detailed discussion of this experiment follows in Chapter 4.

CHAPTER 4

EXPERIMENTAL RESULTS FOR ^{177}Ta

The difficulty encountered in listing the results of
this study is the presentation of the facts in some systematic
sequential order. One often finds that an experiment will yield
not only results that are useful for the present point in question,
but also results that are later found to be relevant to some other
part of the study. The problem arises of whether all the data of
a given experiment should be grouped and presented together or
should the presentation of those facts that are only pertinent to a
later stage of the analysis be postponed until their significance
is appreciated. The latter approach was chosen since it appeared
to be the most logical.

Obviously, only a few of the large quantities of spectra
and data are shown. In making a final decision on the placement
of a γ-ray, several spectra were checked and cross-checked. The
few spectra shown only give an idea of the type of data that were
analyzed.

4.1 Introduction

The nucleus [177]Ta had been investigated to some degree before this project was begun. Most notably, results for the 1-quasi-particle proton bands have been presented by B. Skanberg et al (1970) and D. Barnéoud et al (1970). (See Figure 4.1.) A 3-quasiparticle isomer at 1355.2 keV with a half-life of 5.0 μs had been located. The spin and parity of this isomer were determined to be $21/2^-$ through model-dependent arguments by H. Hübel et al (1971) and the measurement of the multipolarities of de-exciting transitions was made by J.S.Geiger et al (1968). D. Barnéoud et al (1975) have shown results (Figure 4.2) for transitions populating this isomer and have identified the $K^\pi = 23/2^+$ and $25/2^+$ 3-quasiparticle bandheads. The latter group used a 30 MeV α-particle beam with a natural ^{175}Lu target to form the levels in ^{177}Ta via the (α,2n) reaction. States up to 2826.8 keV were populated.

Because of the success in finding 3-quasiparticle states a search was, therefore, begun for a 5-quasiparticle state which should occur at an excitation energy of roughly 2Δ, the pairing gap, or approximately 1500 keV above the 3-quasiparticle states. Facilities at McMaster were incapable of supplying a beam with a high enough value of energy per mass unit of projectile required to excite high angular momentum states, so the experiments were carried out at the Michigan State University cyclotron facilities. The target ^{176}Lu was chosen since its ground state spin is 7^- and was thought to be particularly suitable as a starting point in populating high spin states.

Figure 4.1

Level scheme of ^{177}Ta proposed by Skanberg
et al (1970).

$^{177}_{73}\text{Ta}_{104}$

Band $9/2[514]$

$23/2^-$ — 1576.8
274.8

$21/2^-$ — 1302.0
258.3 ; 533.8 (311.3)

$19/2^-$ — 1043.7
238.7 ; 498.1 (550.0)

$17/2^-$ — 805.0
218.0 ; 456.8

$15/2^-$ — 587.0
195.3 ; 413.6

$13/2^-$ — 391.7
171.6 ; 367.1

$11/2^-$ — 220.1
146.5 ; 318.5

$9/2^-$ — 73.6
73.6

Band $7/2[404]$

$(25/2^-)$ — 1902.6
294.7

$(23/2^-)$ — 1625.9
270.9

$(21/2^-)$ — 1355.0
565 ; T½ 200ns–30µs

$19/2^+$ — 1147.1
$17/2^+$ — 901.5
226.0 ; 471.3

$15/2^+$ — 675.8
204.9 ; 430.0

$13/2^+$ — 470.5
181.6 ; 387.2

$11/2^+$ — 288.6
157.6 ; 339.5

$9/2^+$ — 131.0
131.0 ; 288.6

$7/2^+$ — 0

Band $1/2[541]$

$25/2^-$ — 1449
440.8

$21/2^-$ — 1008
352.6

$17/2^-$ — 655
256.6

$13/2^-$ — 399
$3/2^-$ — 372

$9/2^-$ — 242 ; 217 ; 186.1
$7/2^-$ — 56
$5/2^-$

T½ = 35µs ; 70.6 ; 1153

Band $5/2[402]$

$15/2^+$ — 833.0
200.7

$13/2^+$ — 632.2
177.9 ; 378.6 ; 454.3

$11/2^+$ — 153.9
331.8 ; 300.4

$9/2^+$ — 128.4
282.7 ; 172.0

$7/2^+$ — 101.4 ; 229.6
$5/2^+$ — 70.6

T½ = 53ns

Figure 4.2

Level scheme of transitions populating the
5 μs 21/2⁻ isomer in ^{177}Ta proposed by Barnéọud
et al (1975). The levels at 1355.2, 1698.6
and 1834.9 are assigned 3-quasiparticle
configurations.

33/2⁺ 2826.9

31/2⁺ 2529

29/2⁺ 2271.5 555.4 ~257

234.2

27/2⁺ 20373 202.4

25/2⁺

25/2⁻ ~264 ~437 1834.9

136.3

23/2⁺ 1698.6

400.2

2098.8

25/2⁻ 1920.8

294.7

23/2⁻ 1626.1

270.9

21/2⁻ 1355.2

343.4

T₁/₂ = 5.0 μ·

550.0

311.2

19/2⁻

17/2⁻

9/2⁻[514]

23/2⁻ ~1945 249.0

21/2⁻ ~1696 ~70

~341
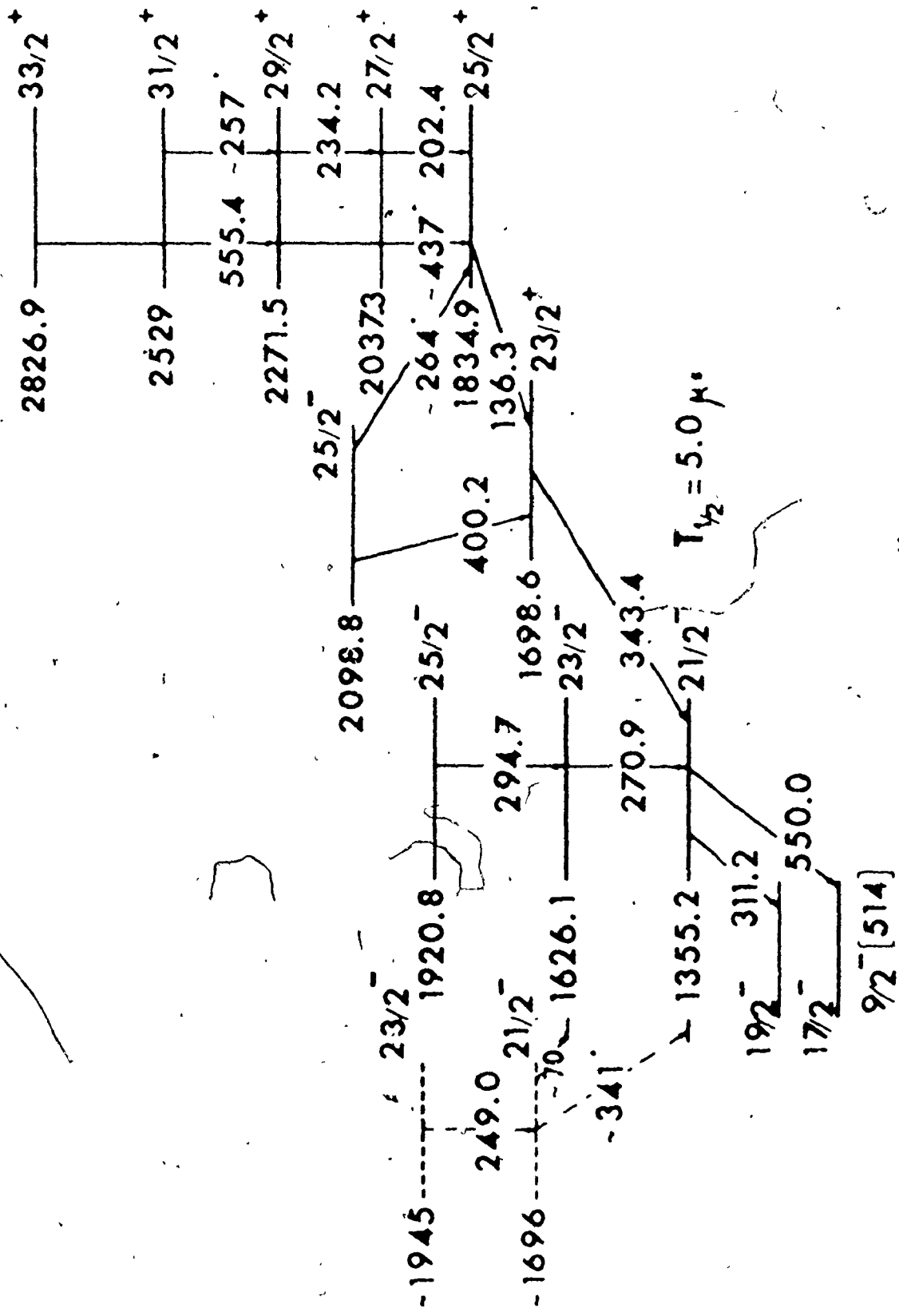
4.2 Delayed γ-Singles Results

4.2.1 Out-of-Beam γ-Singles

An initial attempt was made at the McMaster University Tandem Accelerator facilities to verify the results already recorded by the groups previously mentioned. To do this a ^{11}B beam was used at the maximum energy available, 54 MeV. An enriched ^{170}Er target, 8.5 mg/cm^2, was irradiated periodically for 5 μs with 5 μs beam-off times. The 3.5 μs 1-quasiparticle isomer was verified as well as the 5.0 μs 3-quasiparticle isomer. What was interesting, though, was the presence of the 343.4, 136.3 and 202.7 keV transitions in the out-of-beam spectra. Their intensities were extremely small and another attempt was made at the same experiment but with 1 μs beam on/off times. This time the intensities of these transitions increased to the point that the half-life could be estimated as < 100 nanoseconds, but it was obvious from the very small intensities of the transitions feeding the $^{21}/2^-$ isomer that a beam was required which could supply a higher velocity to the projectile nucleons. The project then was continued at the Michigan State University Cyclotron facilities.

The ^{176}Lu(α,3n) reaction was used to populate the levels of ^{177}Ta. A 1.2 nanoamp beam of 38 MeV α's was used to bombard a rolled target, 3.5 mg/cm^2 thick. Events were detected by an ND10% Ge(Li) detector. The target was irradiated for ∿ 1 ns and eight successive spectra were collected, each separated by 76.6 ns. Table 4.1

Table 4.1

Out-of-beam γ-intensities following the ^{176}Lu(α,3n) Reaction

E_γ (keV)*	I_γ	Assignment $I_i K_i^\pi \rightarrow I_f K_f^\pi$
88.4$^{(d)}$	8.2 ± 1.2	^{178}Ta decay$^{(a)}$; ^{176}Ta decay$^{(6)}$
93.0	4.9 ± 1.0	^{178}Ta decay$^{(a)}$
99.9	12 ± 1	
112.7	6.3 ± 1.0	^{177}Ta decay$^{(c)}$
115.3	30 ± 2	5/2 1/2$^-$ → 5/2 5/2$^+$
121.6	9.5 ± 1.2	
131.3	< .4	
134.3	4.1 ± 1.2	^{176}Ta
136.3	23 ± 6	25/2 25/2$^+$ → 23/2 23/2$^+$
142.1	13 ± 1	
146.5	38 ± 2	11/2 9/2$^-$ → 9/2 9/2$^-$
150.4	4.1 ± 1.1	
159.7	4.8 ± 1.3	
161.3	7.3 ± 1.5	
171.6$^{(d)}$	56 ± 3	13/2 9/2$^-$ → 11/2 9/2$^-$; ^{176}Ta
184.1	67 ± 4	^{176}Lu
186.5$^{(d)}$	15 ± 2	5/2 1/2$^-$ → 7/2 7/2$^+$; ^{176}Ta
192.3	6.0 ± 1.7	
195.3	56 ± 3	15/2 9/2$^-$ → 13/2 9/2$^-$
197.2	36 ± 3	^{19}F(n,n')
198.9	11 ± 2	^{176}Ta

Table 4.1 (continued)

E_γ (keV)*	I_γ	I Assignment $I_i K_i^\pi \rightarrow I_f K_f^\pi$
202.7[d]	40 ± 3	$27/2\ 25/2^+ \rightarrow 25/2\ 25/2^+$; ^{176}Hf
213.5	16 ± 1	^{178}Ta decay[a]
218.0	49 ± 3	$17/2\ 9/2^- \rightarrow 15/2\ 9/2^-$
228.9	7.6 ± 1.5	
234.1	23 ± 2	$29/2\ 25/2^+ \rightarrow 27/2\ 25/2^+$
238.5	67 ± 3	$19/2\ 9/2^- \rightarrow 17/2\ 9/2^-$
242.4	5.9 ± 1.4	
249.4	6.5 ± 1.6	
258.7	9.6 ± 1.5	
261.2	< 4	
270.2	7.7 ± 1.2	
272.3	5.5 ± 1.4	
275.9	12 ± 2	
296.5	15 ± 2	
305.8	4.8 ± 2.0	^{176}Ta
307.0[d]	14 ± 2	partially ^{176}Hf
311.3	100	$21/2\ 21/2^- \rightarrow 19/2\ 9/2^-$
314.4	7.0 ± 1.9	
325.8	21 ± 2	^{178}Ta decay[a]
330.0	< 4	
331.9	13 ± 2	^{178}Ta decay[a]

Table 4.1 (continued)

E_γ (keV)*	I_γ	Assignment $I_i K_i^\pi \rightarrow I_f K_f^\pi$
339.2	< 4	
343.4	76 ± 3	23/2 23/2$^+$ → 21/2 21/2$^-$
352.2	7.4 ± 1.1	
358.5	15 ± 1	
364.4	< 4	
367.1	18 ± 1	15/2 9/2$^-$ → 11/2 9/2$^-$
374.5	5.2 ± 1.0	
381.8	9.3 ± 1.5	
387.4	6.7 ± 1.7	
389.0	5.7 ± 1.7	
393.3	4.6 ± 1.3	^{176}Ta
397.8	7.4 ± 1.4	
400.0	5.1 ± 1.3	(25/2$^-$ 25/2$^-$ → 23/2$^+$ 23/2$^+$)[e]
413.6	23 ± 2	17/2 9/2$^-$ → 13/2 9/2$^-$
426.6	20 ± 2	^{178}Ta decay[a]
434.0	11 ± 1	
436.7	6.5 ± 1.2	29/2 25/2$^+$ → 25/2 25/2$^+$
440.4	< 4	
456.8	39 ± 3	19/2 9/2$^-$ → 15/2 9/2$^-$
461.8	5.9 ± 2.0	

Table 4.1 (continued)

E_γ (keV)	I_γ	Assignment $I_i K_i^\pi \rightarrow I_f K_f^\pi$
463.0	5.9 ± 2.0	
466.2	6.7 ± 1.0	
469.1	12 ± 1	
521.7	4.4 ± 1.4	^{176}Ta decay[b]
526.8	7.5 ± 1.3	
535.6	16 ± 2	
539.8	5.7 ± 1.8	
549.8	14 ± 2	$21/2\ 21/2^- \rightarrow 17/2\ 9/2^-$
555.4	39 ± 3	$31/2\ 31/2^+ \rightarrow 29/2\ 25/2^+$
590.4	15 ± 2	
594.6	6.9 ± 1.4	
610.1	5.5 ± 1.3	
618.4	20 ± 2	^{176}Ta
647.5	7.0 ± 1.2	
658.0	8.6 ± 1.3	
667.4	5.6 ± 1.2	
677.0	6.6 ± 1.2	

Table 4.1 (continued)

E_γ	I_γ	Assignment $I_i K_i^\pi \rightarrow I_f K_f^\pi$
743.1	$\cdot 12 \pm 2$	
753.3	6.6 ± 1.4	
762.9	12 ± 2	
789.4	32 ± 2	$31/2\ 31/2^+ \rightarrow 27/2\ 25/2^+$
793.2	11 ± 2	

(a) decay from 7^- state in ^{178}Ta

(b) decay from 1^- state in ^{176}Ta

(c) decay from $7/2^+$ state in ^{177}Ta

(d) doublet

(e) tentative assignment; see sect. 4.7

* FWHM at 218 keV is equal to 1.3 keV. Energies of low intensity transitions are given to $\pm$ .3 keV.

lists the relative intensities of transitions in the second out-of-beam interval. Detector efficiency corrections have been included. As can easily be seen by the multitude of out-of-beam transitions, even the tool of looking out-of-beam is not as useful as could be hoped. The electron capture decay of the 7^- state in ^{178}Ta to states in ^{178}Hf is seen (C.J. Gallagher, Jr. et al, 1962) as well as the electron capture decay of the 1^- state in ^{176}Ta to states in ^{176}Hf (F.M. Bernthal et al, 1971). In addition, the decay of the $^7/2^+$ state in ^{177}Ta to states in ^{177}Hf is also seen (B.D. Jeltema et al, 1974). A number of transitions, a few of them relatively strong, are as yet unplaced. Because these transitions are not explained through γ-γ coincidence data, their origins are questionable.

The unmistakable presence of transitions which were not known to be delayed by previous authors was seen. (Compare Figure 4.2). Table 4.2 gives the relative intensities of delayed transitions feeding the 5.0 μs 3-quasiparticle isomer at 1354.9 keV. Corrections have been made for contributions from contaminant lines. The 400.0 keV transition is an interesting case in that in addition to appearing in the delayed spectra, later γ-γ prompt coincidence measurements showed this transition to be in prompt coincidence only with the 343.4 keV transition. This evidence points to the possibility of the 2098.4 keV level being isomeric with a half-life $20 \leq t_{1/2} \leq 100$ ns. The delayed nature of the transitions de-exciting the 2826.8 keV level makes the assignment of this level as a member of the rotational band built upon the $K^\pi = ^{25}/2^+$ state, as suggested by previous work

Table 4.2

Delayed γ-transitions feeding the 1354.9 keV isomer

E_γ (keV)	I_γ
136.3	30 ± 8
202.7	44 ± 8 [a]
234.1	31 ± 2
343.4	100 (normalized)
(400.0)	$(6.7 \pm 1.9$ [b]$)$
436.7	8.6 ± 1.5
555.4	52 ± 4
789.4	43 ± 3

[a] Corrected for contribution from contaminant ^{176}Hf transition

[b] tentative placement

(Barnéoud et al, 1975) incorrect. Therefore, the level was interpreted to be a new multi-quasiparticle state.

4.2.2 Half-life Determination of 2826.8 keV Level

The eight consecutive time spectra which were collected were studied for the half-life determination of the 2826.8 keV level. The intensities of the transitions of interest decreased at such a rate that analysis was carried out on the first five spectra only. In addition, the first spectrum was not used because of "seepage" of prompt events into the spectrum. However, the rate of change in intensity of sufficient transitions was studied to make a reasonably accurate estimate of the half-life. Figure 4.3 gives excerpts of the collected spectra showing the change in intensity with time of the 202.7 and 555.4 keV transitions. The time T = 0.0 refers to the first spectrum that was collected out-of-beam. As a reference, the 311.3 keV transition de-exciting the 5.0 μs isomer in ^{177}Ta and the 618.4 keV transition de-exciting the 3.8 μs isomer in ^{176}Ta are shown. It is obvious by comparing the intensities of the 202.7 with the 311.3 keV and the 555.4 with the 618.4 keV transitions through the successive time intervals, that the half-life of the new state in ^{177}Ta is much shorter than a few μs.

Figure 4.4 shows the time rate of change of intensity of the 202.7 keV and 555.4 keV transitions. Values of the half-life using the 202.7, 555.4 and 343.4 keV transitions are 74 ± 4, 80 ± 4, and 80 ± 6 ns which leads to a final value of 78 ± 5 ns.

Figure 4.3

Excerpts of spectra collected during beam off period.
Each period was 76.6 ns long. T = 0.0 represents
the first spectrum out-of-beam, and T = 76.6,
153.2 and 229.8 ns respectively later times. The
311.3 keV and 618.4 keV transitions show de-
excitations of much longer lived isomers.
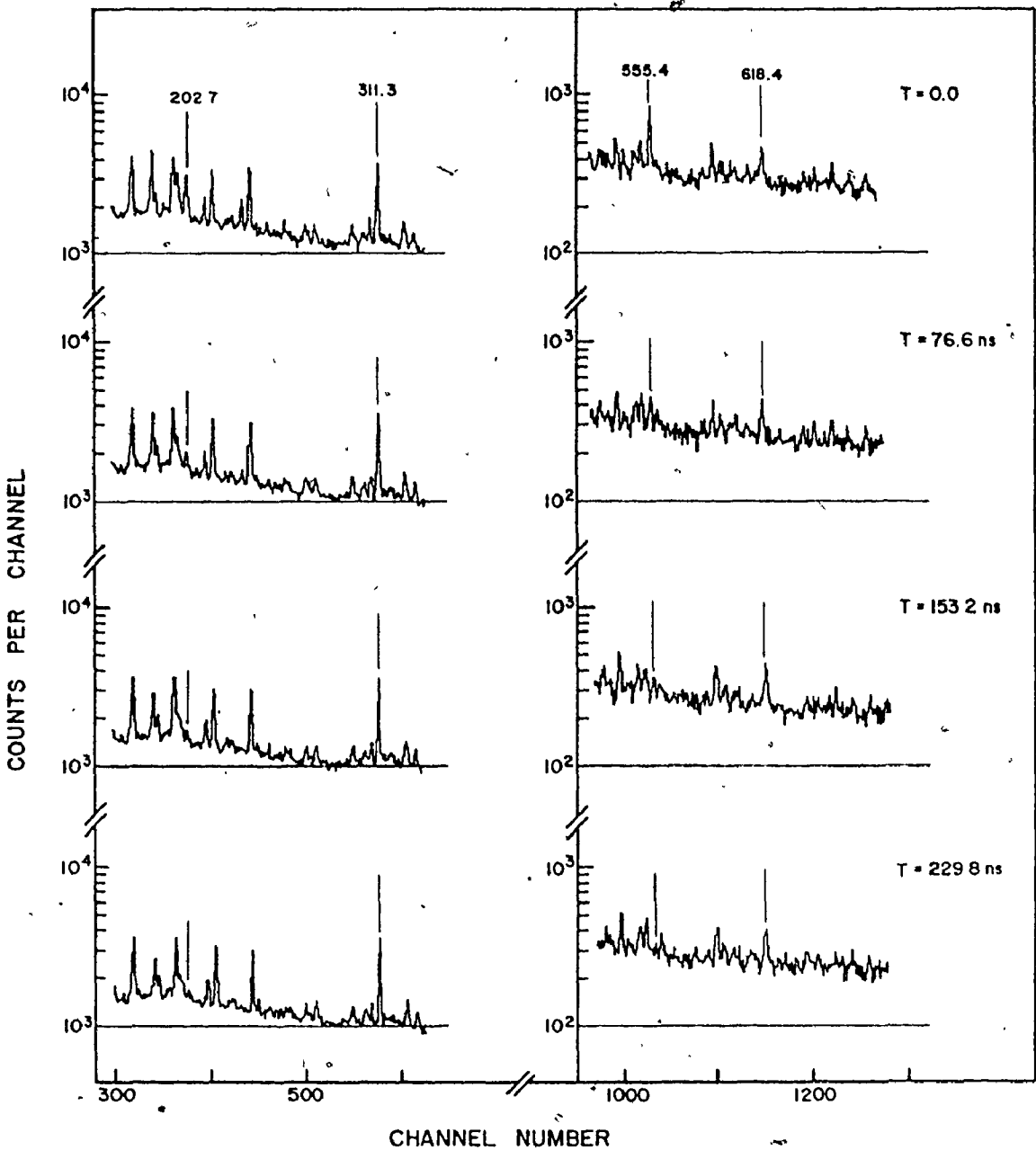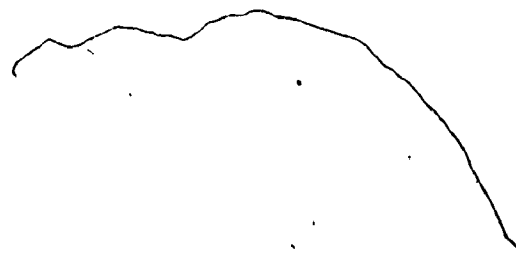
Figure 4.4

Figure illustrating the time rate of change of
intensity of the 202.7 and 555.4 keV transitions.

COUNTS PER CHANNEL

CHANNEL (76.6 ns/channel)

202.7 keV

$T_{1/2} = 74 \pm 4\,ns$

555.4 keV

$T_{1/2} = 80 \pm 4\,ns$
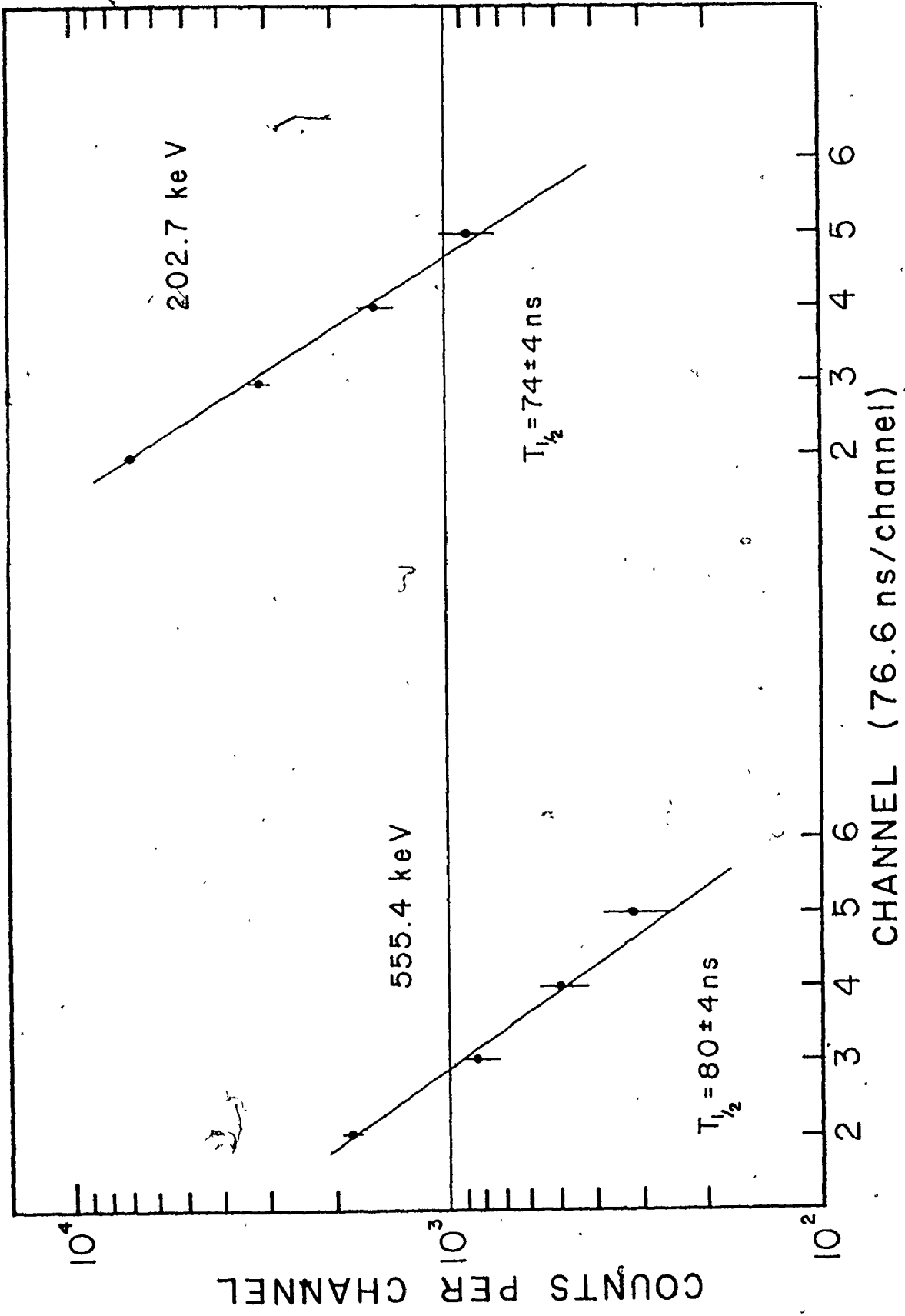
4.3 Internal Conversion Coefficients of 555.4 and 789.4 keV Transitions

In order to establish the spin of the newly found isomer, it was necessary to determine the multipolarities of the 555.4 and 789.4 keV transitions directly de-exciting this isomer. Because the transitions of interest were isomer decay lines, an out-of-beam conversion electron experiment was carried out. A 3 mg/cm^2 self-supporting ^{176}Lu target was bombarded with a 1 nanoamp beam of 38 MeV α's. Approximately 216 nanoseconds elapsed between beam bursts. Gammas were collected in an ND 10% Ge(Li) detector simultaneously with the electrons in the Si(Li) so that there was no need for normalization of counting time between γ's and electrons. Figure 4.5 shows the electron spectrum collected.

To correct for relative efficiences within the Si(Li) electron detector, a ^{207}Bi standard source was used. Since the true relative intensities of 569.6 K, L, M and 1063.5 K, L, M lines are accurately tabulated, one can compare measured intensities with actual intensities to determine the correction required. Since, of course, the conversion coefficient is the relative intensity of electrons to γ's, it is necessary to normalize the intensities of the gammas and electrons as there may be a difference in efficiency for collecting γ's versus electrons. This was particularly simple in the experiment carried out since it was possible to rely on transitions whose multipolarities had already been measured by other authors. In this case, the 549.8 keV transition de-exciting the 5.0 μs isomer in ^{177}Ta was known to be E2 and so this transition was used as a reference.

Figure 4.5

Out-of-beam electron spectrum collected for the
determination of the internal conversion coefficients
of the 555.4 and 789.4 keV transitions found in
^{177}Ta.

(a)   decay of ^{178}Ta

(b)   decay of ^{176}Ta

(c)   transition found in ^{176}Ta
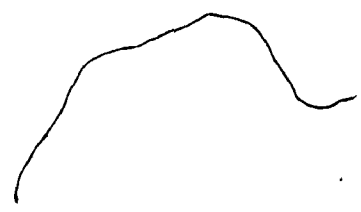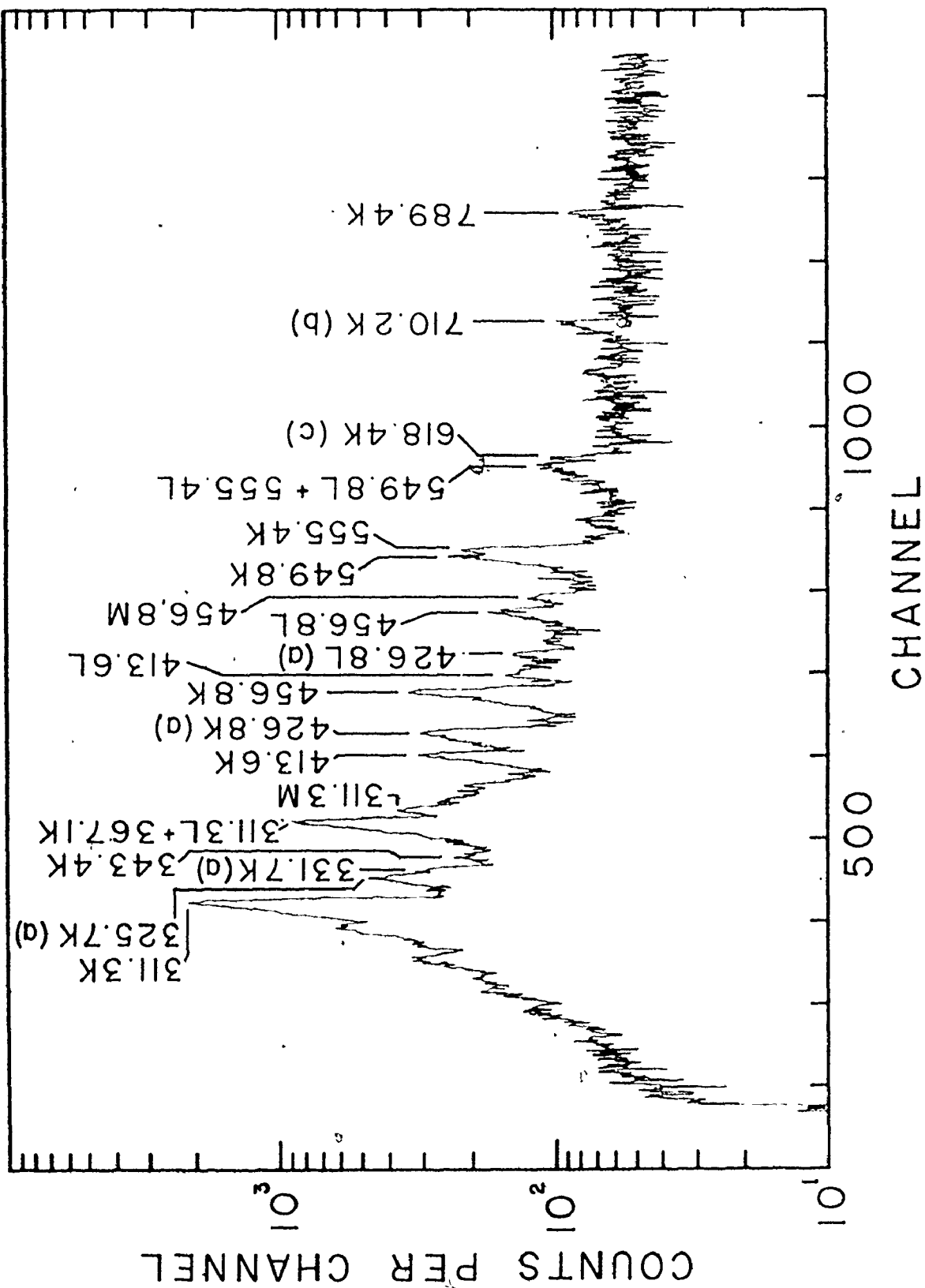
Figure 4.6 illustrates the values of the measured K-shell conversion coefficients for the 555.4 and 789.4 keV transitions. The solid lines were obtained by using the standard values found in internal conversion tables tabulated by R.S. Hager and E.C. Seltzer. The internal conversion coefficient of the 555.4 keV transition, $\alpha^K(555.4)$ was measured to be 0.0236 $\pm$ .0036 in comparison with the values of α^K_{E2} (555.4) = 0.0125 and α^K_{M1} (555.4) = 0.0344. Thus, the 555.4 keV transition appears to be mixed M1 + E2, with a mixing ratio $\delta^2 = I_\gamma(M1)/I_\gamma(E2)$ of 0.92 $\pm$ .30. Also, $\alpha^K(789.4)$ was measured to be 0.0077 $\pm$ 0.0023 in comparison to the values α^K_{E2} (789.4) = 0.0058 and α^K_{M1} (789.4) = 0.0142. Thus the 789.4 keV transition is E2 in nature.

4.4 Prompt-γ-γ Coincidence Results for Transitions not Associated with the 2826.8 keV Level

An extensive amount of γ-γ prompt coincidence data was gathered at MSU with a total of 92 gates set with energies ranging from 72.8 to 1014.6 keV. The ^{176}Lu(α,3n) reaction was used. A 0.4 nanoamp beam of 38 MeV α's bombarded the enriched ^{176}Lu, 3 mg/cm^2 thick. Events were detected by an ND 10% and an EDAC 8% Ge(Li) detector. The results for the 136.3 and 789.4 keV gates are given in Figure 4.7. The results for the transitions between the 1354.9 and 2826.8 keV levels shown in the delayed singles experiment were confirmed. In addition, the rotational band built upon the $K^\pi = 25/2^+$ state was extended to I = 35/2. Several transitions associated with the bands built upon

Figure 4.6

An illustration of the K-shell conversion coef-
ficients for the 555.4 and 789.4 keV transitions
in ^{177}Ta. The solid lines were obtained by
using the standard values found in internal conversion
tables tabulated by Hager and Seltzer. The 456.8
and 549.8 keV transitions are known E2 transitions.
The 618.4 keV transition is associated with the
isomer decay found in ^{176}Ta.
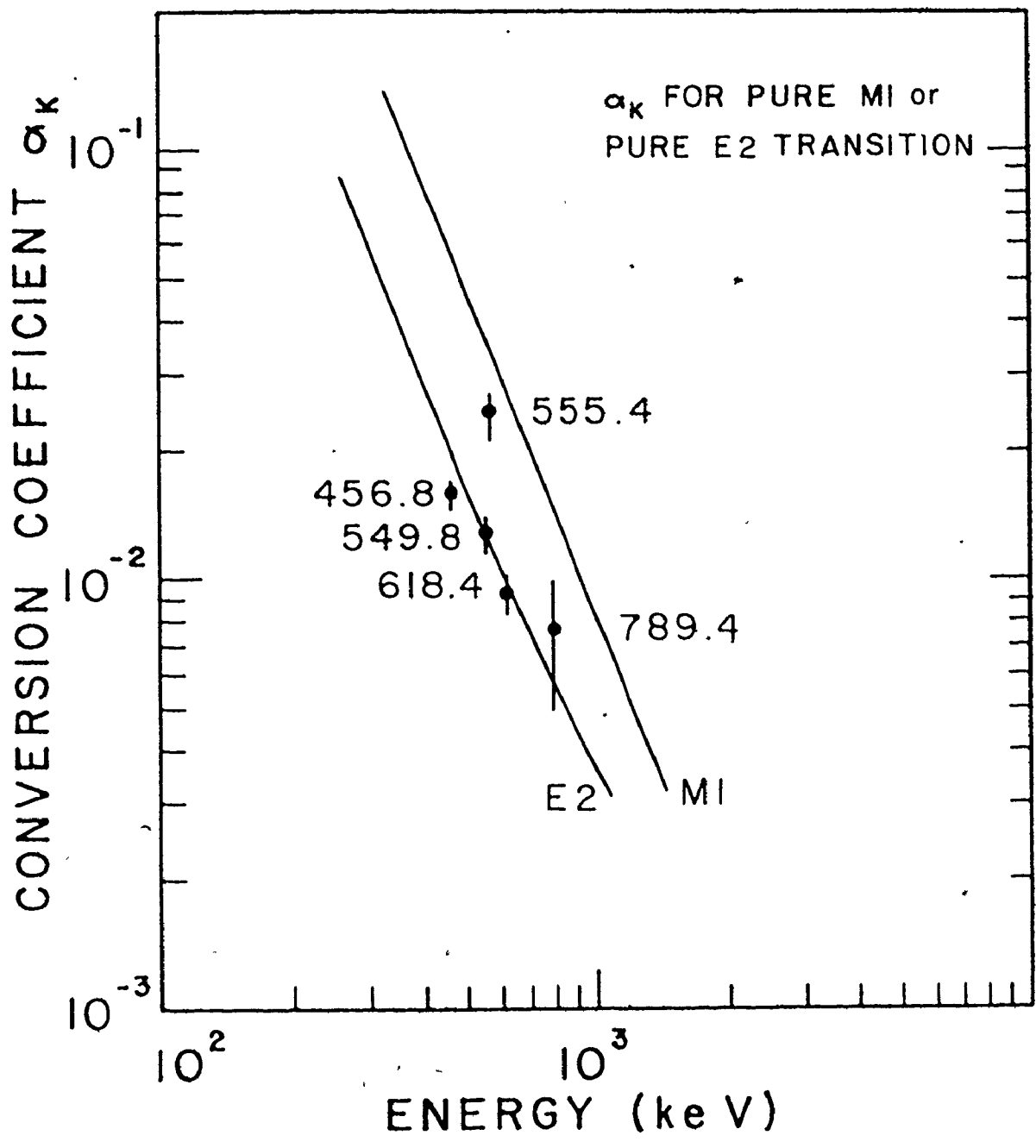
Figure 4.7

The results for the 136.3 and 789.4 keV prompt
γ-γ coincidence gates.

(a) transitions associated with the 134.3 keV
transition in ^{176}Ta
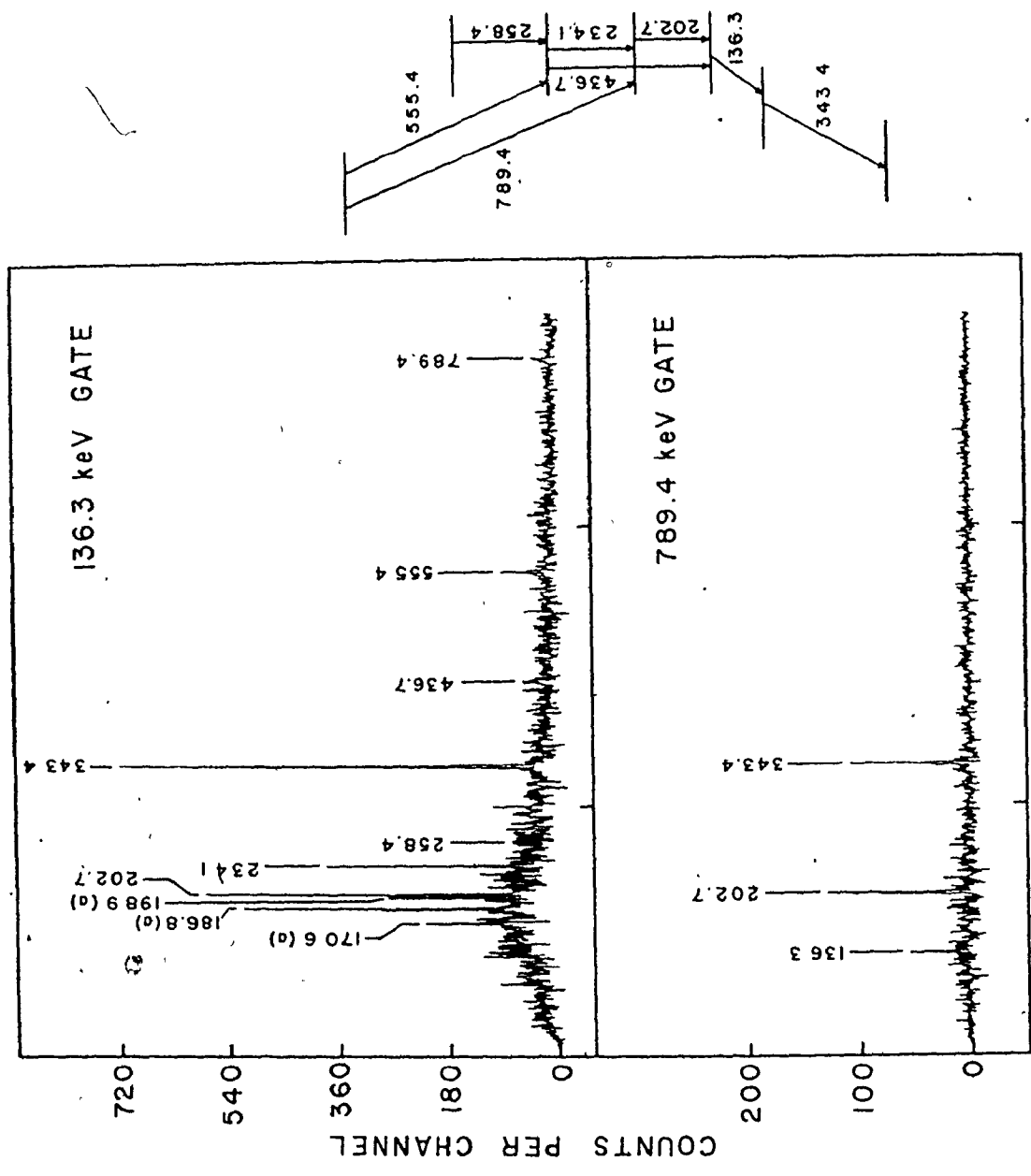
the $7/2^+[404]$, $1/2^-[541]$, $5/2^+[402]$ and $9/2^-[514]$ states were added
to the previously known decay scheme. The results for the $1/2^-$
[541] band are especially good since it is yrast until spin $I = 33/2$.
The rather large abundance of gates was necessary because of the
competition of transitions in other nuclei which made the unique
determination of a level scheme difficult. The final decay scheme is
given in Figure 4.8.

Transitions populating the 2826.8 keV level are discussed
in section 4.6

4.5 Delayed γ-γ Coincidence Results

Having established the presence of an isomer of half-life
78 $\pm$ 5 nanoseconds at 2826.8 keV energy, it was decided to investigate
the transitions feeding into this isomer. The reason for this is
twofold: first, the extension of the level scheme to as high an
energy and spin as possible; second, to give further evidence of the
configuration of the 2826.8 keV level. Often the decision between two
or more plausible configurations is made easier by knowing the nature
of the transitions that feed into this level.

The results of the prompt γ-γ coincidence experiment discussed
in section 4.4 were part of a larger experiment which yielded delayed
γ-γ coincidence results also. See section 3.9.2. A beam sweeper
was used to turn the beam off for 350 nanosecond intervals between
beam bursts. The coincidence data collected in the three parameter

Figure 4.8

Proposed decay scheme of levels found in ^{177}Ta.
Bracketed spins have not been definitely assigned.
A 5-quasiparticle interpretation is given to the
isomeric level found with a proposed 7-quasi-
particle interpretation forthe level found at
4082.6 keV.

$\gamma_1 - \gamma_2 - t$ mode were sorted for delayed times' 't'.

Figure 4.9 shows the same energy gate, 343.4 keV, used with different time gates. In the lower spectrum the sorting was carried out having specified that coincident γ events should occur within a prompt time of the gating 343.4 signal. The upper spectrum was obtained with a time gate of 120 nanoseconds, almost twice the measured half-life of the isomer, immediately following the prompt time gate. Therefore, the sorting brought out the γ's that were in delayed coincidence with the 343.4 keV 'stop' signal.

The use of the delayed coincidence experiment was extremely important for two reasons. First, because the transitions feeding the isomer would not be seen in prompt coincidence with already established transitions, there had to be some way of establishing a connection between the unknown isomer feeding transitions and the known isomer decay transitions. In addition, the specific nature of the delayed coincidence experiment permits even low intensity transitions to be more visible. A large number of gates were set in this way to isolate those transitions that fed into the isomer. Having done this, other measures were used to determine the level scheme above the isomer.

Figure 4.9

Figure illustrating the transitions in delayed and
prompt γ-γ coincidence with the 343.4 keV gate.

(a) doublet
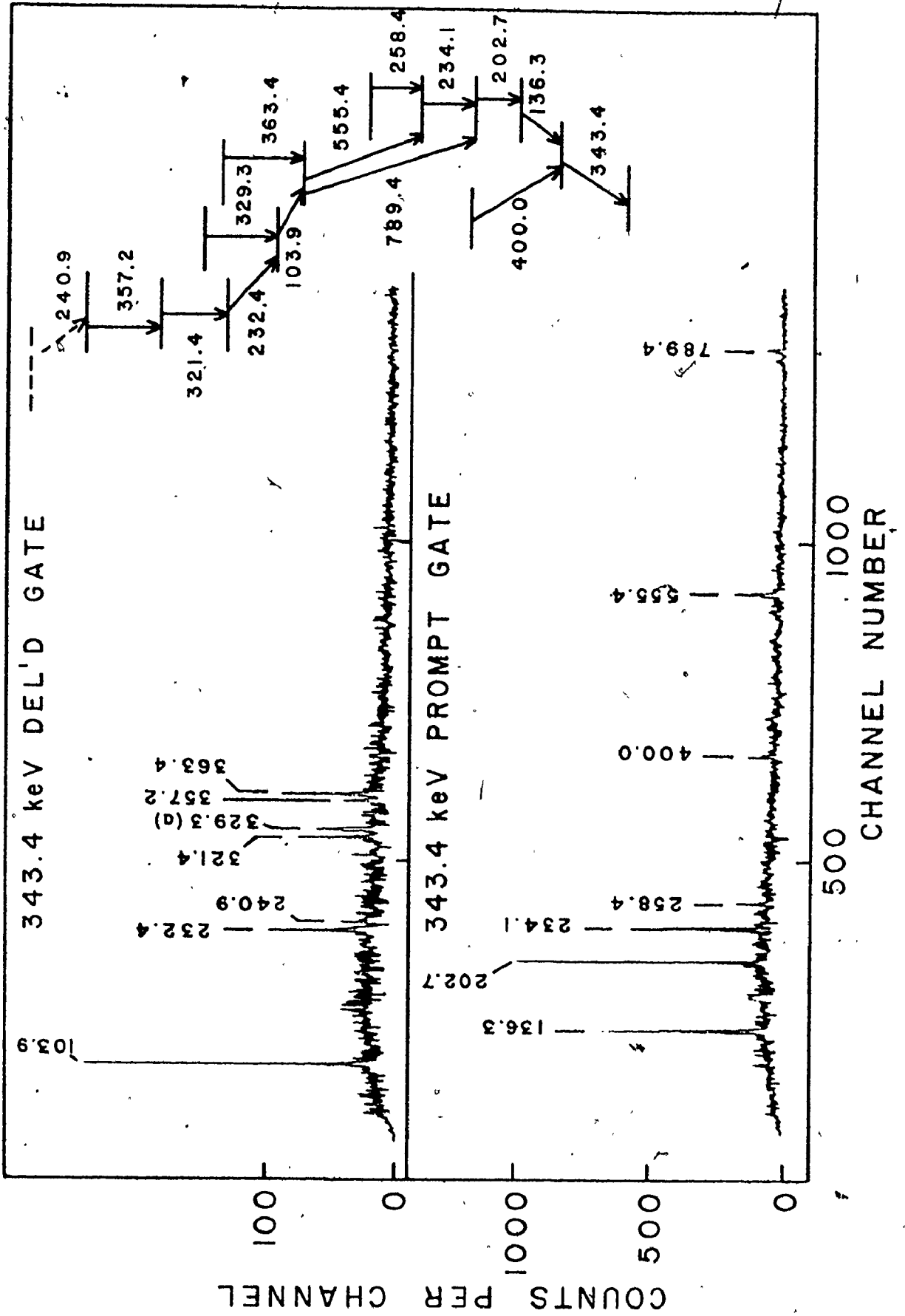
4.6 Transitions Feeding Into the 2826.8 keV Isomer

4.6.1 Prompt γ-γ Coincidence Results

Although it is possible to learn which transitions are 'above' by looking from 'below', and perhaps, from their relative intensities, an estimate of the level ordering can be·derived, prompt γ-γ coincidence data are a necessary tool in determining a level scheme.

The same prompt γ-γ coincidence experiment discussed in section 4.4 contained information that was useful for investigating prompt coincidences between γ-rays feeding the 2826.8 keV isomer. The spectrum of transitions in coincidence with the strongest isomer feeding transition, the 103.9 keV, is shown in Figure 4.10. By this point it is obvious that the intensities that were dealt with were' much smaller and, hence, the results not as straightforward to determine. Unfortunately, although a gate was set on the second most intense transition, the 232.4 keV, the interference of the 234.2 keV transition in the $K^{\pi} = 25/2^+$ band contributed most of the information in this gate. Several transitions were found in coincidence with the . eight most prominent transitions above the isomer, however, only the most definite were placed in the final level scheme of Figure 4.8. The. very rapid decrease in intensity with energy made positive identification more and more difficult.

The 363.4 keV transition was placed directly feeding the isomer because of its prominence in the delayed γ-γ coincidence work and the lack of any coincidences with transitions associated with the 103.9 keV line. The energy is also favourable in considering it to be a

Figure 4.10

Figure illustrating the transitions in prompt

coincidence with the 103.9 keV transition feeding

the 78 ns isomer at 2826.8 keV

(a) doublet
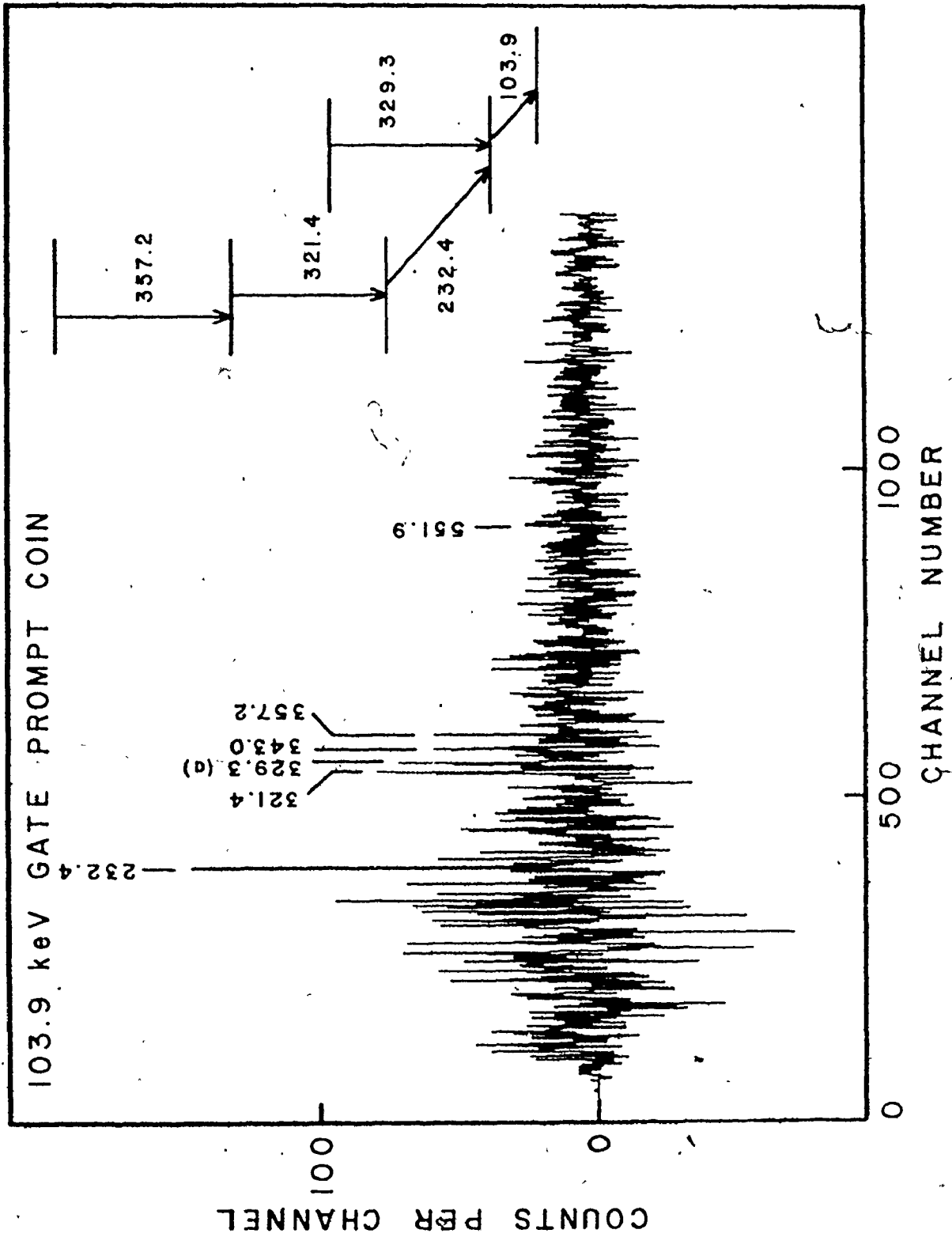
part of the rotational band built upon the 2826.8 keV level.

4.6.2 Multipolarity of the 103.9 keV Transition

The determination of the multipolarity of a very weak, low energy (< 200 keV) transition using a conversion electron experiment is difficult, if not impossible. Similarly, angular distribution measurements of low intensity transitions are usually ambiguous and are best when used in conjunction with some other more reliable data. This makes it necessary to use some other method to try to determine the multipolarity of such a transition. One method is to use prompt γ-γ coincidence data.
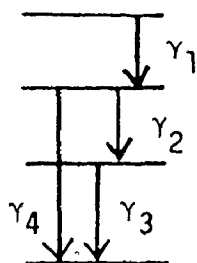
As the figure at the left illustrates, by looking at the gate set on transition γ_1, one should see the transitions γ_2, γ_3 and γ_4. What is of interest, though, is the fact that for every γ_2 event that occurs, so must a γ_3 to de-excite the level populated by the γ_2 transition. In other words, the intensity of the γ_2 transition as seen by the γ_1 transition must equal the intensity of the γ_3 transition. Allowing for angular distribution effects, any difference between the intensities measured would be due to unseen converted intensity.

Using the 321.4 keV gate, the measured relative intensities of the 103.9 keV and 232.4 keV transitions, corrected for detector and coincidence efficiency were.
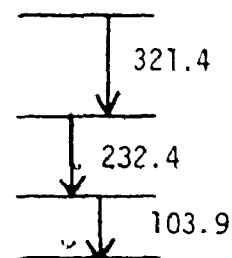
400 $\pm$ 33 and 408 $\pm$ 28 respectively. The majority of the error is due to coincidence efficiency correction. Although the multipolarity of the 232.4 keV transition is not known, it must be E1, M1 or E2 because it is prompt. Similarly with the 103.9 keV transition. Table 4.3 tabulates the possible ratios of the total intensities, $I_T(103.9)/I_T(232.4)$ using the different conversion coefficients for pure E1, M1 or E2 transitions. For the gate in question this value should be 1.0. It is obvious that only the possibility of an E1 multipolarity for the 103.9 keV transition is consistent with the intensities measured. The determination of the multipolarity of the 232.4 keV transition is not as clear as all three multipolarities give values in agreement with 1.0.

4.6.3 γ-Angular Distribution Results

A γ-angular distribution experiment was carried out to see if it would be possible to gain more information about the multipolarities of the transitions feeding the 2826.8 keV level. Again the ^{176}Lu $(\alpha,3n)$ reaction was used, a 0.4 nanoamp beam of 38 MeV α's bombarding the target. Data were collected at θ = 90°, 107°, 125°, 136°, 147° and 159° to the beam direction. An ND 10% Ge(Li) was used to collect the γ-events.

The intensities of the isomer feeding transitions compared to the lower lying transitions were quite small and easily masked by the much stronger transitions of similar energies. The 363.4 keV transition was not analyzed due to difficulties in consistently

Table 4.3

Ratios of $I_T(103.9)/I_T(232.4)$ Assuming Different

Possible Assignment of Multipolarities*

103.9 keV

		E1	M1	E2
	E1	1.26 ± .20	4.87 ± .82	3.92 ± .67
232.4 keV	M1	0.95 ± .20	3.68 ± .62	2.96 ± .50
	E2	1.17 ± .20	4.55 ± .77	3.66 ± .62

* Angular distribution effects which could alter intensities up

to 30% were not included. Their inclusion would not have

changed the conclusion presented.

extracting its areas from neighbouring peaks. Also, the 240.9 keV transition is a doublet, with only 25% of its intensity being isomer feeding. The other isomer feeding transitions, except the 103.9 keV, had too much uncertainty with their relatively small intensities to have any conclusive results. In the 103.9 keV case, though, the A_2 and A_4 coefficients were measured to be $-.204 \pm .046$ and $-.035 \pm .081$, characteristic of a 'stretched' dipole and therefore supporting the previous evidence for the E1 multipolarity of this transition.

The relative intensities of transitions at $\theta = 125°$ were used to check the consistency of the placement of these transitions in the proposed level scheme. The relative intensities of those isomer-feeding transitions which could be measured to a reasonable degree of accuracy are given in Table 4.4. The 311.3 keV is included for comparison purposes. Detector efficiency corrections have been included.

4.7 Spin and Parity Assignments

The final level scheme with proposed spin and parity assignments was given in Figure 4.8. The rotational bands built upon the 1-quasiparticle proton states have been extended in a natural sequence to, in the case of the $K^\pi = 1/2^-$ band, spin $I = 37/2^-$. The bands built upon the $5/2^+[402]$, $7/2^+[404]$ and $9/2^-[514]$ are not yrast and hence the intensities were too small to detect after spins $21/2^+$, $25/2^+$ and $27/2^-$ respectively.

Table 4.4

Relative Intensities of Some Isomer Feeding Transitions
At $\theta = 125°$ to the Beam Direction

E_γ (keV)	I_γ
103.9	100
232.4	44 ± 6
240.9 a)	16 ± 4
321.4	36 ± 6
329.3 b)	44 ± 6
357.2	27 ± 4
363.4	41 ± 29
311.3 c)	678 ± 31

a) doublet

b) corrected for contribution from lower lying transition

c) isomer decay transition included for comparison

Having measured the multipolarity of the 555.4 keV transition de-exciting the 2826.8 keV level into the I, $K^\pi = 29/2$, $25/2^+$ level to be M1 + E2 with a mixing ratio $\delta^2 = .92 \pm .30$, therefore the parity of this level must be positive with the spin satisfying the relationship

$$27/2 \leq I \leq 31/2. \tag{4.7.1}$$

The choice of spin $I \leq 29/2$ is highly unlikely as one would then expect to see E2 transitions from this level to the $25/2^+$ member of the $K^\pi = 25/2^+$ band. There is no such evidence. Also, since states near the yrast band are preferentially populated, a high lying level of low spin would not be populated significantly. Again, the choice of low spin does not seem likely.

Therefore, the conclusion must be that the 78 nanosecond isomer at 2826.8 keV has spin and parity $31/2^+$.

The angular distribution and prompt coincidence data showed the multipolarity of the 103.9 keV transition feeding the $31/2^+$ isomer to be stretched E1, meaning $|I_i - 31/2| = 1$. The spin and parity of this level must be either $29/2^-$ or $33/2^-$. Again, population of states near yrast band makes the choice of $29/2^-$ highly unlikely and so the level at 2930.7 keV is assigned a spin and parity of $33/2^-$.

Assuming the 363.4 keV transition to be the first member of
a rotational band built upon the $31/2^+$ state would lead to a spin
and parity assignment of $33/2^+$ for the 3190.2 keV level. What is
surprising, though, is the sudden absence of any transitions feeding
this level as the 363.4 prompt coincidence gate shows essentially
no transitions. Although this suddeness is unusual the same
behaviour is found to a lesser extent in ^{178}Ta where the rotational
band on che ground state is only seen for a few levels (F. Dubbers
et al, 1975).

The 329.3 keV transition which decays into the 2930.7 keV level
most likely depopulates the $35/2^-$ member of the $K^{\pi} = 33/2^-$ band.
The coincidence data are very ambiguous at this point beyond the fact
that the 329.3 keV is in prompt coincidence with a transition of
energy approximately 332 keV. Because of the lack of conclusive
data to establish the band built upon the $33/2^-$ state, only the
3260.9 keV level is tentatively assigned a spin and parity $(35/2^-)$.

As the multipolarities of the other isomer feeding
transitions were not extracted because of a lack of experimental
information, the assignments of the spins and parities of the
remaining levels were predicted using model dependent arguments.
This discussion is given in Chapter 6.

CHAPTER 5

EXPERIMENTAL RESULTS FOR ^{176}Ta

5.1 Introduction

The method of study used to investigate states in ^{177}Ta was extended also to ^{176}Ta ($Z = 73$, $N = 103$) in the hope of gaining some information in the, as yet, little explored field of high angular momentum states in doubly odd deformed nuclei. Numerous γ-transitions were found in the delayed studies on ^{177}Ta which did not appear to belong to any scheme yet proposed. The possibility arose that isomer decay transitions in ^{176}Ta were being seen.

Low spin levels up to an energy of 195.1 keV had been reported by J. Valentin et al (1963). These authors used electron capture of ^{176}W to populate levels in ^{176}Ta. Their results are given in Figure 5.1. Unfortunately, the ground state spin has never been measured absolutely. Dzhelepov et al (1958) determined that the spin should be 6^- or 1^-. Using model dependent arguments and similar considerations, Valentin et al (1963) had decided upon a ground state spin assignment of 1^-.

Further work has been introduced in an annual laboratory report by Elfström et al (1976) who had used the ^{175}Lu(α,3n) reaction to carry out coincidence, angular distribution and time distribution measurements. A tentative level scheme, Figure 5.2, was proposed by

Figure 5.1

Low spin levels in ^{176}Ta reported by Valentin et al (1963).

0^+ ^{176}W

e.c.

1^+ 195.1

1^+ 184.3

2^+ 133,8

0^+ 100.2

1^- 0
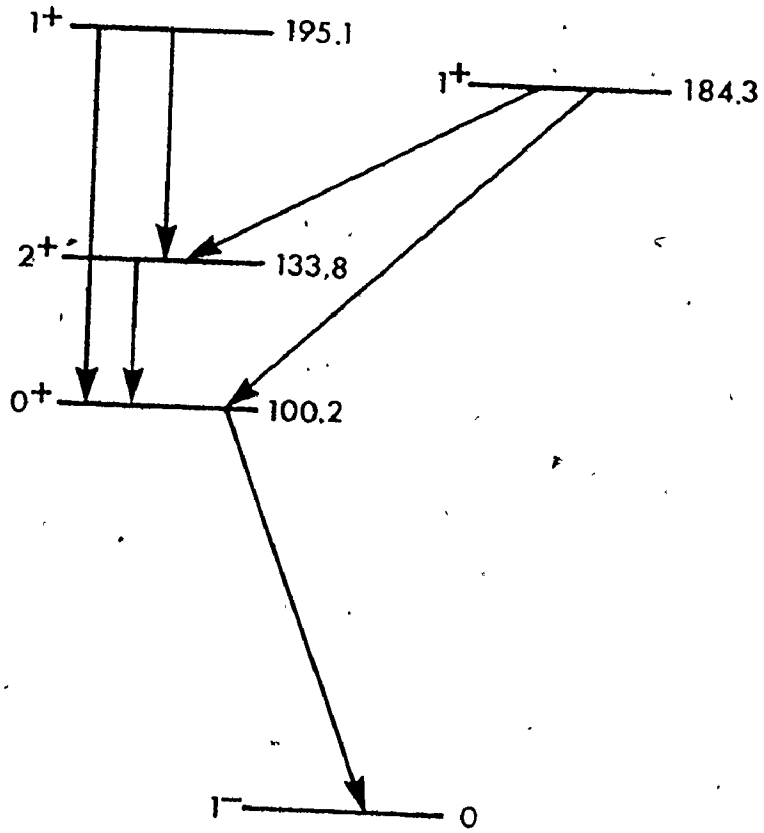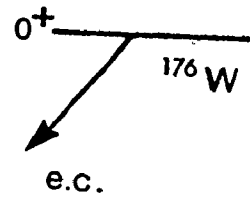
Figure 5.2

Tentative level scheme of ^{176}Ta proposed by
Elfström et al (1976).
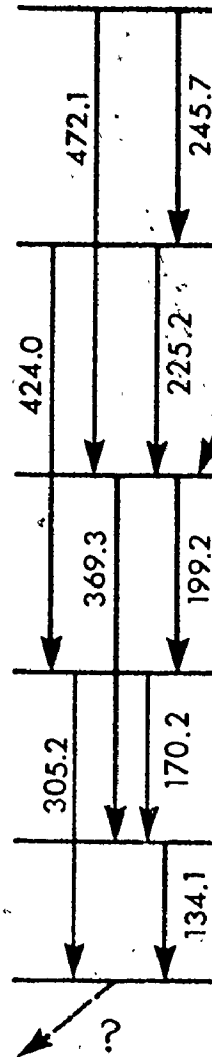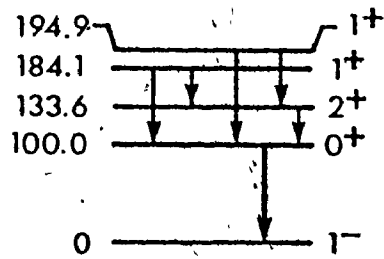
these authors which was basically consistent with the results that had independently been determined at McMaster, however, this group gave no information regarding the existence of a higher-lying isomer.

5.2 Delayed γ-Singles Results

5.2.1 Out-of-Beam Singles

Data collected while studying the delayed transitions in ^{177}Ta gave evidence for various other transitions which could be attributed to the de-excitation of an isomeric state in ^{176}Ta. These transitions appeared to decay with a half-life in the 1-10 μs range.

In order to enhance these transitions, the ^{170}Er(^{10}B,4n) reaction was used and delayed γ spectra were collected in the manner described in Section 2.9. A 0.3 nanoamp beam of 54 MeV ^{10}B from the McMaster Tandem accelerator bombarded a rolled target of ^{170}Er, 8.5 mg/cm^2 thick, placed in the Orange line γ-target chamber. The beam was pulsed at 40 μs intervals and a 17% Ge(Li) detector was used to detect γ-rays during the beam-off period. Figure 5.3 shows some of the sixteen spectra which were collected. Each spectrum represents a 1.18 μs interval. The time T = 0.0 represents the first spectrum which occurred out-of-beam, while the T = 2.4 μs and T = 11.8 μs spectra represent respectively later times.

Gamma transitions are present not only from the (^{10}B,4n) but also from the (^{10}B,5n) reaction, as well as transitions found

Figure 5.3

Spectra collected during beam off period. Each
period was 1.18 µs long. T = 0.0 µs·represents
the first spectrum collected out-of-beam, and
T = 2.4 µs and T = 11.8 µs represent the
respectively later times.

(a) lines found in ^{175}Hf

(b) lines found in ^{176}Hf

(c) lines found in ^{175}Ta
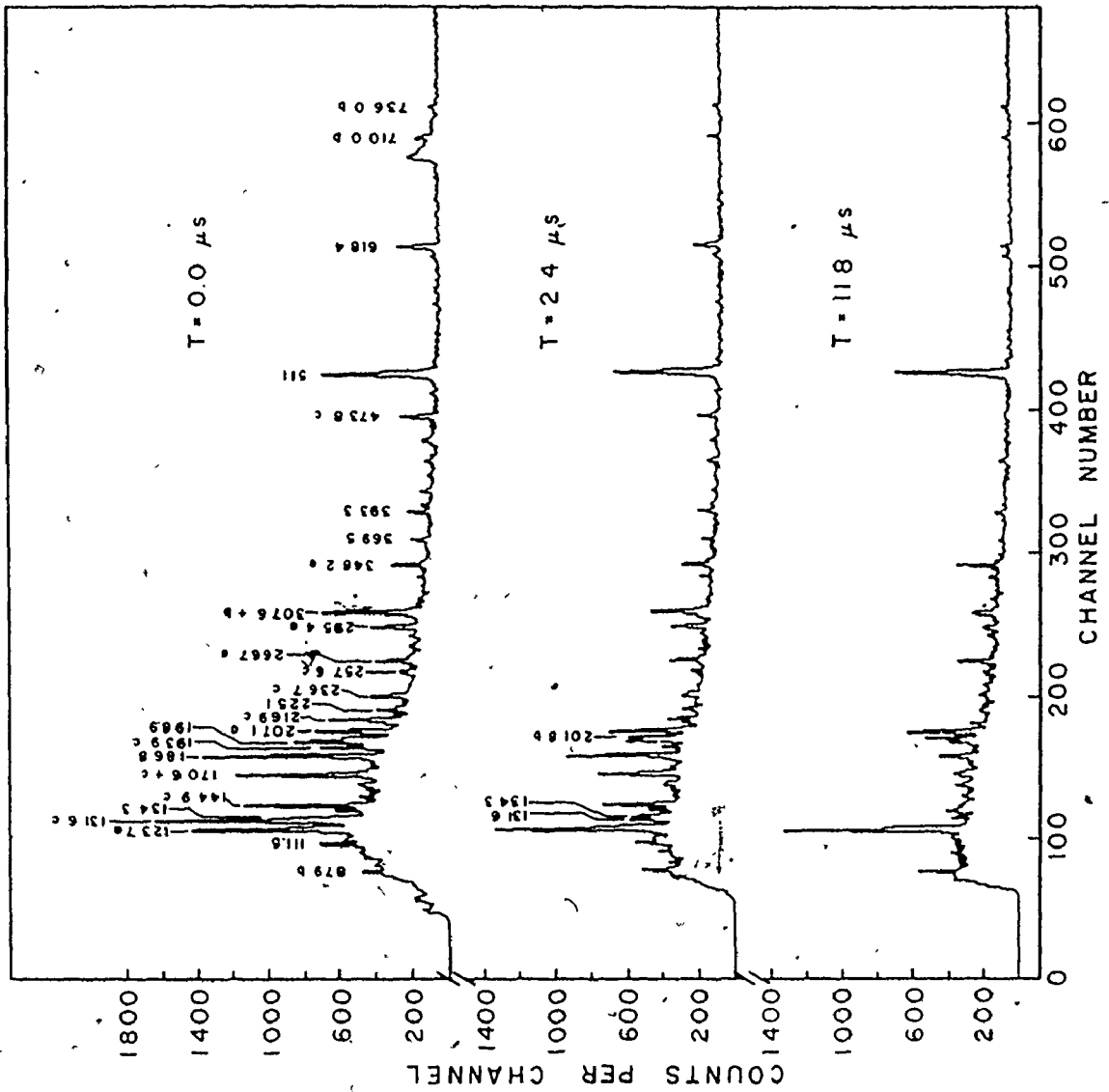
in ^{175}Hf and ^{176}Hf from the decays of ^{175}Ta and ^{176}Ta, respectively. Upon accounting for transitions in neighbouring nuclei and transitions whose energies or intensities would not fit in a proposed decay scheme, the 134.3 - 170.6 - 186.8 - 198.9 - 225.1 - (305.8) - 369.5 - 393.3 - 618.4 keV transitions were isolated. It is to be noted at this point that prompt γ-γ coincidence data were extensively used to build up the level ordering of transitions. For example, the 307.6 keV triplet peak is strong enough so as to mask the 305.8 keV transition found in ^{176}Ta.

Table 5.1 gives a listing of γ-intensities found in the T = 0.0 μs spectrum along with their relative intensities corrected for detector efficiency and attenuation in absorbers placed between the target and the detector. The abundance of contaminant decay lines is brought about by the 8.08 and 10.5 hour half-lives of the ground states of ^{176}Ta and ^{175}Ta, respectively. It is, therefore, mandatory that while preparing the experimental set-up, the beam should irradiate the target as little as possible and thereby lessen the problems of built-up radioactivity in the target.

The extremely large intensity of the 307.6 keV triplet transition cannot be explained. The components from ^{176}Ta and its decay constitute less than half of its intensity thereby still leaving a large unaccounted intensity. A comparison with prompt γ-γ coincidence data shows no such strong intensity for a transition of this energy. Its presence as well as that of the relatively strong 152.4 and 295.4 keV transitions could be associated with another

Table 5.1

Out-of-beam γ-intensities in ^{176}Ta using the

^{170}Er(^{10}B,4n) reaction

E_γ (keV)	I_γ	Assignment $I_i K_i^\pi \rightarrow I_f K_f^\pi$
87.9	x	^{176}Ta decay[a]
111.5	x	
123.7[d]	119 ± 12	partly ^{175}Ta decay[6]
131.6	145 ± 17	^{175}Ta
134.3		$(9)(8^-) \rightarrow (8)(8^-)$
140.7	11 ± 3	
144.9	69 ± 9	^{175}Ta
152.4	15 ± 9	
162.1	14 ± 7	
170.6[d]	82 ± 9	$(10)(8^-) \rightarrow (9)(8^-)$; ^{175}Ta
186.8	100	$(8)(8^-) \rightarrow (7)(7^+)$; other
193.9	32 ± 3	^{175}Ta
198.9	85 ± 5	$(11)(8^-) \rightarrow (10)(8^-)$
201.8		^{176}Ta decay[a]
207.1	38 ± 5	^{175}Ta decay[b]
216.9	31 ± 5	^{175}Ta
225.1	12 ± 3	$(12)(8^-) \rightarrow (11)(8^-)$
236.7	24 ± 4	^{175}Ta

Table 5.1 (continued)

E_γ (keV)	I_γ	Assignment $I_i K_i^\pi \to I_f K_f^\pi$
257.6	9 ± 2	^{175}Ta
266.7	24 ± 4	^{175}Ta decay[b]
279.5	5 ± 2	
289.1	6 ± 2	
295.4	35 ± 5	
307.6[t]	72 ± 8	^{176}Ta decay; $(10)(8^-) \to (8)(8^-)$; other
348.2	23 ± 4	^{175}Ta decay
369.5	9 ± 2	$(11)(8^-) \to (9)(8^-)$
393.3	14 ± 3	$(13)(13^-) \to (12)(8^-)$
399.2	7 ± 2	
410.7	7 ± 2	
424.6	5 ± 2	$(12(8^-) \to (10)(8^-)$
436.4	7 ± 2	^{175}Ta decay[b]
453.8	13 ± 3	^{175}Ta
473.8	23 ± 3	^{175}Ta
494.0	2 ± 1	^{175}Ta
609.8	5 ± 1	
618.4	30 ± 4	$(13(13^-) \to (11)(8^-)$
710.0	xx	^{176}Ta decay[a]
736.0	xx	
857.7	3 ± 1	^{175}Ta decay[b]

Table 5.1 (continued)

E_γ (keV)	I_γ	Assignment $I_i K_i^\pi \to I_f K_f^\pi$
936.0[d]	3 ± 1	partly ^{176}Ta decay[a]
1023.1	2 ± 1	^{176}Ta decay[a]
1159.0	16 ± 2	^{176}Ta decay[a]
1188.0	2 ± 1	

[a] decay from the 1^- state in ^{176}Ta

[b] decay from the 7/2+ state in ^{175}Ta

[d] doublet

x no intensity measurement due to low-energy cut-off

xx no intensity measurement due to presence of neutron
peak

FWHM at 307 keV equals 2.4 keV Energies of low intensity
transitions accurate to ± .4 keV

[t] triplet

isomer in the nucleus. There is no other evidence for this and it is only put forward as a suggestion.

The relative intensities of the isomer decay transitions in ^{176}Ta were only assigned after prompt and delayed γ-γ coincidence data were studied. These values are given in Table 5.4.

5.2.2 Half-life Determination of the 1309.0 keV Level

The decay of various transitions was followed and their time distributions determined. Of the 16 consecutive spectra collected, the first three were eliminated because of beam "seepage". The results for two of the transitions, 618.4 and 186.8 are illustrated in Figure 5.4. Because the 618.4 keV transition is clearly isolated from neighbouring peaks, interest was focussed on its behaviour for the clearest indication of the half-life of the isomer.

To account for the background component to the time distributions a least-squares fitting routine was used to fit to the data a function of the form

$$Y = A_1 \quad + A_2 \times \exp(-A_3 \times t) \qquad (5.2.1)$$

linear back-   exponential
ground con-   isomer decay
tribution

The fitted values of A_2 and A_3 give the intensity of the decaying component at $t = 0$ and the isomer lifetime, respectively. A measure of the goodness of fit is obtained through defining a quantity χ^2.

Figure 5.4

Figure illustrating the time rate of change of
intensity of the 186.8 and 618.4 keV transitions.
In each case, constant background contribution is
subtracted to yield exponential decay curve.
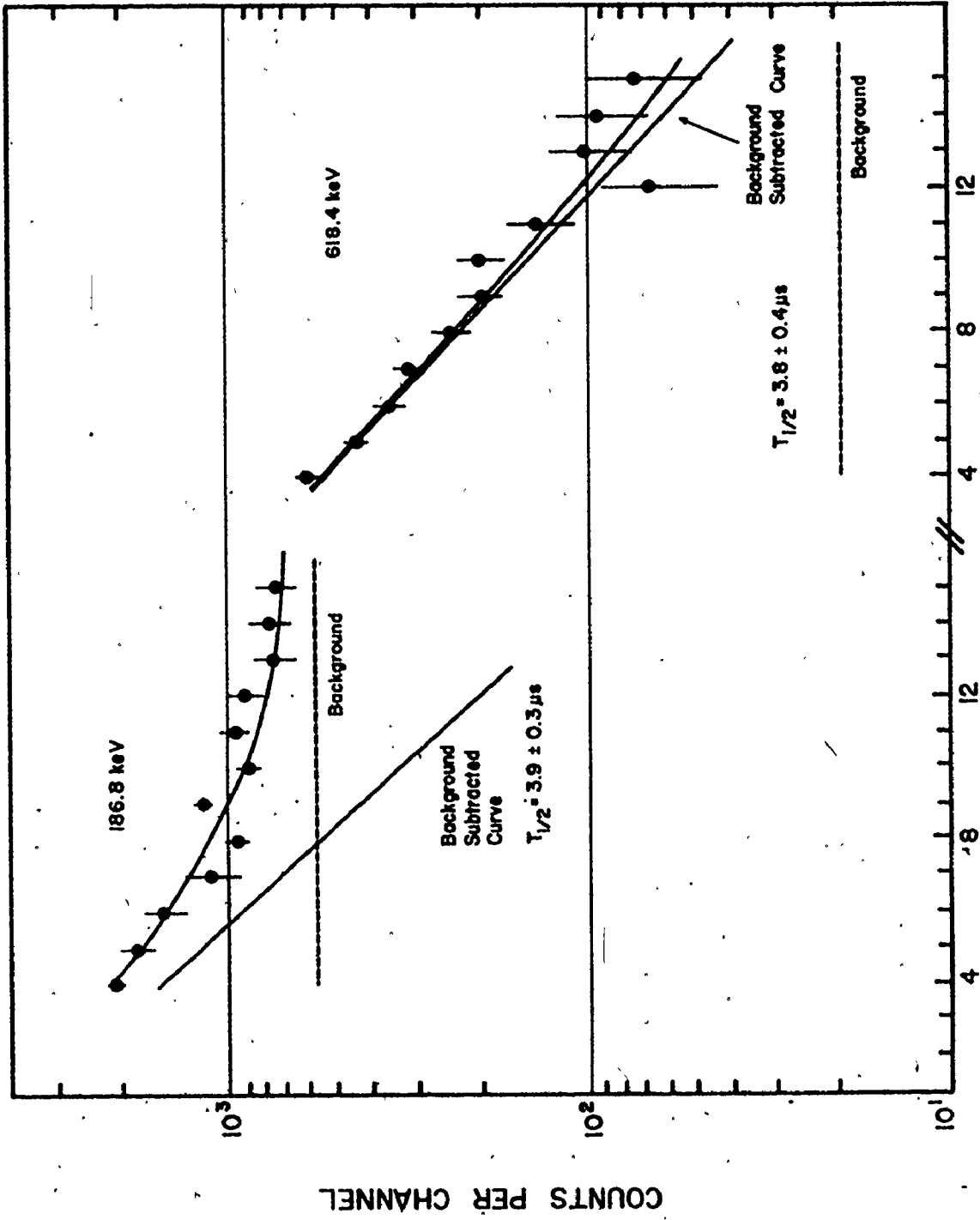
given by

$$\chi^2 = \Sigma \{\frac{1}{\sigma_i^2} [\mathring{y}_i - Y(t_i)]^2\} ; \qquad (5.2.2)$$

where the σ_i are the uncertainties in the measured data points. According to the method of least-squares, the optimum values of the parameters A_1, A_2 and A_3 are obtained by minimizing χ^2 with respect to each of these parameters. An explanation of the programme used, named Chifit, for this minimization procedure is given by P. Bevington (1969).

The values obtained using the 186.8 and 618.4 keV transitions were 3.9 ± 0.3 µs and 3.8 ± 0.4 µs respectively. Using these values and those of other transitions, the value of 3.8 ± 0.4 µs has been adopted as the isomer half-life.

5.3 Internal Conversion Coefficient of the 618.4 keV Transition

An out-of-beam conversion electron experiment was carried out at MSU cyclotron facilities to primarily obtain the multipolarities of the 555.4 and 789.4 keV transitions depopulating the 78 ns isomer in ^{177}Ta (see Section 4.3). At the same time, valuable data were also obtained which could be used in determining the multipolarity of the 618.4 keV transition depopulating the 3.8 µs isomer in ^{176}Ta. The measured value for $\alpha^K(618.4)$ was found to be 0.0088 ± 0.0018. This is to be compared with $\alpha_{E1}^K(618.4) = 0.0029$, $\alpha_{E2}^K(618.4) = 0.009$ and $\alpha_{M1}^K(618.4) = 0.026$. Clearly, the 618.4 keV transition is E2. The position of the measured conversion coefficient relative to the

calculated coefficients for M1 and E2 transitions is given in Figure 4.6.

5.4 Prompt γ-γ Coincidence Results

5.4.1 In-Beam Prompt Coincidence Results

To obtain γ-γ coincidence data, a 0.1 nanoamp .36 MeV ^{7}Li beam was used on a 3 mg/cm^2 target of ^{173}Yb. A 10 cm^3 planar Ge(Li) and a 17% Ge(Li) collected the events. Extensive data were collected to establish the ordering of transitions, with a total of 32 gates being set. Representative results for a few of the gates are shown in Figures 5.5 and 5.6. The 186.8, 134.3 and 198.9 keV gates were set on the smaller 10 cm^3 Ge(Li) detector and coincidences were sought in the larger 17% Ge(Li). The opposite procedure was used for the 618.4 keV gate.

The 186.8 keV gate clearly shows a large number of the transitions in the proposed decay scheme. The 618.4 keV gate, also, by its isolated position gives a very clean spectrum. Problems arise quickly with the other gates set since neighbouring nuclei have transitions whose energies are very similar to the energies of interest in ^{176}Ta, and their presence makes setting a gate difficult. The 170.6 keV and 170.3 keV transitions in ^{176}Ta and ^{175}Ta are a good example of this. Because of the doublet and even triplet nature of a number of transitions, the results for a few isolated peaks like 186.8, 393.3 and 618.4 keV were heavily weighted.

Figure 5.5

Figure illustrating the transitions in prompt
coincidence with the 186.8 and the 618.4 keV
gates. The 152.5 keV transition has not been
assigned.

124
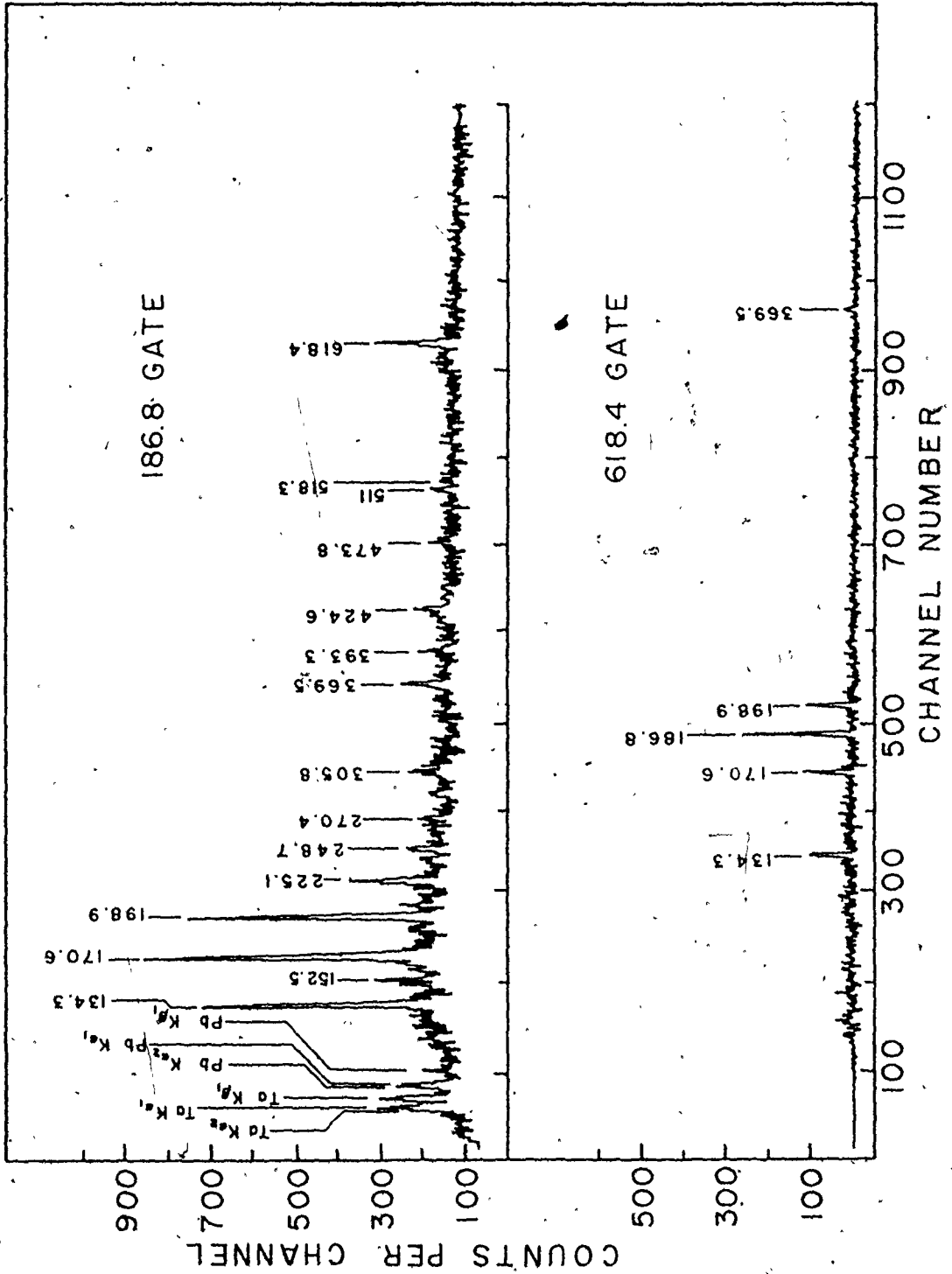
Figure 5.6

Figure illustrating transitions in prompt
coincidence with the 198.9 and 134.3 keV
gates.
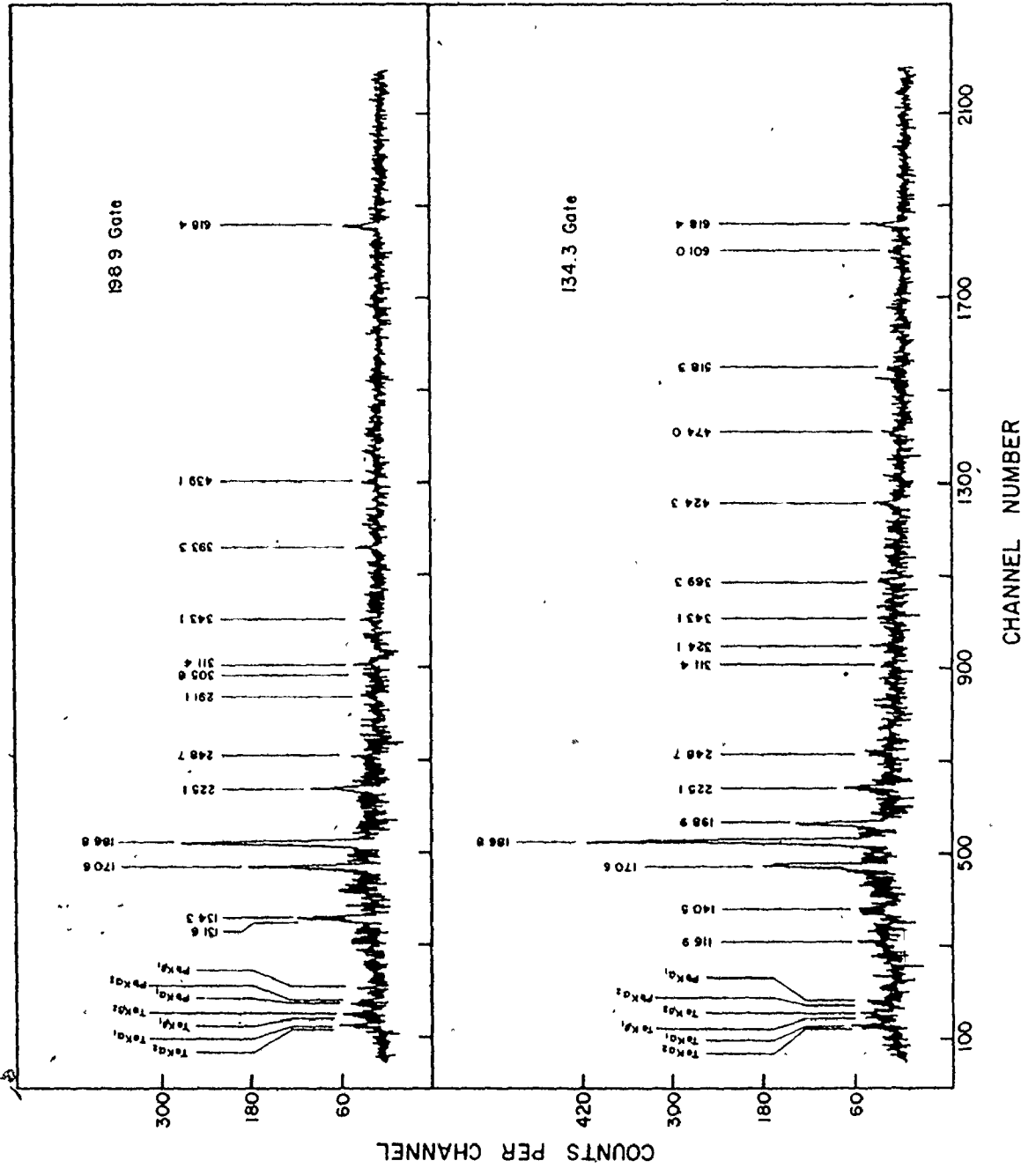
Although a large amount of coincidence data was collected and strong coincidences were seen among many transitions, some of these could not be related to the proposed decay scheme of [176]Ta. Whether they actually belonged to [176]Ta or not was questionable and they were therefore omitted from the discussion.

The final decay scheme is given in Figure 5.7. It should be noted that the lowest lying state seen is labelled at zero energy even though it is not the ground state. The energies of other levels are given relative to this lowest lying level. Because of the weak intensity of the transitions feeding into the 1309.0 keV isomer, it was not profitable to use coincidence data to investigate these transitions. A discussion of these transitions follows in Section 5.5.

5.4.2 Multipolarities of the 186.8 and 134.3 keV transitions

As shown in Section 4.6, the multipolarity of a transition can, in some cases, be extracted from prompt γ-γ coincidence results. Using the 198.9 keV gate, the total intensity of the 170.6 keV transition must equal that of the 134.3 keV. Apart from angular distribution effects any imbalance is due to converted intensity. Table 5.2 shows the ratios of transition intensities $I_T(170.6)/I_T(134.3)$ assuming E1, M1 and E2 multipolarities for the 170.6 keV transition and similarly E1, M1 and E2 multipolarities for the 134.3 keV. The gamma intensities of the 134.3 and 170.6 keV transitions were 815 ± 42 and 1567 ± 58, respectively. The ratio of the total intensities should equal 1.0. From the values

Figure 5.7

Proposed level scheme for ^{176}Ta. Spins are
bracketed due to the uncertainty of the spin
of the lowest lying 2-quasiparticle bandhead
seen. A 4-quasiparticle interpretation is
given to the isomeric level found. Although
all energies are given relative to the lowest level
which was detected, this level is not the
ground state.

$^{176}_{73}Ta_{103}$

$K^{\pi} = (13^-)$
$T_{1/2} = 3 8 \pm 0.4 \mu S$

$K^{\pi} = (8^-,9^-)$

$K^{\pi} = (7^+)$
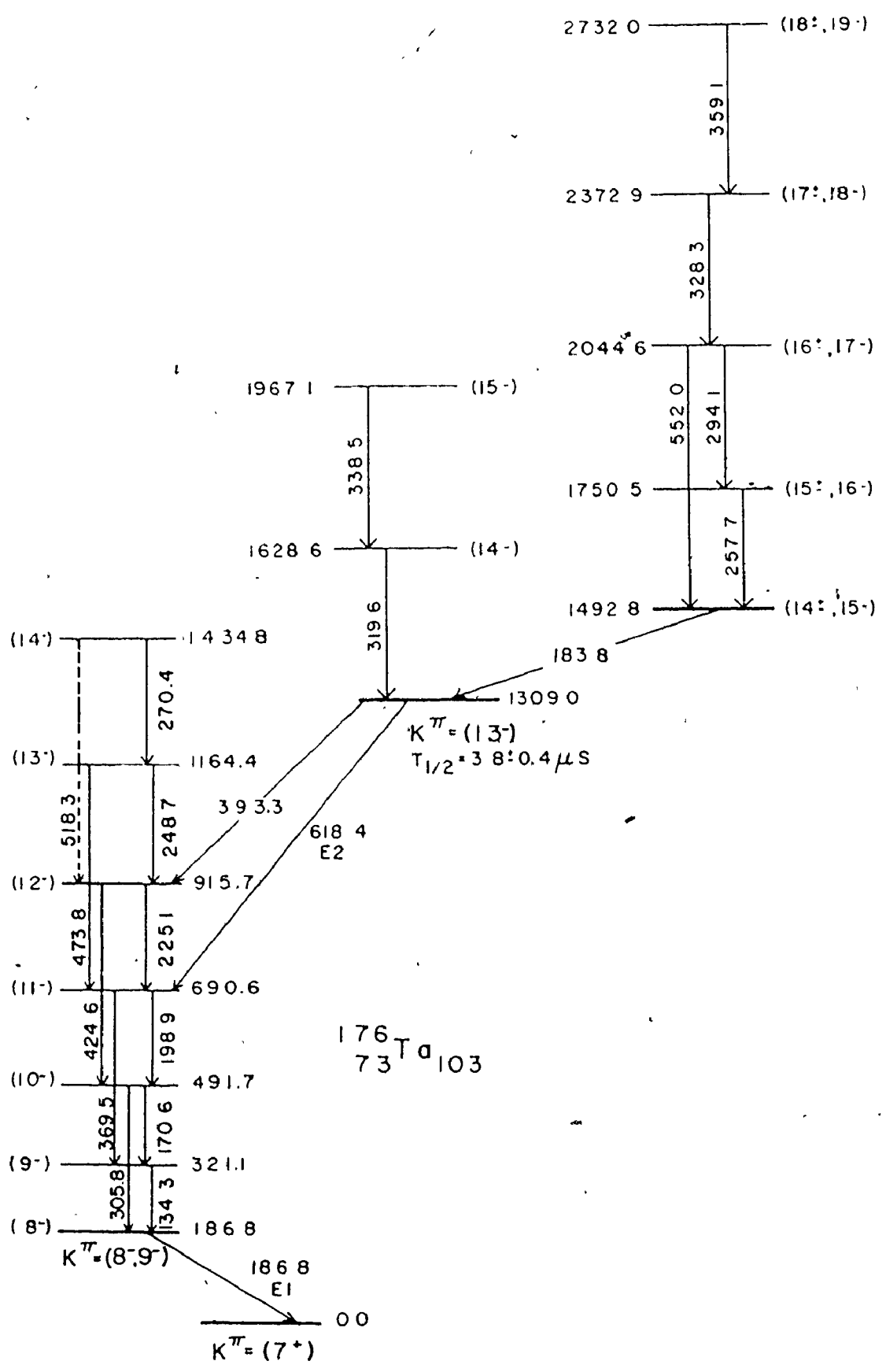
Table 5.2

Ratios of $I_T(170.6)/I_T(134.3)$ Assuming Different

Possible Assignment of Multipolarities*

		170.6 keV		
		E1	M1	E2
134.3 keV	E1	1.80 ± .16	3.29 ± .30	2.51 ± .22
	M1	0.71 ± .06	1.30 ± .12	0.99 ± .09
	E2	0.97 ± .09	1.68 ± .15	1.28 ± .12

* See footnote to table 4.3.

calculated, the choice of mixed M1 + E2 for the 134.3 keV transition gives the best agreement for all three choices of multipolarity for the 170.6 keV transition. In actual fact, the 170.6 keV is part of a rotational band and is, therefore, M1 + E2.
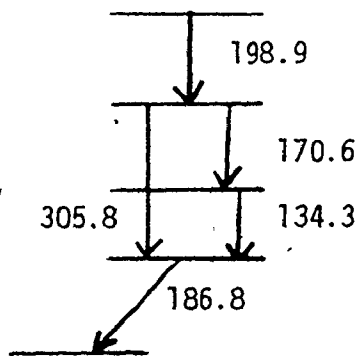
Carrying the calculation one step further it is also possible to obtain the multipolarity of the 186.8 keV transition. Again using the 198.9 keV gate, intensity balance requires that

$$I_T(305.8) + I_T(134.3) = I_T(186.8). \quad (5.4.1)$$

The 305.8 keV transition is a cross-over transition within a rotational band and therefore must be E2. Assuming this and that the 134.3 keV transition is M1 + E2, the ratios $[I_T(305.8) + I_T(134.3)]/I_T(186.8)$ for various multipolarities of the 186.8 keV transition are given in Table 5.3. The intensity of the 186.8 keV was 2453 ± 59, while the intensity of the 305.8 keV was too small to be accurately measured and so was included as an extra error in the determination of the ratio. It is clear that the best agreement is shown by choosing the multipolarity of the 186.8 keV to be E1. The multipolarity of the 134.3 keV transition is also shown to be mostly M1 consistent with the previous calculation.

Table 5.3

Ratios of $[I_T(305.8) + I_T(134.3)]/I_T(186.8)$

Assuming Different Possible Assignment of Multipolarities

Multipolarity of 134.3

		M1	E2
	E1	.92 ± .08	.68 ± .06
186.8 keV	M1	.55 ± .05	.41 ± .04
	E2	.70 ± .06	.52 ± .05

5.4.3 Half-life of the 186.8 keV Level

Since the 186.8 keV transition is a transition between two different particle states, an attempt was made to see if its de-excitation of the 186.8 keV level is delayed, with a half-life less than the timing resolution for prompt coincidences, that is, approximately 20 nanoseconds. To do this, the same gating and sorting procedure was carried out as used for previous results except that the gates were set on two energy signals with the resultant sorted spectrum showing the time distribution between them.

Since 134.3, 170.6 and 198.9 keV transitions are part of the same rotational band, they must necessarily be in prompt coincidence with each other and can, therefore, be used in determining a 'standard' time distribution for transitions in prompt coincidence. A shift in the centroid of the time distribution between two events compared to the time distribution between the 134.3 - 170.6 keV or the 170.6 - 198.9 keV would indicate the presence of an isomer. Figure 5.8 illustrates the time distributions of the 134.3 - 170.6, 186.8 - 170.6 and 198.9 - 170.6 keV transitions. No discernible shift could be detected and so no delay greater than 5 nanoseconds was detected between these transitions.

Figure 5.8

Figure illustrating the time spectra between
coincident γ rays. The 134.3 - 170.6 and
198.9 - 170.6 are used as 'standard' prompt
coincident events. No shift greater than 5 ns
was found in comparing the 186.8 - 170.6 coin-
cidence with the 'standards'.

134.3 - 170.6

186.8 - 170.6

198.9 - 170.6

Counts per Channel

Channel (.78 ns / channel)
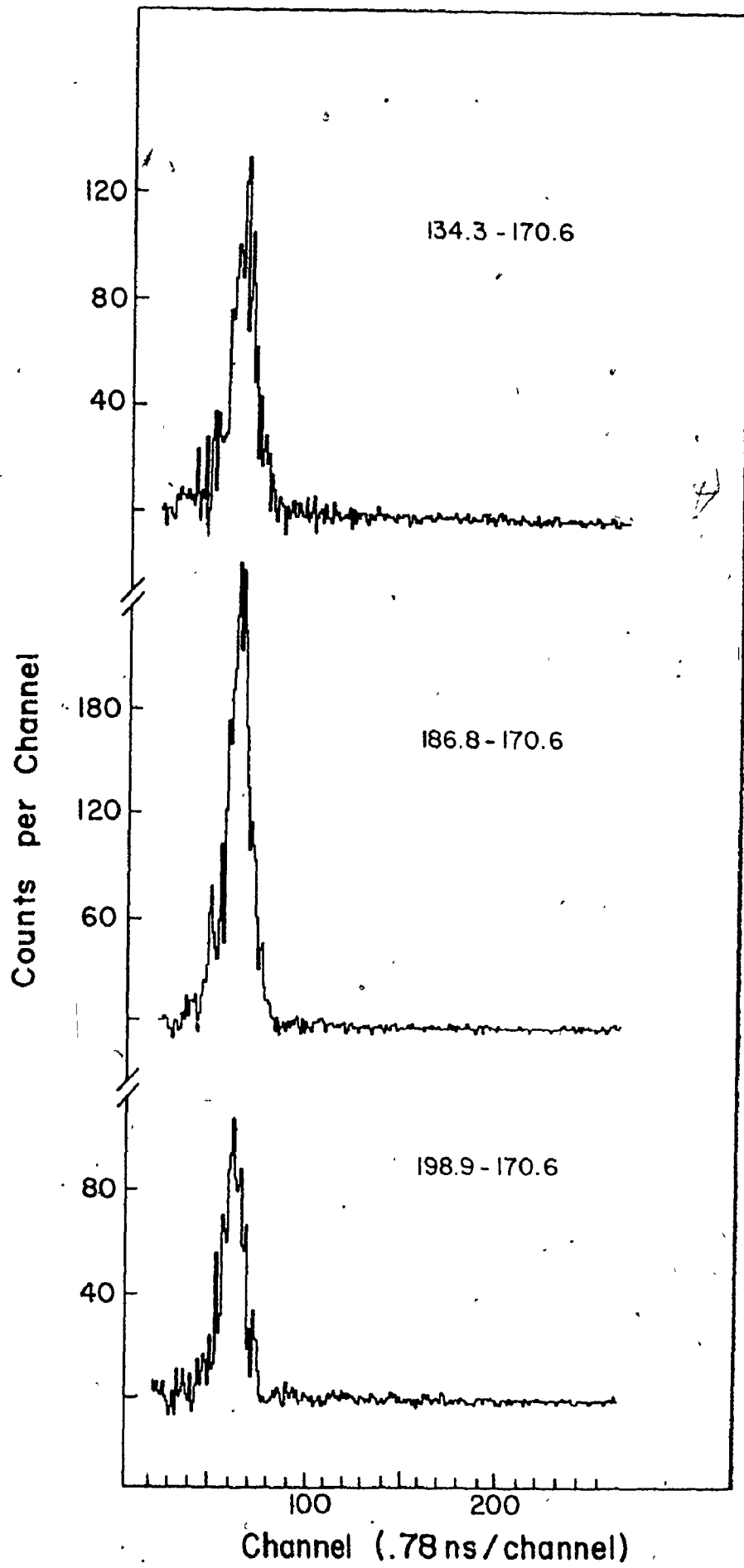
5.4.4 Out-of-Beam Prompt Coincidence Results

An experiment was carried out at MSU to study out-of-beam prompt coincidences between transitions de-exciting the 78 nanosecond isomer in ^{177}Ta. The ^{176}Lu(α,3n) reaction was used. A 0.1 nanoamp beam of 38 MeV α's bombarded the self-supporting target with resultant γ-events collected in an ND 10% Ge(Li) detector. The advantage of such an experiment is that weak in-beam lines can be particularly emphasized and be made 'visible'. Although this advantage was not particularly necessary in the case of ^{177}Ta, the usefulness of the method was seen as applied to the case of the 186.8 keV transition in ^{176}Ta.

Figure 5.9 illustrates two spectra of transitions in prompt coincidence with the 186.8 keV gate. Whereas in the upper in-beam spectrum the 369.5 keV transition is too weak to detect, it is clearly visible in the lower out-of-beam spectrum. What should be noticed is the lower statistics but greater prominence of the 369.5 keV transition making it's identification possible.

5.5 Delayed γ-γ Coincidence Results

5.5.1 Transitions populating the 1309.0 keV Level

To extend the study of ^{176}Ta to transitions feeding the newly established 3.8 μs isomer, an experiment was carried out to isolate delayed coincidences between those transitions which populate the isomer and those which were identified as decaying from the isomer. Again, the ^{170}Er(^{10}B,4n) reaction was used with a 0.3 nanoamp beam of 54 MeV ^{10}B

Figure 5.9

Figure illustrating transitions in prompt γ-γ
coincidence with the 186.8 keV gate. Data in
upper spectrum were collected with the beam
on target while the data in the lower spectrum
were collected with the beam off target.

134
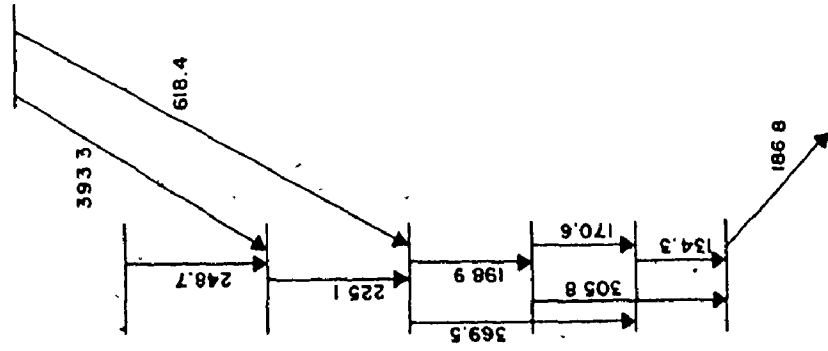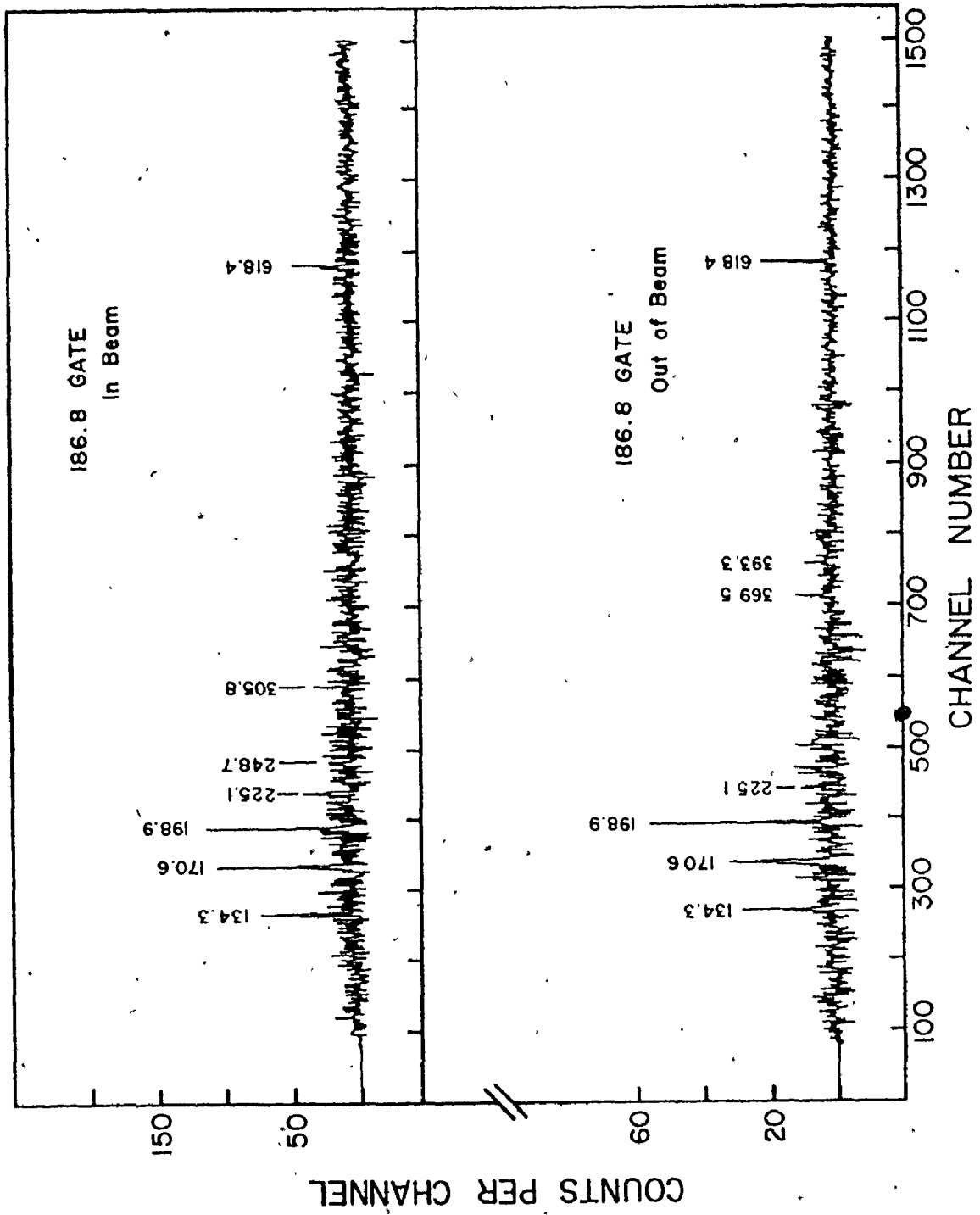
8.5 mg/cm^2 thick. A 17% Ge(Li) detector was used to await possible 'start' events and a 65 cc Ge(Li) was used to detect any coincident 'stop' signals that occurred during the 30 μs that the beam was pulsed off.

Figure 5.10 shows γ-transitions in delayed coincidence with the 618.4 and 198.9 keV transitions. It is obvious that the intensity of levels above the isomer is very small with most of the strength in only a few transitions, namely the 183.8, 257.7, 294.1, 319.6 and 328.3 keV transitions. Only the transitions that have appeared consistently in various delayed gates were put into the decay scheme shown in Figure 5.7.

Apart from a single case, no prompt γ-γ coincidence data could be used to help in establishing the level ordering above the isomer. This was brought about because the strongest of the above isomer transitions which could have possibly been used in prompt coincidence analysis were all heavily masked by other much stronger transitions. Consequently, the level ordering relied almost solely on the relative intensities of transitions 'above' as seen from 'below'. Table 5.4 lists the more accurately measureable intensities. Detector efficiencies have been included.

An estimate of the multipolarity of the 183.8 keV transition was determined using prompt coincidence information obtained by A. Larabee while studying the neighbouring ^{175}Ta nucleus. A 294.1 keV gate was set which rather weakly saw the 257.7 and 183.8 keV transitions.

Figure 5.10

Figure illustrating transitions in delayed coin-
cidence with the 618.4 and 198.9 keV 'stop'
gates.

(a) ^{170}Er Coulen

(b) associated with the 172.7 - 201.8 delayed
     coincidence in ^{176}Hf.
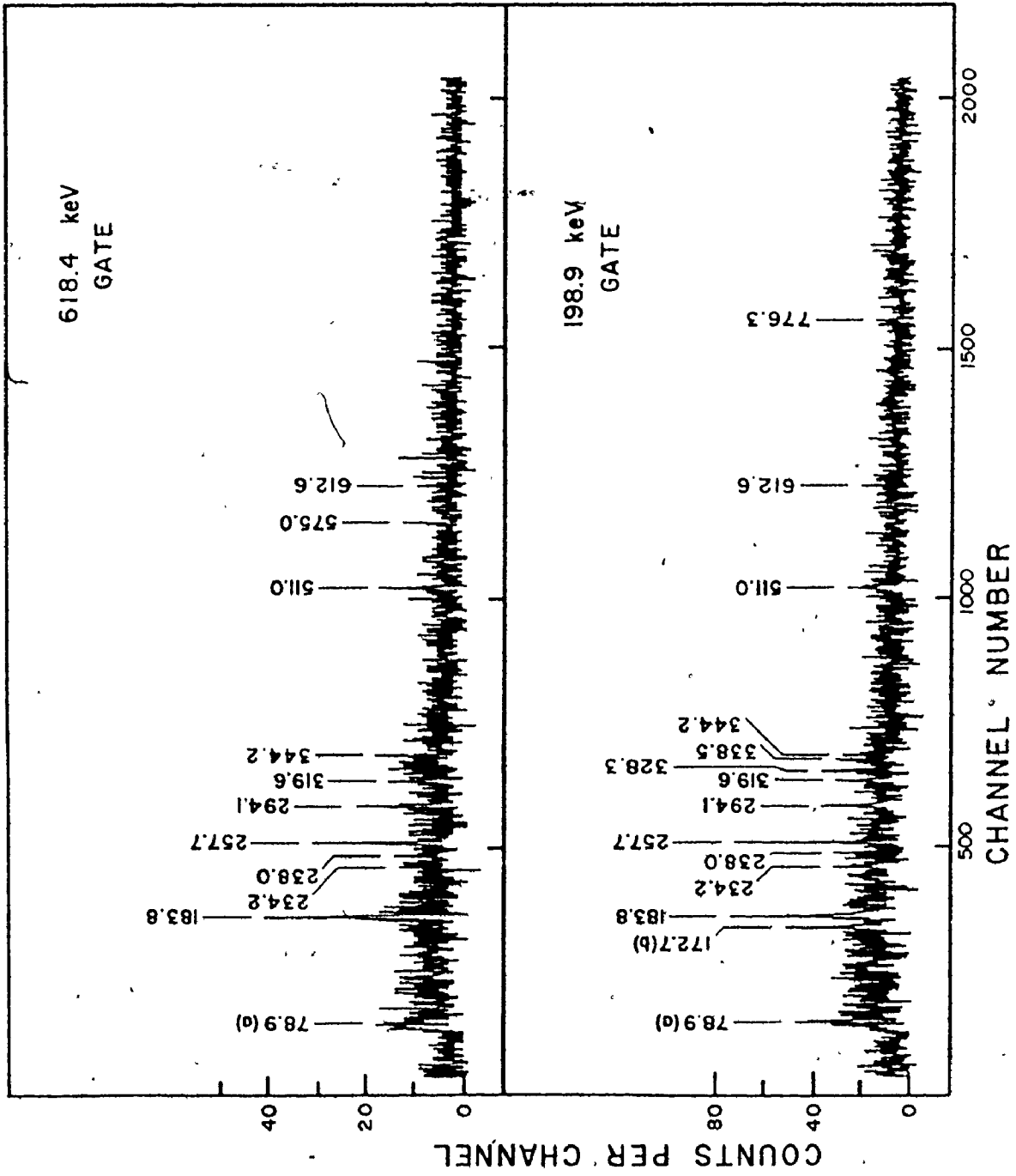
Table 5.4

Relative Intensities of some Isomer
Feeding Lines in ^{176}Ta.

E_γ (keV)	I_γ
183.8	100
257.7	59 ± 5
294.1	36 ± 4
319.6	35 ± 4
328.3	28 ± 3
338.5	28 ± 3

Although the intensities are too small to narrow down the exact multipolarity, only the choice of E1 or E2 give results close to the measured value of the conversion coefficient which was 0.0 ± .35. The tabulated values of the conversion coefficient for a 183.8 keV transition are: $\alpha_{E1}(183.8) = .07$, $\alpha_{M1}(183.8) = .76$, $\alpha_{E2}(183.8) = .34$.

5.5.2 Further Evidence for Transitions De-exciting the 1309.0 keV Isomer

The use of simple out-of-beam singles did not provide sufficient information for establishing the relative intensities of isomer decay transitions. Table 5.1 gives a clear indication why. Therefore, the results from the prompt and delayed coincidence experiments were analyzed before a final conclusion was reached. The relative intensities of the 305.8 keV and 424.6 keV transitions could not, because of their weak nature, be accurately determined. The values are listed in Table 5.5.

The intensities decaying into and out of each level are consistent throughout the rotational $K^{\pi} = (8^-, 9^-)$ band, but assuming only the 618.4 and 393.3 keV transitions feed into it, not enough intensity is brought in by these transitions to account for the intensity within the band. Another weak isomer decay branch must feed into the band, but it's presence has not been detected.

Table 5.5

Out-of-beam γ-ray Intensities in ^{176}Ta. Another relatively weak decay branch out of the isomer remains undetected.

E_γ (keV)	I_γ *
134.3	32 ± 8
170.6	48 ± 11
186.8	100
198.9	46 ± 10
225.1	17 ± 4
305.8	∿ 12[a]
369.5	14 ± 3[a]
393.3	19 ± 3
424.6	11 ± 7
618.4	55 ± 5

[a] Obtained from out-of-beam prompt γ-γ coincidence data

* The normalization of these intensities to the 186.8 keV intensity differs from Table 5.1 in that the intensity of the 186.8 keV used is strictly due to the isomer decay transition.

5.6 Spin and Parity Assignments

At the present time it is not possible to determine the spins of the states in ^{176}Ta without resorting to model-dependent arguments. The difficulty stems largely from the lack of an absolute measurement of the spin of the lowest energy bandhead seen in this work, this bandhead not being the ground state of the nucleus. Also disturbing was the inability to isolate transitions de-exciting this level, as this would have facilitated the interpretation.

The spin of the lowest energy bandhead seen is assigned a value of (7^+) for reasons discussed in the next chapter with the $(8^-,9^-)$ band being a strongly Coriolis mixed rotational band de-excited by the 186.8 keV E1 transition. The (13^-) isomer is de-excited by a 618.4 keV E2 transition to the 11^- member of the $(8,9^-)$ band. The assignment of (13^-) followed from the lack of any visible transition to the 10^- member of this band.

A full discussion of the considerations used in assigning these levels is given in Chapter 6.

CHAPTER 6

DISCUSSION OF EXPERIMENTAL RESULTS

6.1 Introduction

This chapter deals with the interpretation of the-experimentally determined level schemes of Chapters 4 and 5. The spins and parities of the individual many-quasiparticle states are discussed in terms of model dependent arguments and the most favourable configurations are suggested.

A semi-empirical calculation of the energies of the 3, 5, 7-quasiparticle states in ^{177}Ta is presented following the guidelines of Section 2.6. Various many-quasiparticle states in ^{176}Hf are used in the calculation, this nucleus being an isotone of ^{177}Ta. This type of calculation was not extended to the case of ^{176}Ta because of the shortage of information about many-quasiparticle states in this nucleus. However, a splitting energy calculation was carried out for the possible 2-quasiparticle states in this nucleus.

6.2 2-Quasiparticle States in ^{176}Ta

The configurations considered for the states populated in this nucleus are those formed from the Nilsson single particle proton and neutron orbitals near the Fermi level. The $9/2^-[514]_p$, $7/2^+[404]_p$ $5/2^+[402]_p$ and $1/2^-[541]_p$ proton orbitals and the $7/2^+[633]_n$,

$1/2^-[521]_n$, $5/2^-[512]_n$, $7/2^-[514]_n$ and $9/2^+[624]_n$ neutron orbitals are available. The 2-quasiparticle states that can be formed from these orbitals are shown in Table 6.1. Both the singlet (S) and triplet (T) configurations are given as well as their relative energies

$$E_{u_\ell} = \epsilon_p + \epsilon_n + \frac{\hbar^2}{2\mathcal{J}} (K) \pm \frac{S}{2} \qquad (6.2.1)$$

where S is the calculated splitting energy.

Since the $7/2^+[633]$ and $9/2^+[624]$ neutron orbitals are found at 207.4 and 644.2 keV, respectively, in ^{175}Hf, it is expected that the 2-quasiparticle states in ^{176}Ta involving the $7/2^+[633]$ neutron orbital will be lower in energy than those involving the $9/2^+[624]_n$ neutron.

Since the 186.8 keV E1 transition decays promptly (<5ns) it can be assumed to involve only a single particle transition. Thus, if the only configurations involved are those shown in Table 6.1, it would proceed as a $7/2^+[633]_n \rightarrow 5/2^-[512]_n$. This can be seen by comparing the energy differences between states that can be connected by an E1 transition. All transitions involving the $7/2^+[633]_n \rightarrow 5/2^-[512]_n$ neutron orbitals, namely $7^+ \rightarrow 6^-$, $8^- \rightarrow 7^+$ and $6^+ \rightarrow 5^-$ can possibly explain the 186.8 keV transition between the two states. This argument is supported by the structure of the rotational band above the 186.8 keV transition. The band is very compressed with a rotational parameter ~7.5 keV. Such Coriolis coupled bands with small rotational parameters have been found

Table 6.1

Configurations of Some Low-Lying 2-Quasiparticle States Expected in ^{176}Ta. The Bracketed Symbols Represent Singlet (S) or Triplet (T) Configurations.

	$7/2^+[404]\downarrow_p(0)^*$		$9/2^-[514]\uparrow_p(131.6)$		$5/2^+[402]\uparrow_p(36.4)$	
$7/2^+[633]\uparrow_n(207.6)$	7^+(S)	340	1^-(S)	403	1^+(S)	286
	0^+(T)	160	8^-(T)	383	6^+(T)	286
$5/2^-[512]\uparrow_n(0)$	6^-(S)	112	2^+(S)	225	0^-(S)	110
	1^-(T)	-28	7^+(T)	147	5^-(T)	22
$7/2^-[514]\downarrow_n(348.3)$	0^-(S)	430	8^+(S)	710	6^-(S)	507
	7^-(T)	350	1^+(T)	358	1^-(T)	347
$9/2^+[624]\uparrow_n(644.2)$	8^+(S)	806	0^-(S)	856	2^+(S)	749
	1^+(T)	590	9^-(T)	804	7^+(T)	721

*Energies shown after the proton and neutron orbitals represent the energies of those orbitals in ^{175}Ta and ^{175}Hf, respectively.

throughout the rare earth region to involve the $i_{13/2}$ orbitals.

It is not possible to determine the identity of the proton, at this time, but the higher spin bands formed with the $9/2^-[514]_p$ proton are expected to be the yrast states and therefore the most strongly populated. For the above reasons, the tentative spin and parity assignments shown in Figure 5.7 have been made. The bandhead of the $K^\pi = (7^+)$, $9/2^-[514]_p + 5/2^-[512]_n$ configuration is populated by an E1 transition from the 186.8 keV state. The energy of this state is given with respect to the 7^+ state, not the ground state.

6.3 Coriolis Coupling Calculation for the $K^\pi = (8^-,9^-)$ Band in ^{176}Ta

In order to test the conjecture that the perturbed structure of the 134.3 - 170.6 - 198.9 - 225.1 - 248.7 - 270.4 band results from Coriolis coupling between two $i_{13/2}$ orbitals, a simple two band mixing calculation was carried out. Following the procedure outlined in Section 2.7, the existence of two unperturbed rotational bands $K^\pi = 8^-$, $9/2^-[514]_p + 7/2^+[633]_n$ and $K^\pi = 9^-$, $9/2^-[514]_p + 9/2^+[624]_n$ was assumed. In addition, the calculation carried out assumed both unperturbed bands had the same rotational parameter, namely 13 keV, similar to that for the ground state of ^{176}Hf. This last requirement is a simplification which allows the energy difference between like-spin members of the two unperturbed rotational bands to be constant.

The values of E_+ as given by equation 2.7.6 are easily obtained by comparing the energy of a given unperturbed spin state, $\frac{\hbar^2}{2\mathcal{J}} \{I(I+1)-K^2\}$ to the measured energy of the state. It is then

straightforward to generate a series of equations and solve for the

the quantity $E_a - E_b$, the energy difference between the unperturbed

bands. The final result leads to the conclusion that two unperturbed

bands, separated by $E_a - E_b \sim 900$ keV with a rotational parameter

$\hbar^2/2\vartheta = 13$ keV can Coriolis couple to form the experimentally seen

134.3 - 170.6 - 198.9 - 225.1 - 248.7 - 270.4 keV band. The Coriolis

matrix element is unattenuated. Thus the small 134.3 keV spacing

results from the fact that, in this simple model, there is only one

spin 8 state and all other members are lowered relative to it. The

higher-lying perturbed band is not seen experimentally as it lies too

far off the yrast band.

A more complex calculation with fewer simplifying assumptions

should show essentially the same features.

6.4 4-Quasiparticle States in ^{176}Ta

6.4.1 The $K^{\pi} = (13^-)$ Isomer State at 1309.0 keV

The E2 multipolarity of the 618.4 keV transition leads to the

assignment of $K^{\pi} = (13^-)$ for the 3.8 µs isomer level (see Section 5.7).

Several states have been found in nuclei in this mass region which

have very hindered decays. These isomers have been attributed to

K-forbiddeness. A useful parameter often used in the consideration

of such cases is the hindrance factor F_W defined in Section 2.8.

The value of F_W for the 618.4 keV transition has been calculated to

be 3.27×10^4 which is consistent with the values quoted by Löbner (1968)

for a twice forbidden E2 transition.

Table 6.2 lists some possible 4-quasiparticle configurations for $K^\pi = 13^-$, 14^+, 15^- constructed of single particle Nilsson states located reasonably close to the Fermi surface. The possibility that the isomer is another 2-quasiparticle state is not considered because of the unavailability of two single particle states with high enough spin to produce a $K^\pi = 13^-$. There is, at present, not enough evidence to choose between the two possible configurations for the $K^\pi = (13^-)$ state. It should be noted, however, that the $\{5/2^+[402]_p + 7/2^+[633]_n + 5/2^-[512]_n + 9/2^+[624]_n\}$ configuration might lie lower in energy but would require a two-particle transition to decay into the $K^\pi = (8^-,9^-)$ band. If so, it would probably decay through small admixtures of other configurations.

Also to be noticed is the level spacing of the rotational band built upon the $K^\pi = (13^-)$ state as seen in Figure 5.7. Its rotational parameter of 11.5 keV is not characteristic of mixing between configurations with $i_{13/2}$ particles. Of the two possible configurations, the $\{9/2^-[514]_p + 9/2^+[624]_n + 1/2^-[521]_n + 7/2^-[514]_n\}$ would be able to mix with a configuration having the $7/2^+[633]_n$ and, consequently, produce a small rotational parameter. However, the $\{5/2^+[402]_p + 7/2^+[633]_n + 5/2^-[512]_n + 9/2^+[624]_n\}$ configuration already contains all the $i_{13/2}$ neutrons whose energies are close enough to be considered and would not produce a compressed band.

Still, there is no clear cut reason to definitely choose one configuration over another. Further evidence would be required before a decision could be made.

Table 6.2

Configurations of Possible 4-Quasiparticle Bandheads in ^{176}Ta

K^π	Configuration
13^-	$9/2^-[514]\uparrow_p + 9/2^+[624]\uparrow_n +$ $1/2^-[521]\downarrow_n + 7/2^-[514]\downarrow_n$
13^-	$5/2^+[402]\downarrow_p + 7/2^+[633]\uparrow_n +$ $5/2^-[512]\uparrow_n + 9/2^+[624]\uparrow_n$
14^+	$9/2^-[514]\uparrow_p + 7/2^+[404]\downarrow_p +$ $5/2^+[402]\uparrow_p + 7/2^-[514]\downarrow_n$
14^+	$7/2^+[404]\uparrow_p + 7/2^-[514]\downarrow_n +$ $5/2^-[512]\uparrow_n + 9/2^+[624]\uparrow_n$
14^-	$9/2^-[514]\uparrow_p + 7/2^+[404]\downarrow_p +$ $5/2^+[402]\uparrow_p + 9/2^+[624]\uparrow_n$
14^-	$9/2^-[514]\uparrow_p + 7/2^+[633]\uparrow_n +$ $5/2^-[512]\uparrow_n + 7/2^-[514]\downarrow_n$
14^-	$7/2^+[404]\downarrow_p + 7/2^+[633]\uparrow_n +$ $5/2^-[512]\uparrow_n + 7/2^+[624]\uparrow_n$

Table 6.2 (continued)

K^{π}	Configuration
14^-	$5/2^+[402]\uparrow_p + 7/2^+[633]\uparrow_n +$ $7/2^-[514]\downarrow_n + 9/2^+[624]\uparrow_n$
15^-	$9/2^-[514]\uparrow_p + 7/2^+[404]\downarrow_p +$ $5/2^+[402]\uparrow_p + 9/2^+[624]\uparrow_n$
15^-	$7/2^+[404]\downarrow_p + 7/2^+[633]\uparrow_n +$ $7/2^-[514]\downarrow_n + 9/2^+[624]\uparrow_n$
15^-	$9/2^-[514]\uparrow_p + 5/2^-[512]\uparrow_n +$ $7/2^-[514]\downarrow_n + 9/2^+[624]\uparrow_n$

6.4.2 The $K^\pi = (14^{\pm}, 15^-)$ State at 1492.8 keV

The 183.8 keV transition populating the 1309.0 keV $K^\pi = (13^-)$ level was shown in Section 5.5 to be either E1 or E2. This leads to the possibilities of $K^\pi = 14^{\pm}$ or 15^- for the 1492.8 keV level, lower spin assignments being eliminated due to yrast considerations.

Dubbers et al (1976) in their study of ^{178}Ta found the lowest 4-quasiparticle state to be $K^\pi = 15^- \{9/2^-[514]_p + 9/2^+[624]_n\} +$
$6^+[\frac{7/2^-[514]_n + 5/2^-[512]_n}{7/2^+[404]_p + 5/2^+[402]_p}]$.

This configuration can be formed through the combination of the $9/2^+[624]_n$ to the lowest lying 3-quasiparticle state in ^{177}Ta having $K^\pi = 21/2^-$ (see Section 6.5). The analogy is further substantiated by the decay of the $K^\pi = 15^-$ isomer to the $K^\pi = 9^- \{9/2^-[514]_p + 9/2^+[624]_n\}$ which is the addition of the $9/2^-[624]_n$ to the $9/2^-[514]_p$ 1-quasiparticle band found in ^{177}Ta to which the $K^\pi = 21/2^-$ decays.

Thus, the most favourable configuration is $K^\pi = 15^-$ $\{9/2^-[514]_p + 5/2^-[512]_n + 7/2^-[514]_n + 9/2^+[624]_n\}$ for the 1492.8 keV level. Unlike the $K^\pi = 15^-$ level in ^{178}Ta which is an isomer with a half-life of 60 ms, the 1492.8 keV level decays first to the $K^\pi = 13^-$ 3.8 μs isomer which subsequently decays to the 2-quasiparticle $K^\pi = (8^-, 9^-)$ band.

The evident small rotational parameter of this band, $\hbar^2/2\Im \sim$ 8 keV, leads to the choice of a configuration with an $i_{13/2}$ neutron which could mix with another such configuration. The presence of the $9/2^+[624]_n$ adds further emphasis for the choice of this configuration

for the 1492.8 keV level.

6.5 3-Quasiparticle States in ^{177}Ta

The 3-quasiparticle states in ^{177}Ta seen in Figure 4.8 at energies 1354.9, 1698.4 and 1834.7 keV have been studied by Barneoud et al (1975) who assigned these states with spins and parities $K^\pi = 21/2^-$, $23/2^+$ and $25/2^+$ respectively. The proposed configurations for these states are given in Table 6.3.

The decay of the $K^\pi = 21/2^-$ state at 1354.9 keV to the $K^\pi = 9/2^-[514]$ 1-quasiproton band is a K-forbidden transition with a half-life of 5.0 μs. To construct this state, one would expect to couple the $9/2^-[514]_p$ to a 6^+ configuration. Looking to the 2-quasiparticle states in ^{176}Hf, there are two possible 6^+ states. A 2-quasiproton state, $6^+\{7/2^+[404]_p + 5/2^+[402]_p\}$, is found at 1333.1 keV while a 2-quasineutron state, $6^+\{7/2^-[514]_n + 5/2^-[512]_n\}$ is found at 1761.5 keV. These two states are heavily mixed with the lower energy band containing 62% of the 2-quasiproton configuration and 38% of the 2-quasineutron configuration (Khoo et al, 1972). One would similarly expect two mixed $21/2^-$ states in ^{177}Ta, the lower energy configuration containing the largely 2-quasiproton 6^+ state found in ^{176}Hf.

The $K^\pi = 23/2^+$ and $25/2^+$ configurations follow in a straightforward manner. The undelayed nature of the 343.4 and 136.3 keV transitions de-exciting these levels implies a single particle transition thereby making the proposed $9/2^-[514]_p + 7^-\{9/2^+[624]_n +$

Table 6.3

Proposed Configurations of Observed 3-Quasiparticle States in ^{177}Ta

E (keV)	K^{π}	Configuration
1354.9	21/2$^-$	$9/2^-[514]\uparrow_p + 6^+\left\{\begin{array}{l}7/2^+[404]\downarrow_p + 5/2^+[402]\uparrow_p \\ 7/2^-[514]\downarrow_n + 5/2^-[512]\uparrow_n\end{array}\right\}$
1698.4	23/2$^+$	$9/2^-[514]\uparrow_p + 7^-\{9/2^+[624]\uparrow_n + 5/2^-[512]\uparrow_n\}$
1834.7	25/2$^+$	$9/2^-[514]\uparrow_p + 8^-\{9/2^+[624]\uparrow_n + 7/2^-[514]\downarrow_n\}$

$5/2^-[512]_n\}$ and $9/2^-[514]_p + 8^-\{9/2^+[624]_n + 7/2^-[514]_n\}$ configurations favourable. The 7^- and 8^+ configurations are found in ^{176}Hf at energies 1798.8 and 1860.3 keV, respectively. The rotational band built upon the $K^\pi = 25/2^+$ level is also seen to have a small rotational parameter, $\hbar^2/2\vartheta \sim 7$ keV, which is consistent with the small rotational parameter found for the $K^\pi = 8^-$ band in ^{176}Hf, $\hbar^2/2\vartheta \sim 8$ keV.

6.6 5-Quasiparticle States in ^{177}Ta

6.6.1 The $K^\pi = 31/2^+$ Isomer State at 2826.8 keV

The spin and parity of the 78 ns level at 2826.8 keV, as seen in Figure 4.8 was determined to be $31/2^+$. Table 6.4 gives the two most favourable configurations for this state. Again, the presence of the mixed $K^\pi = 21/2^-$ states is seen which in this case is coupled to a 2-quasineutron $5^-\{9/2^+[624]_n + 1/2^-[521]_n\}$ state. Because the 3-quasiproton $K^\pi = 21/2^-$ state is lower in energy than the other $K^\pi = 21/2^-$ configuration, one would, therefore, expect to assign the $\{3\text{-quasiproton} + 5^-\}$ configuration as the predominant contribution to this state. The decay of this state to the $K^\pi = 25/2^+\{9/2^-[514]_p + 9/2^+[624]_n + 7/2^-[514]_n\}$ band proceeds through the admixture of the configuration containing the higher-lying $K^\pi = 21/2^-$ configuration.

The isomerism of this state is attributed to K-forbiddeness, the 555.4 keV transition being a twice forbidden M1 transition. The value of F_W for the 555.4 keV transition has been calculated to be 2.29×10^5 which is consistent with the values given by Löbner(1968) for a twice forbidden M1 transition.

Table 6.4

Proposed Configurations of Observed 5-Quasiparticle States in ^{177}Ta

K^π	Configuration
$31/2^+$	$21/2^-\left\{\begin{array}{l}9/2^-[514]\uparrow_p + 7/2^+[404]\downarrow_p + 5/2^+[402]\uparrow_p \\ 9/2^-[514]\uparrow_p + 7/2^-[514]\downarrow_n + 5/2^-[512]\uparrow_n\end{array}\right\} + 5^-\{9/2^+[624]\uparrow_n + 1/2^-[521]\downarrow_n\}$
$33/2^-$	$21/2^- \{9/2^-[514]\uparrow_p + 7/2^+[404]\downarrow_p + 5/2^+[402]\uparrow_p\} + 6^+\{7/2^-[514]\downarrow_n + 5/2^-[512]\uparrow_n\}$ $23/2^+ \{9/2^-[514]\uparrow_p + 9/2^+[624]\uparrow_n + 7/2^-[514]\downarrow_n\} + 4^-\{7/2^+[633]\uparrow_n + 1/2^-[521]\downarrow_n\}$
$35/2^+$	$21/2^- \{9/2^-[514]\uparrow_p + 7/2^+[404]\downarrow_p + 5/2^+[402]\uparrow_p\} + 7^-\{9/2^+[624]\uparrow_n + 5/2^-[512]\uparrow_n\}$ $7/2^+[404]\downarrow_p + 9/2^+[624]\uparrow_n + 7/2^-[514]\downarrow_n + 7/2^+[633]\uparrow_n + 5/2^-[512]\uparrow_n$
$37/2^-$	$21/2^- \{9/2^-[514]\uparrow_p + 7/2^+[404]\downarrow_p + 5/2^+[402]\uparrow_p\} + 8^+\{9/2^+[624]\uparrow_n + 7/2^+[633]\uparrow_n\}$ $25/2^+ \{9/2^-[514]\uparrow_p + 9/2^+[624]\uparrow_n + 7/2^-[514]\downarrow_n\} + 6^-\{7/2^+[633]\uparrow_n + 5/2^-[512]\uparrow_n\}$

6.6.2 The $K^\pi = 33/2^-$ and $37/2^-$ States at 2930.7 and 3163.1 keV

The 'stretched' E1 multipolarity of the 103.9 keV transition de-exciting the 2930.7 keV level makes the assignment of the spin and parity of this level $K^\pi = 33/2^-$. Of the two most favourable configurations for this state given in Table 6.4, the {3-quasiproton + 2-quasineutron} should be lower lying in energy. The reason for this is obvious. One of the configurations can be thought of as the coupling of the low-lying $K^\pi = 21/2^-$ 3-quasiparticle state with the $K^\pi = 6^+$ 2-quasineutron state found in ^{176}Hf. The other is a coupling of the higher-lying $K^\pi = 25/2^+$ 3-quasiparticle state with the higher lying $K^\pi = 4^-$ 2-quasineutron state.

The actual configuration of this state is probably mixed to some extent as the 103.9 keV transition is undelayed and, therefore, most probably a one-particle transition. The dominant contribution is from the lower-lying {3-quasiproton + 2-quasineutron} configuration.

Although there is no experimental proof for the actual multipolarity of the 232.4 keV transition, the undelayed nature of this transition limits it to either E1, M1 or E2. A spin of 33/2 or lower for the state at 3163 keV is rejected because of yrast arguments. A spin of $35/2^-$ is not likely as it is impossible to construct a configuration of this spin and parity which would de-excite promptly to the 2930.7 keV level. One is left, therefore, with the possibilities of $35/2^+$ or $37/2^-$.

There is no definite reason for the elimination of the choice of $35/2^+$ for this state, indeed, as can be seen in Table 6.4, one of the $35/2^+$ configurations would easily decay into the $33/2^-$ level. The argument is not so much against the choice of $35/2^+$ as for the choice of $37/2^-$. There could be both a $35/2^+$ and $37/2^-$ bandhead present and if they are near each other, the higher spin $37/2^-$ will get the majority of the population. In addition, by comparing the 5-quasiparticle states in ^{177}Ta to the 6-quasiparticle states in ^{176}Hf proposed by Khoo et al (1976) in Table 6.5, the results would suggest a spin of $37/2^-$.

Table 6.4 shows the possible $K^{\pi} = 37/2^-$ configurations. Again, the two possibilities can be thought of as a union of a 3-quasiparticle state in ^{177}Ta with a 2-quasineutron state in ^{176}Hf. The first configuration listed consists of the $K^{\pi} = 8^+$ 2-quasineutron state while the second one consists of the $K^{\pi} = 23/2^+$ state with the $K^{\pi} = 6^-$ 2-quasineutron state. Although the $K^{\pi} = 8^+$ state is not seen experimentally in ^{176}Hf, its energy is estimated in Section 6.8.1 to be 2.0 MeV. This is higher than the energy of the corresponding $K^{\pi} = 6^-$ state, 1.9 MeV, but the $K^{\pi} = 21/2^-$ level is seen 479 keV lower than the $K^{\pi} = 25/2^+$ level. This could put the configuration that includes the $K^{\pi} = 21/2^-$ contribution slightly lower in energy.

Table 6.5

Suggested Configurations for 4- and 6-quasiparticle States Observed in ^{176}Hf(a)

Band-head energy (keV)	K^π	Configuration(b)
2866	14^-	$7/2^+_p\ 9/2^-_p\ 7/2^-_n\ 5/2^-_n$
3080	15^+	$7/2^+_p\ 9/2^-_p\ 9/2^+_n\ 5/2^-_n$
3266	16^+	$7/2^+_p\ 9/2^-_p\ 7/2^-_n\ 9/2^+_n$
4377	19^+	$7/2^+_p\ 9/2^-_p\ 7/2^-_n\ 9/2^+_n\ 5/2^-_n\ 1/2^-_n$
4766	20^-	$7/2^+_p\ 9/2^-_p\ 7/2^-_n\ 9/2^+_n\ 7/2^+_n\ 1/2^-_n$
4864	22^-	$7/2^+_p\ 9/2^-_p\ 7/2^-_n\ 9/2^+_n\ 7/2^+_n\ 5/2^-_n$

(a) ref. Khoo et al (1976)

(b) single-particle orbitals are $7/2^+[404]_p$, $9/2^-[514]_p$, $7/2^-[514]_n$, $5/2^-[512]_n$, $9/2^+[624]_n$, $7/2^+[633]_n$, $1/2^-[521]_n$.

6.7 7-Quasiparticle State in ^{177}Ta

Having assigned the 3163.1 keV level with a spin and parity of 35/2$^+$ or 37/2$^-$, the latter being more favourable, the two members of the rotational band built upon this state would have spins 37/2$^+$ and 39/2$^+$ in the former case, or 39/2$^-$ and 41/2$^-$ in the latter case. The 240.9 keV transition is obviously not a member of this band as the energy spacing is not rotational, but feeds into it from another many-quasiparticle state.

An interesting situation arises at this point. Although the multipolarity of the de-exciting 240.9 keV transition could not be measured because of the strong contribution of another transition of the same energy, the spin of the 4082.6 keV level must be in the vicinity of 41/2. To account for a spin that high, one must add another two quasiparticles as no combination of five quasiparticles can yield a spin greater than 37/2.

To construct the lowest-lying 7-quasiparticle state, the most favourable choice would be the K^π = 31/2$^+$ 5-quasiparticle configuration coupled with the low-lying K^π = 6$^+$ 2-quasineutron state in ^{176}Hf. This combination would decay via a single particle transition to the K^π = 37/2$^-$ configuration by a twice K-forbidden E1 transition. This would lead to a half-life of about 15 ns. Alternatively, if the band to which it decayed had spin and parity 35/2$^+$, it would decay via a single particle once K-forbidden E2 transition. The half-life in this case would be about 1 µs. The weakness of this transition made

the calculation of a half-life impossible, in fact there was no direct evidence that the transition was delayed. Nevertheless, the state from which it decays does appear to have a 7-quasiparticle configuration.

6.8 Theoretical Estimates of the Energies of the Many-Quasiparticle States in ^{177}Ta

6.8.1 Estimates of the Energies of the $K^{\pi} = 5^-$ and 8^+ States in ^{176}Hf

Before a presentation of the theoretical calculations of the energies of the many-quasiparticle states seen in ^{177}Ta is given, a preliminary estimate must be made for the energies of two 2-quasi-neutron states in ^{176}Hf which are not seen experimentally. Table 6.6 lists the various 2-quasiparticle states which have been seen experimentally in ^{176}Hf by Khoo et al (1972) and Zaitz et al (1972). To calculate the energy at which the $5^-\{9/2^+[624]\downarrow_n + 1/2^-[521]\downarrow_n\}$ configuration would appear, it is best to compare this state with the experimentally seen $7^-\{9/2^+[624]\downarrow_n + 5/2^-[512]\downarrow_n\}$ configuration. Using the method of calculation explained in Section 2.6, three factors contribute to the difference: 1) the difference in quasiparticle energy of the $5/2^-[512]_n$ and $1/2^-[521]_n$ states, 2) the difference in neutron-neutron interaction within the 5^- and 7^- states, 3) the difference in neutron-proton interaction within the 5^- and 7^- states. The first quantity can be obtained by using experimentally determined values in ^{175}Hf, the second and third can

Table 6.6

Configurations of Some 2-Quasiparticle States Seen in ^{176}Hf*

Energy (keV)	K^{π}	Configuration
1333.1	6^+	$7/2^+[404]\downarrow_p + 5/2^+[402]\uparrow_p$
1559.4	8^-	$7/2^+[404]\downarrow_p + 9/2^-[514]\uparrow_p$
1761.5	6^+	$7/2^-[514]\downarrow_n + 5/2^-[512]\uparrow_n$
1798.0	7^-	$5/2^-[512]\uparrow_n + 9/2^+[624]\uparrow_n$
1860.3	8^-	$7/2^-[514]\downarrow_n + 9/2^+[624]\uparrow_n$
1888.0	4^+	$7/2^-[514]\downarrow_n + 1/2^-[521]\uparrow_n$

* ref. Khoo et al (1972) and Zaitz et al (1972).

be calculated using the procedure prescribed in Section 2.6.

Alternatively, a comparison of the $4^+\{7/2^-[514]_n + 1/2^-[521]_n\}$

with the $6^+\{7/2^-[514]_n + 5/2^-[512]_n\}$ configuration also gives

an estimate of the latter two quantities, the difference between

the two methods being about 20 keV. The estimated energy of the

5^- state is then found to be 1605 keV.

The energy of the $8^+\{9/2^+[624]\uparrow_n + 7/2^+[633]\uparrow_n\}$ state can

also be estimated following the same procedure. By comparing the

8^+ state with the $7^-\{9/2^+[624]_n + 5/2^-[512]_n\}$ the value obtained

is equal to 2005 keV. Alternatively, by using the estimated value

of the energy of the 5^- state, the energy is 2008 keV.

6.8.2   Energies of the 3-Quasiparticle States in ^{177}Ta.

There are two types of 3-quasiparticle states in ^{177}Ta,

the 1 proton + 2 neutron case and the 3 proton case. The calculation

of the former type of configuration will be treated first.

Aside from residual interactions, a 3-quasiparticle state in

^{177}Ta consisting of one proton and two neutrons can be treated as

a 1-quasiproton state in ^{177}Ta coupled with a 2-quasineutron state

in ^{176}Hf. The difference in the nucleon-nucleon interactions can

be calculated and, in addition, two simplifying assumptions are made.

The difference between the neutron-proton interaction within a

one-quasiproton excited state and the ground state is essentially zero.

This can be seen by the fact that the neutron-proton interaction

in this case only varies by 5-20 keV depending on which proton is the

quasiproton. Also the difference between the neutron-proton inter-action within a 2-quasineutron excited state and the ground state in ^{176}Hf is approximately equal to the difference between the neutron-proton interaction in a 3-quasiparticle state and the ground state in ^{177}Ta, where the 3-quasiparticle state consists of the $7/2^+[404]_p$ and the 2-quasineutron state in ^{176}Hf. What should be noted at this point is that ^{176}Hf and ^{177}Ta are isotones which leads to a great deal of simplification in the calculations.

Also to be considered is the mixing of states that must be included in the energy determination. This can be partially accounted for by using the mixed 2-quasiparticle energies as one would more or less expect the same amount of mixing to occur with or without the presence of the 'spectator' proton depending on whether the energy separation of the states were about the same in both cases.

Therefore, to carry out the calculation for the $21/2^-$ state, the $9/2^-[514]_p$ state found at 74 keV in ^{177}Ta was coupled to the $6^+\{5/2^-[512]_n + 7/2^-[514]_n\}$ state in ^{176}Hf. Similarly, the energies of the $23/2^+$ and $25/2^+$ were determined by coupling the $9/2^-[514]_p$ to the $7^-\{5/2^-[512]_n + 9/2^+[624]\}$ and $8^-\{7/2^-[514]_n + 9/2^+[624]_n\}$ states in ^{176}Hf.

The calculation of the energy of the 3-quasiproton $21/2^-$ configuration is somewhat more difficult as the D' correction as given by equation 2.6.2 must also be considered. The simplifying

assumption that the proton-proton interaction is approximately the same in a 1-quasiproton excited state and the ground state in ^{177}Ta can be verified in the same manner as the neutron-proton interaction was shown to be approximately the same in a 1-quasiproton excited state and the ground state in ^{177}Ta. There are two groupings which can be used, the $9/2^-[514]_p$, $+ 6^+\{7/2^+[404]_p + 5/2^+[402]_p\}$ or $5/2^+[402]_p + 8^-\{7/2^+[404]_p + 9/2^-[514]_p\}$. There is a sizable difference in energy obtained by using the groupings because unlike the 8^- state, the 6^+ is strongly mixed. Using the "unmixed" value of the energy of the 6^+ state, the values calculated using the two methods differ by only 40 keV.

The values of the calculated energies are given in Table 6.8. It should be noted that the 3-quasiproton $21/2^-$ state lies lower in energy than the other $21/2^-$ state, as predicted. Also the calculated energies of the $23/2^+$ and $25/2^+$ states are 170 and 99 keV larger than the experimentally found values which is within the accuracy one would expect using this method.

6.8.3 Energies of the 5-Quasiparticle States in ^{177}Ta

There are two ways in which the energy of a 5-quasiparticle state can be calculated, either as a combination of a 3-quasiparticle state in ^{177}Ta with a 2-quasiparticle state in ^{176}Hf, or else a 1-quasiproton state in ^{177}Ta with a 4-quasiparticle state in ^{176}Hf. The advantage of using one method over another will be discussed in Chapter 7.

Table 6.5 lists various 4-quasiparticle states seen by
Khoo et al (1976). For the purposes of the calculations about to be
presented, it was necessary to use the energies of other 4-quasi-
particle states, even though such states have not been experimentally
seen. Therefore, estimates were made of their energies by using the
known energies of various 6-quasiparticle states seen. The idea
was to isolate the 4-quasiparticle energies by considering the
6-quasiparticle states to be composed of known 2-quasiparticle
energies and the contribution from the unknown 4-quasiparticle
state. The estimated energy is then combined with a quasiproton
state to use in a further calculation of the 5-quasiparticle states.

Table 6.7 lists the final energies derived for the 4-quasi-
particle states.

The first thing to be considered at this point is whether
it is reasonable that the $31/2^+$ state should be the lowest 5-quasi-
particle state to be populated in this nucleus. It is possible
to construct a $29/2^+$ state by combining the $7/2^+[404]_p$ with the
$11^-\{5/2^-[512]_n + 9/2^+[624]_n + 7/2^-[514]_n + 1/2^-[521]_n\}$ state. But
a calculation of the energy of this state (see Table 6.8) shows it to
be of higher excitation than the proposed $31/2^+$. Of the two possible
$31/2^+$ configurations, the state having the contribution from the
3-quasiproton $21/2^-$ state is found to be lower, as was previously
argued in Section 6.6.

Table 6.7

Estimates of the Energies of 4-Quasiparticle States in ^{176}Hf

K^{π}	6-Quasiparticle Configuration Used		4-Quasiparticle Energy Derived	
	Configuration*	Exp. Energy $\quad K^{\pi}$	Configuration*	Calc. Energy
19^{+}	$\{7/2^{-}_{n}\ 9/2^{+}_{n}\ 5/2^{-}_{n}\ 1/2^{-}_{n} +$ $7/2^{+}_{p}\ 9/2^{-}_{p}\}$	$4377 \qquad 11^{-}$	$\{7/2^{-}_{n}\ 9/2^{+}_{n}\ 5/2^{-}_{n}\ 1/2^{-}_{n}\}$	2998
20^{-}	$\{7/2^{-}_{n}\ 9/2^{+}_{n}\ 7/2^{+}_{n}\ 1/2^{-}_{n} +$ $7/2^{+}_{p}\ 9/2^{-}_{p}\}$	$4766 \qquad 12^{+}$	$\{7/2^{-}_{n}\ 9/2^{+}_{n}\ 7/2^{+}_{n}\ 1/2^{-}_{n}\}$	3479
22^{-}	$\{7/2^{-}_{n}\ 9/2^{+}_{n}\ 5/2^{-}_{n}\ 7/2^{+}_{n} +$ $7/2^{+}_{p}\ 9/2^{-}_{p}\}$	$4864 \qquad 14^{+}$	$\{7/2^{-}_{n}\ 9/2^{+}_{n}\ 5/2^{-}_{n}\ 7/2^{+}_{n}\}$	3513
22^{-}	$\{9/2^{-}_{p}\ 7/2^{+}_{p}\ 9/2^{+}_{n}\ 7/2^{+}_{n} +$ $7/2^{-}_{n}\ 5/2^{-}_{n}\}$	$4864 \qquad 16^{+}$	$\{9/2^{-}_{p}\ 7/2^{+}_{p}\ 9/2^{+}_{n}\ 7/2^{+}_{n}\}$	3687

* single particle orbitals $7/2^{+}[404]_{p}$, $9/2^{-}[514]_{p}$, $1/2^{-}[521]_{n}$, $7/2^{+}[633]_{n}$, $5/2^{-}[512]_{n}$, $7/2^{-}[514]_{n}$, $9/2^{+}[624]_{n}$.

Table 6.8

Theoretical Calculations of the Excitation Energies of

Many-Quasiparticle States Seen in ^{177}Ta

K^π	Exp. Energy	Calc. Energy	Configuration(a)	Calc. Energy
$21/2^-$		1835	$9/2^-_p + 6^+\{5/2^-_n + 7/2^-_n\}$	
$21/2^-$	1355	1415(1578)(b)	$9/2^-_p + 6^+\{7/2^+_p + 5/2^+_p\}$	
$23/2^+$	1699	1872	$9/2^-_p + 7^-\{5/2^-_n + 9/2^+_n\}$	
$25/2^+$	1835	1934	$9/2^-_p + 8^-\{7/2^-_n + 9/2^+_n\}$	
$31/2^+$	2827	2857	$21/2^-\{9/2^-_p + 7/2^+_p + 5/2^+_p\} + 5^-\{9/2^+_n + 1/2^-_n\}$	
$31/2^+$		3315	$23/2^+\{9/2^-_p + 5/2^-_n + 9/2^+_n\} + 4^+\{7/2^-_n + 1/2^-_n\}$	
$29/2^+$		3020	$7/2^+_p + 11^-\{5/2^-_n + 9/2^+_n + 7/2^-_n + 1/2^-_n\}$	

K^π	Configuration(a)	Exp. Energy	Calc. Energy	Configuration(a)	Calc. Energy
$33/2^-$	$21/2^-\{9/2^-_p +7/2^+_p +5/2^+_p\}+$ $6^+\{7/2^-_n +5/2^-_n\}$	2931	3141(c)	$5/2^+_p +$ $14^-\{7/2^+_p +9/2^-_p +7/2^-_n +5/2^-_n\}$	3186
$33/2^-$	$9/2^+_p +$ $12^+\{9/2^+_p +7/2^-_n +7/2^+_n +1/2^-_n\}$		3479		
$35/2^+$	$5/2^+_p +$ $15^+\{9/2^-_p +7/2^+_p +9/2^+_n +5/2^-_n\}$		3221		
$35/2^+$	$7/2^+_p +$ $14^+\{9/2^+_n +7/2^-_n +7/2^+_n +5/2^-_n\}$		3513		
$37/2^-$	$21/2^-\{9/2^-_p +7/2^+_p +5/2^+_p\}+$ $8^+\{9/2^+_n +7/2^+_n\}$	3163	3477	$5/2^+_p +$ $16^+\{9/2^+_p +7/2^+_p +9/2^+_n +7/2^+_n\}$	3536
$37/2^-$	$9/2^+_p +$ $14^+\{9/2^+_n 7/2^-_n 7/2^+_n 5/2^-_n\}$		3597		
$43/2^+$	$31/2^+\{9/2^-_p +7/2^+_p +5/2^+_p$ $9/2^+_n +1/2^-_n\}+$ $6^+\{5/2^-_n +7/2^-_n\}$	4083	4407	$5/2^+_p +$ $19^+\{7/2^+_p +9/2^-_p +7/2^-_n$ $9/2^+_n +5/2^-_n +1/2^-_n\}$	4262

(a) Configuration is written grouped in the manner the calculation was carried out
(b) Unmixed energy of the 6^+ used for value in bracket   (c) Unmixed energy of the 6^+ used

166

The energy of the 33/2$^-$ configuration containing the 3-proton 21/2$^-$ contribution was calculated in two ways. The first method combined the 3-quasiproton 21/2$^-$ state with the 2-quasineutron 6$^+$ state in ^{176}Hf while the second method used the 14$^-$ 4-quasiparticle state with the 5/2$^+$[402]$_p$ state. Both methods gave consistent results that agreed with the experimentally measured energy of this level. The other possible configuration for a state of this spin and parity is seen to give a result 550 keV higher in energy.

Although the estimates of the energies of the 35/2$^+$ configurations are closer in magnitude to the measured value of 3163 keV than the calculated energies of the 27/2$^-$ configuration, the difference is not great enough to exclude the possibility that the spin and parity of the state may still be 37/2$^-$. Another way of interpreting this is to note that the difference between the calculated energies of 33/2$^-$ and 37/2$^-$ states is about 330 keV which is in reasonable agreement with the measured transition energy of 232 keV. This also substantiates the previous prediction discussed in Section 6.6.2 that a 35/2$^+$ and 37/2$^-$ state may lie close in energy, but yrast arguments would explain the greater population of the 37/2$^-$ state as opposed to the 35/2$^+$.

6.8.4 Energy·of the 7-Quasiparticle State in ^{177}Ta

    ·The energy of the proposed 7-quasiparticle state at
4082.6 keV was calculated assuming two different combinations of
lower-order quasiparticle states: the lower-lying 5-quasiparticle
configuration of spin $31/2^+$ with the 2-quasineutron 6^+ state₀ in
^{176}Hf and also the $5/2^+[402]_p$ state with the 19^+ 6-quasiparticle
state in ^{176}Hf. The former combination gave an estimate of somewhat
poorer agreement with experimental values then the latter, the
difference being 324 and 179 keV, respectively, but still reasonable
enough to assume the $43/2^+$ state to be a 7-quasiparticle state. This
$43/2^+$ configuration is the lowest energy 7-quasiparticle config-
uration that can be constructed, other 7-quasiparticle configurations
having calculated energies that are greater by at least 400 keV.

CHAPTER 7

SUMMARY AND CONCLUDING REMARKS

The experimental results of this study have extended the knowledge of high spin states in ^{177}Ta, to I = 43/2 as well as I = (18,19) in the case of ^{176}Ta. The interpretation of the high spin states has been carried out within the framework of the quasiparticle model, these states being assigned many-quasiparticle configurations.

Also, the experimentally measured half-lives of the K^{π} = 21/2$^-$, 31/2$^+$, and 13$^-$ states in ^{177}Ta and ^{176}Ta agree favourably with the predicted values using the K-selection rule for electromagnetic transitions.

The agreement of the semi-empirically calculated energy values for the 3-quasiparticle states and for the 5-quasiparticle 31/2$^+$ and 33/2$^-$ states with experimentally determined values is very satisfactory and illustrates the applicability of the δ-force interaction for the nucleon-nucelon residual interaction. Although the agreement is not quite as good for the higher energy states, this is not a reflection on the theory used. Some of the disagreement most probably is brought about by the fact that mixing between states of the same spin and parity was not taken into explicit consideration. The mixing calculations were not carried out because of the absence

of experimental information on the states with which the experimentally
detected states would mix. Whereas for the 21/2$^-$ and 31/2$^+$ states
the mixing seems to have been taken care of by using 'mixed' values
for the constituent lower-order quasiparticle states, the mixing
for most of the other states could not be included so easily.

The calculation of the energy of a configuration using two
different combinations of lower-order states, was an interesting
exercise, not so much to check the consistency of themethod used,
which at first thought should yield the same answer, but rather
to check for inconsistencies. The discrepencies would have, to
some extent, reflected the inaccuracies of the interaction matrix
elements and, potentially, also a difference in pairing energy of
a nucleon pair in a few-quasiparticle system as opposed to a many-
quasiparticle system. However, no such discrepencies were found in
the cases seen in this study.

The 'story' of ^{176}Ta has just been begun with only a beginning
presented in this study. It is not a trivial subject for study,
but the paucity of data on many-quasiparticle states in-odd-odd nuclei
in the rare earth region is great and should be further explored.
The difficulties encountered in the analysis of experimental data
stems from the great similarity of transition energies in neighbouring
nuclei, thus making the analysis inherently difficult. The most
important first step in furthering information on this nucleus would
be to gain information on the method of decay of the $K^\pi = (7^+)$ state

to the actual ground state, thereby eliminating the confusion of high intensity transitions that do not seem to have a relationship with the levels so far placed and also putting spin assignments on a surer footing.

Whereas it was once thought that very high spin states could not be reached experimentally before one enters the fission region, recent experiments by groups such as Pederson et al. (1977) have shown results to spin ~ 40 in the mass region with neutron number $N \sim 82$. How far the knowledge of high spin states can be extended for the Ta nuclei is questionable, as although the $(43/2^+)$ state found in ^{177}Ta is only at 4 MeV of excitation, nevertheless seven of the highest Ω states available near the Fermi level were required to construct its configuration. What is yet to be found, or not found, remains to be the subject for further investigations.

BIBLIOGRAPHY

Barden, J., Cooper, L.N. and Schrieffer, J.R., 1957. Phys. Rev. $\underline{106}$, 162.

Barnéoud, D., Foin, C., Baudry, A., Gizon, A. and Valentin, J., 1970. Nucl. Phys. $\underline{A154}$, 653.

Barnéoud, D., André S. and Foin, C., 1975. Phys. Lett. $\underline{55B}$, 443.

Bernthal, F.M., Rasmussen, J.O. and Hollander, J.M., 1971. Phys. Rev. $\underline{C3}$, 1294.

Bertsch, G.F., 1972. The Practitioner's Shell Model, North Holland Publ. Co., Amsterdam.

Bevington, P., 1969. Data Reduction and Error Analysis for the Physical Sciences, McGraw-Hill, New York.

Bohr, A., 1952. Mat. Fys. Medd. Dan. Vid. Selsk. $\underline{26}$, #14.

Bohr, A. and Mottelson, B.R., 1953. Mat Fys. Medd. Dan. Vid. Selsk. $\underline{27}$, #16.

Bohr, A., Mottelson, B.R. and Pines, D., 1958. Phys. Rev. $\underline{110}$, 936.

Bohr, N., 1936. Nature $\underline{137}$, 344.

Boisson, J.P., Piepenbring, R. and Ogle, W., 1976. Physics Reports $\underline{26C}$, 99.

Cheung, H.C., 1975. McMaster University computer programme SPLIT, unpublished.

Chi, B.E., 1967. State University of New York, Department of Physics, preprint. Corrected from Chi, B.E., 1966. Nucl. Phys. $\underline{83}$, 97.

Cook, W.B., 1972. McMaster University, Ph.D. thesis.

dePinho. A.G. and Picard, J., 1965. Nucl. Phys. $\underline{65}$, 426.

172

Dubbers, F., Funke, L. Kemnitz, P., Schilling, K.-D., Strusny, H., Will, E., Winter, G. and Balodis, M.K., 1975. Zentralinstitut für Kernforschung, Rossendorf ZfK - 295.

Dubbers, F., Funke, L., Kemnitz, P., Schilling, K.-D., Strusny, H., Will, E., Winter, G. and Balodis, M.K., 1976. Zentralinstitut für Kernforschung, Rossendorf ZfK - 315.

Dzhelepov, B.S. and Peker, L.K., 1958. Decay Schemes of Radio-active Nuclei, Academy of Science (Moscow).

Elfström, S., Dubbers, F., Funke, L., Kemnitz, P., Lindblad, Th., Linden, C.G. and Winter, G., 1976. Research Institute of Physics (Stockholm) Annual Report.

Foin, C., Lindblad, Th., Skanberg, B. and Ryde, H., 1972. Nucl. Phys. A195, 465.

Gallagher, C.J. Jr. and Moszkowski, S.A., 1958. Phys. Rev. 111, 1282.

Gallagher, C.J. Jr. and Nielsen, H.L., 1962. Phys. Rev. 126, 1520.

Geiger, J.S., Graham. R.L. and Ward, D., 1968. AECL Report. AECL3257.

Hager, R.S. and Seltzer, E.C., 1968. Nuclear Data 4, 1.

Hübel, J., Naumann, R.A. and Spejewski, E.H., 1971. Phys. Rev. C4, 2272.

Hultberg, S., Rezenka, I. and Ryde, H., 1973. Nucl. Phys. A205, 321.

Jeltema, B.D. and Bernthal, F.M., 1974. Phys. Rev. C10, 778.

Jones, H.D., Onishi, N., Hess, T. and Sheline, R.K., 1971. Phys. Rev. C3, 529.

Kerman, A.K., 1956. Mat. Fys. Medd. Dan. Vid. Selsk. 30, #15.

Khoo, T.L., 1972. McMaster University, Ph.D. thesis.

Khoo, T.L., Waddington, J.C., O'Neil, R.A., Preibitz, Z., Burke, D.G. and Johns, M.W., 1972. Phys. Rev. Lett. 28, 1717.

Khoo, T.L., Bernthal, F.M., Warner, R.A., Bertsch, G.F. and Hamilton, G., 1975. Phys. Rev. Lett. 35, 1256.

Khoo, T.L., Bernthal, F.M., Robertson, R.G.H. and Warner, R.A., 1976. Phys. Rev. Lett. 37, 823.

Khoo, T.L., 1978. Private Communication.

Löbner, K.E.G., 1968. Phys. Lett. 26B, 369.

Mayer, M.G. and Jensen, J.H.D., 1955. Elementary Theory of Nuclear Shell Structure, John Wiley and Sons, Inc., New York.

Nathan, O. and Nilsson, S.G., 1965. Alpha Beta and Gamma Ray Spectroscopy, 601. ed. K. Siegbahn, North Holland Publ. Co., Amsterdam.

Newby, N.D., 1962. Phys. Rev. 125, 2063.

Newton, J.O., Stephens, F.S., Diamond, R.M., Kotajima, K. and Matthias, E., 1967. Nucl. Phys. A95.

Newton, J.O., 1969. Prog. in Nucl. Phys. Vol. 2, Ed. by Brink, D.M. and Mulvey, J.H. Pergamon Press, Oxford.

Newton, J.O., Stephens, F.S., Diamond, R.M., Kelly, W.H. and Ward, D., 1970. Nulc. Phys. A141, 631.

Nilsson, S.G., 1955. Mat. Fys. Medd. Dan. Vid. Selsk. 29, #16.

Pederson, J., Back. B.B., Bernthal, F.M., Bjorholm, S., Borggreen, J., Christensen, O., Folkmann, F., Herskind, B., Khoo, T.L., Neiman, M., Pühlhofer, F. and Sletter, G., 1977. Phys. Rev. Lett., 39. 990.

Preston, M.A. and Bhaduri, R.K., 1975. Structure of the Nucleus, Addison-Wesley Publ. Co. Inc., Massachusetts.

Pyatov, N.I., 1963. Ivz. Akad, Nauk, SSSR Ser. Fiz. 27, 1436 (Trans. Bull. Acad. Sci. USSR Phys. Ser. 27, 1409).

Rowe, D.J., 1970. Nuclear Collective Motion, Methuen and Co. Ltd., London.

Skänberg, B., Hjorth, S.A., and Ryde, H., 1970. Nucl. Phys. A154, 641.

Stephens, F.S. and Simon, R.S., 1972. Nucl. Phys. A183, 257.

Valentin, J. and Santoni, A., 1963. Nucl. Phys. 47, 303.

Weisskopf, V.F., 1952, in Theoretical Nuclear Physics, by Blatt and Weisskopf, John Wiley and Sons, Inc., New York.

Zaitz, J.I. and Sheline, R.K., 1972. Phys. Rev. C6, 506.